

ALMA MATER STUDIORUM  
UNIVERSITÀ DEGLI STUDI DI BOLOGNA

Dipartimento di Elettronica Informatica e Sistemistica

---

Dottorato di Ricerca in Ingegneria Elettronica, Informatica  
e delle Telecomunicazioni  
XX Ciclo

# Wireless Systems for the Fourth Generation

Tesi di:  
Ing. Enrica Salbaroli

Coordinatore:  
Chiar.mo Prof. Ing. Paolo Bassi

Relatore:  
Chiar.mo Prof. Ing. Oreste Andrisano

Settore scientifico-disciplinare:  
ING-INF/03 TELECOMUNICAZIONI

Correlatore:  
Dott. Ing. Alberto Zanella



# Contents

<b>1</b>	<b>Introduction</b>	<b>1</b>
1.1	Fourth Generation Wireless Systems . . . . .	1
1.2	Connectivity models and system performance . . . . .	4
1.3	Thesis Outline . . . . .	5
<b>2</b>	<b>Connectivity models for the infinite area case</b>	<b>9</b>
2.1	Notations and Scenario Description . . . . .	11
2.2	Statistic model for the received power . . . . .	13
2.2.1	Distribution of $T$ . . . . .	14
2.2.2	Distribution of $G$ . . . . .	16
2.3	Distribution of the received power: comparison with simulations . . . . .	18
<b>3</b>	<b>Connectivity models and Interference analysis for finite areas</b>	<b>23</b>
3.1	Propagation environment . . . . .	26
3.2	Distribution of $G$ . . . . .	27
3.2.1	Distribution of $G$ : general case . . . . .	27
3.2.2	Distribution of $G$ : external circular area . . . . .	28
3.2.3	Distribution of $G$ : the circular annulus case . . . . .	29
3.2.4	Distribution of $G$ : the circular area case . . . . .	30
3.3	Interference analysis . . . . .	31
3.3.1	Evaluation of the Moments of the Interference . . . . .	32
3.3.2	The moments of $G$ : circular annulus scenario . . . . .	35

3.3.3	The moments of $G$ : circular area scenario . . . . .	38
3.4	Numerical results . . . . .	38
3.4.1	External Circular Area Case: Scenario b) . . . . .	38
3.4.2	Circular Annulus Case: Scenario c) . . . . .	38
3.4.3	Circular area case: Scenario d) . . . . .	39
<b>4</b>	<b>Achievable Rate of networks with multiple-antenna sinks</b>	<b>45</b>
4.1	System Description . . . . .	48
4.1.1	Notations . . . . .	48
4.1.2	The scenario . . . . .	48
4.1.3	System Model . . . . .	50
4.1.4	The Achievable Rate . . . . .	51
4.2	Evaluation of the Achievable Rate . . . . .	52
4.2.1	Evaluation of $\Upsilon(n, \mathbf{E})$ . . . . .	52
4.2.2	Evaluation of $\mathcal{E}(n)$ . . . . .	55
4.2.3	Spatial Correlation model . . . . .	56
4.3	Achievable Rate analysis: numerical results . . . . .	57
<b>5</b>	<b>Experimental Activity: development and performance evaluation of a Multi-Hop IEEE802.15.4 Wireless Sensor Network</b>	<b>63</b>
5.1	TCS Application Scenario . . . . .	64
5.1.1	Description and Requirements . . . . .	64
5.1.2	Tests . . . . .	65
5.2	TCS with IEEE802.15.4: Interference and Selection of the Transmission Modes	73
5.3	TCS with IEEE802.15.4: System Design . . . . .	78
5.3.1	Possible implementations: Beacon Enabled or Non Beacon Enabled; Static or Dynamic . . . . .	78
5.3.2	Leaky Bucket . . . . .	80

---

5.3.3	Final Test: Scenarios . . . . .	81
5.3.4	Final Test: Results . . . . .	84
<b>6</b>	<b>Conclusions</b>	<b>89</b>
<b>A</b>	<b>Discussion on the p.d.f. of the distance between a pair of communicating nodes</b>	<b>93</b>
A.1	Review of eq. (7) of [23] . . . . .	94
A.2	Distribution of the distance between audible nodes and discussion on the validity of the other results of [23] . . . . .	96
A.2.1	Evaluation of $f_{D c}(\cdot)$ . . . . .	96
A.2.2	Discussion on the other results of [23] . . . . .	97



# Chapter 1

## Introduction

### 1.1 Fourth Generation Wireless Systems

Today, third generation networks are consolidated realities (see for instance [1–5]), and user expectations on new applications and services characterized by different quality of service (depending on the tolerable delay, or packet error rate, ...) are becoming higher and higher. Therefore, new systems and technologies are necessary to move towards the market needs and the user requirements, and to watch to the future. This has driven the development of fourth generation networks. The telecommunications technological growth offers to the market new systems and applications, and the cost reduction, jointly with the larger and larger demand, will led to a rapid spreading of the innovative solutions.

”Wireless network for the fourth generation” is the expression used to describe the next step in wireless communications ( [6–11]). There is no formal definition for what these fourth generation networks are; however, we can say that the next generation networks will be based

on the coexistence of heterogeneous networks (for instance, devices belonging to a Personal Area Network which can connect to the Internet through a wide band Access Point, active RFID remote controlled through the web and an IEEE802.11 network, ...), on the integration with the existing radio access network (e.g. GPRS, UMTS, WIFI, ...) and, in particular, on new emerging architectures that are obtaining more and more relevance, as Wireless Ad Hoc and Sensor Networks (WASN) [12–14]. Thanks to their characteristics, fourth generation wireless systems will be able to offer custom-made solutions and applications personalized according to the user requirements; they will offer all types of services at an affordable cost, and solutions characterized by flexibility, scalability and reconfigurability.

WASNs, with their specific characteristic and problems, have received a lot of attention in the past years, both from research and enterprise world. This interest is expected to increase in the next years due to the advent of new architectures and communication technologies. Among the most investigated next generation network we can find the Wireless Sensor Networks (WSNs) (see [15–20]), which represent a new and innovative opportunity to collect and analyse information from the environment (see for instance Fig. 1.1). Owing to their characteristics, WSNs are becoming very popular. As a matter of fact, their avant-garde technology allows the development of low cost applications, hardy and flexible, with large coverage areas, and the capability of automatic network creation and maintenance. IEEE standard 802.15.4 is the main protocol used by WSNs, and is the ideal technology for every application aiming at the collection of data from the real world. Among the huge number of WSNs possible application scenarios, we cite some application example:

- environmental monitoring (i.e. fire control; monitoring of amount of light, temperature, humidity, ...);
- home automation;
- emergency scenarios (i.e. earthquakes, eruptions, or flooding control);
- medical applications;

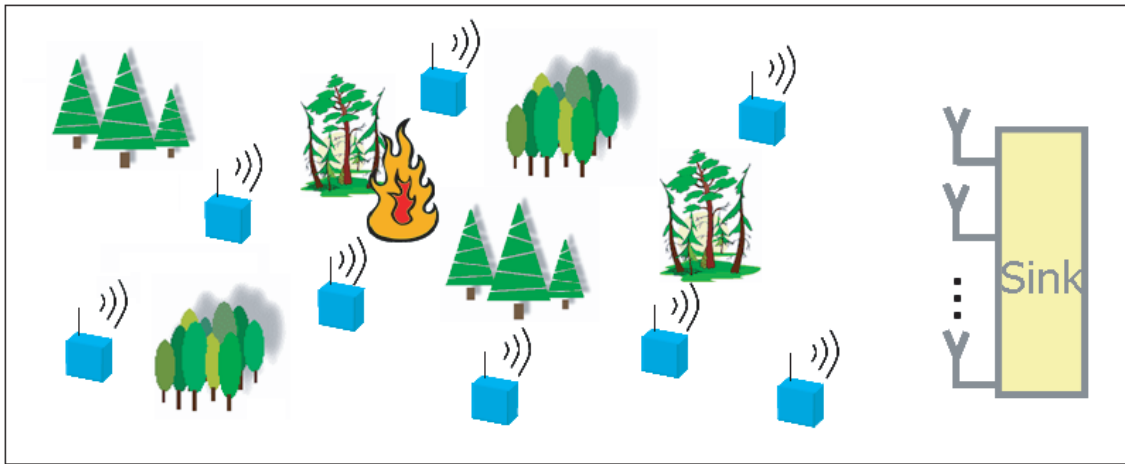


Figure 1.1: Deployment of a Wireless Sensor Network for environmental monitoring.

- industrial applications (i.e. localization, object tracking);
- traffic control;
- security (i.e. surveillance of houses or city districts);
- military applications (i.e. movement detection).

My PhD's work has been focused on WASNs, autoconfiguring networks (see Figure 1.2) which are not based on a fixed infrastructure, but are characterized by being infrastructure less, where devices have to automatically generate the network in the initial phase, and maintain it through reconfiguration procedures (if nodes' mobility, or energy drain, etc..., cause disconnections). The main part of my PhD activity has been focused on an analytical study on connectivity models for wireless ad hoc and sensor networks, nevertheless a small part of my work was experimental. Anyway, both the theoretical and experimental activities have had a common aim, related to the performance evaluation of WASNs. Concerning the theoretical analysis, the objective of the connectivity studies has been the evaluation of models for the interference estimation. This is due to the fact that interference is the most important performance degradation cause in WASNs. As a consequence, is very important to find an accurate model that allows its investigation, and I've tried to obtain a model the most realistic and general as possible, in

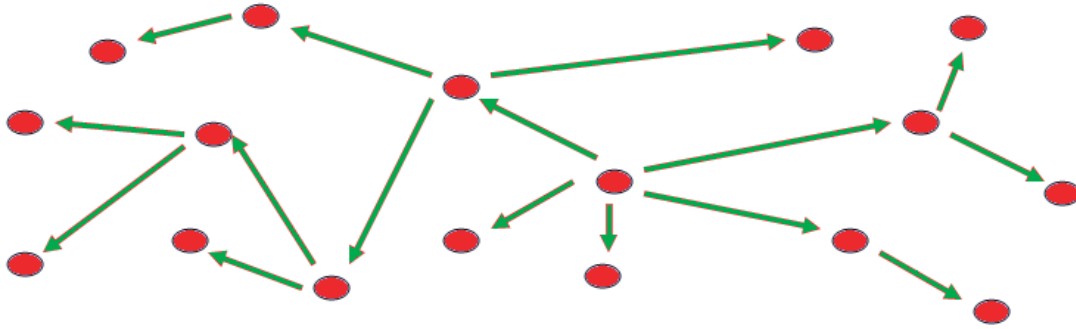


Figure 1.2: An example of Wireless autoconfiguring Ad Hoc Network.

particular for the evaluation of the interference coming from bounded interfering areas (i.e. a WiFi hot spot, a wireless covered research laboratory, ...). On the other hand, the experimental activity has led to Throughput and Packet Error Rate measurements on a real Wireless Sensor Network.

## 1.2 Connectivity models and system performance

The connectivity properties<sup>1</sup> of infrastructure-less systems, jointly with interference, play a crucial role in the next generation wireless systems. In particular, theoretical analysis of wireless ad hoc and sensor networks requires the development of accurate link models which are able to take the peculiarities of decentralized architectures into account. In recent years, the sudden spread of these kind of networks has led to the investigation of tens of models addressing the connectivity aspects of nodes in a Poisson field of interferers [21–26], and to the appearance in the literature of several analytical models that try to model the interference with the aim of predict and evaluate the performance of wireless ad hoc and sensor networks.

It is well known that the presence of co-channel interference represents the most important cause of performance degradation in wireless networks [27, 28]. The use of a Gaussian distribution for modelling the interference is the easiest way to characterize its effect in wireless

<sup>1</sup>Connectivity is commonly denoted as the capability that a node to communicate with others. A node is assumed to be able to communicate with another one when the value of received power is sufficient to warrant an acceptable quality of the radio link. In the absence of interference, this is generally obtained when the received power is larger than a given threshold which depends on the receiver sensitivity.

systems but, although this assumption has the undoubted merit to be simple and analytically tractable, it appears to be too simplistic in many practical situations and in particular when the number of interferers is small. Interference analysis in wireless communications systems is further complicated by the complexity of the propagation environment and by the inherent random nature of the users' positions. This consideration has led to the proposal of several statistical models to estimate the amount of interference in wireless systems (see for instance [29–31]). In the recent years the advent of new technological and architectural paradigms, such as: a) radio-access technologies sharing unlicensed frequency bands, i.e. the industrial, scientific and medical (ISM) band; b) infrastructure-less wireless networks; c) ultra wideband (UWB) systems, has made the research for interference models much more challenging. The difficulty is due to the fact that in such systems, the number and position of transmitting and receiving nodes cannot be easily predicted and/or controlled. A largely accepted model to characterize the spatial distribution of nodes in wireless networks is the Poisson Point Process (PPP) [32]. It represents a good tradeoff between the complexity of the model and its capability to describe realistic situations. For such reason, the use of PPP for the performance evaluation of wireless network is known since the 1980s [33].

### 1.3 Thesis Outline

This thesis is organized in chapters that develop several issues strictly connected to the analysis of connectivity models for fourth generation wireless system.

- In the second chapter a scenario composed by nodes which are uniformly and randomly distributed in an infinite area is considered, and the distribution of the power received by a given terminal is derived. The model, which takes a propagation environment characterized by distance-dependent loss and log-normally distributed shadowing into account, can be used to evaluate the distribution of the received power in wireless ad hoc and sensor networks. In particular, the model is suited to investigate the distribution of the received useful and the interference power in a scenario where all the terminals can communicate

with each other using the same radio resource.

- In the third Chapter we try to overcome some of the limitations of the existing interference models and propose an analytical framework for the evaluation of any statistical moment of the interference provided by a Poisson field of nodes located on a given region of limited area. The propagation environment we consider is characterized by a deterministic distance-dependent path-loss model and log-normal shadowing. The proposed methodology can be used to provide a fast and accurate evaluation of the amount of interference in many practical situations. Closed form expressions are given for some specific cases.
- In the fourth chapter the performance of a wireless sensor network where nodes, which are uniformly and randomly distributed in a given area, transmit information to a sink equipped with smart antennas, are investigated. We assume that the sensors are uniformly distributed in a two-dimensional space and consider a propagation environment composed by a distance-dependent loss, shadowing and Rayleigh fading. Owing to the propagation conditions and the randomness of the node locations, the achievable rate of such system is equivalent to that of a multiple-input-multiple-output scheme where both the number of the transmit antennas and the received power (averaged over the fast fading) at the sink are random variables. We give an integral expression for the average (over the node locations and fading fluctuations) achievable rate at the sink. The impact of correlation among the data sensed by sensors is also considered.
- In the fifth chapter the development of a real wireless sensor network is described, and its performance are evaluated. The aim of this Chapter is to move from theory to practice, completing the performance analysis carried out analytically through the interference study with the investigation of a real-world applications of WASNs, and the evaluation of its performance through Link and Throughput measurements. The methodologies used to design a WASN suited to a defined application are illustrated in this Chapter, by describing the scenario, the measurements done, the design methodology used, and by providing

samples of the measurements performed over the field.

- Chapter 6 shows some conclusions concerning the issues described in the previous chapters.
- Finally, in the Appendix we discuss the correctness of one of the main results of [23] about the probability density function of the distance between two *audible* nodes in an infinite 2-dimensional scenario. We prove that result [23, eq. (7) ] is wrong and derive an alternative expression which is valid for an infinite  $m$ -dimensional area. Since [23, eq. (7) ] was used in [23] to obtain other results, we discuss their validity.



## Chapter 2

# Connectivity models for the infinite area case

Recently, the development of wireless systems characterized by decentralized architectures has given rise to a great interest towards the investigation of capacity limits of networks based on the *ad hoc* paradigm [34, 35]. After the fundamental works of Gupta and Kumar, several contributions appeared in the open literature addressing connectivity issues on ad hoc systems (see for instance [23, 24, 36–38]).

Some of the works cited previously consider a spatial model based on the Poisson point process and address either the transmission range of a node or the probability that the network is fully connected. Other papers evaluate the effect of interference using a deterministic model for the path-loss [37]. An extension to the connectivity theory in the case of log-normal shadowing is given in [23], where authors derive the distribution of the distance between two nodes which are in communication (see comments in Appendix) and the distribution of nodes that are in

communication (i.e. those whose received power is larger than a given threshold) with another one in a propagation environment characterized by distance-dependent loss and shadowing. Here, we extend that model and derive the distribution of the power received by any terminal when the number of communicating nodes is exactly  $N$  (the distribution of  $N$  is given in [23]).

Two possible scenarios, that can be investigated using the model proposed here, are shown in Fig.2.1 and Fig.2.2. In the first scenario, all the terminals can communicate with each other using the same radio resource (i.e. in case of code division multiple access) and are potentially interferers. Although in such a scenario each terminal can interfere with potentially all the other nodes, in practice only few can provide a significant contribution. The approach presented here takes this fact into account and considers only the terminals that provide a received signal larger than a given value. In this scenario the model can be used to evaluate the distribution of the received useful power (i.e. by considering the node that provide the largest received signal) and

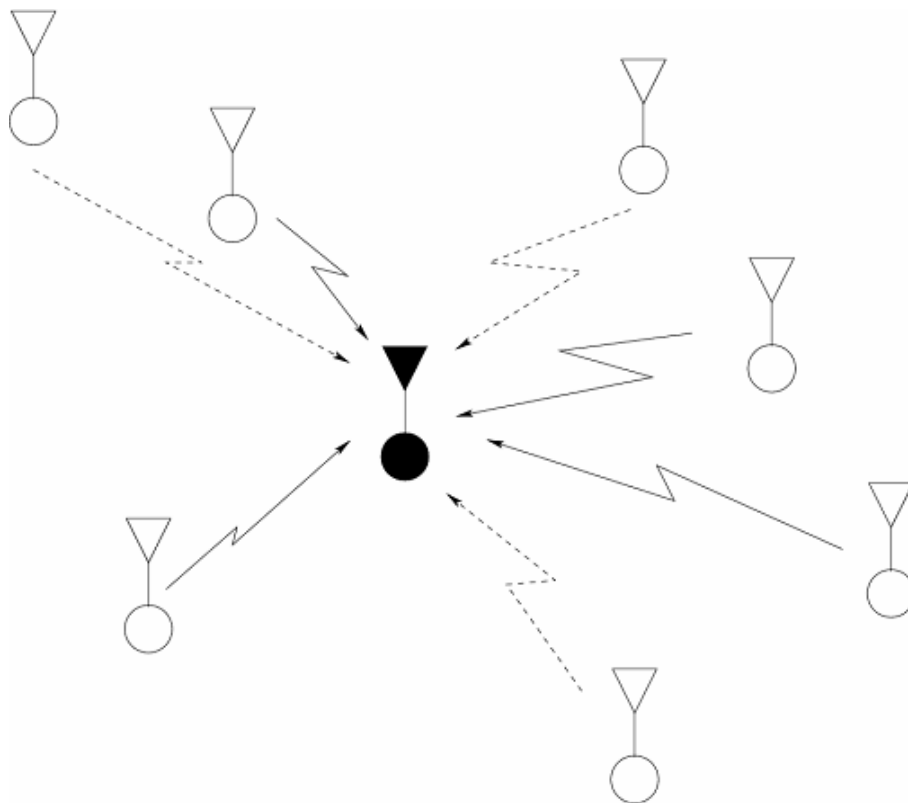


Figure 2.1: Scenario 1: Wireless Ad Hoc Network.

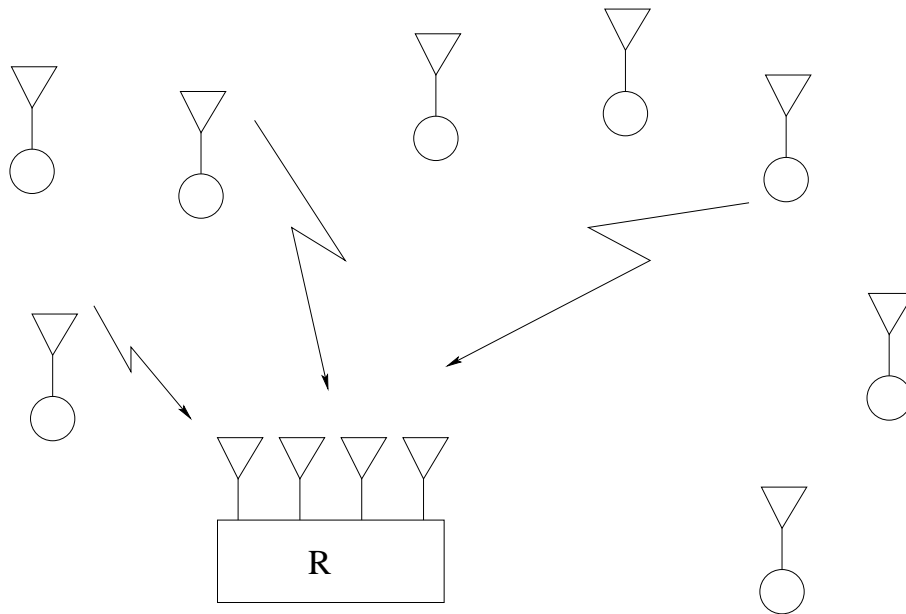


Figure 2.2: Scenario 2: Wireless Sensor Network where the supervisor is equipped with multiple antennas.

the interference (for instance the expected value). A second scenario is related to a wireless sensor network where the nodes, distributed in a given area, have to send messages to a given supervisor, which is equipped with a smart antennas device. In such a scenario only a subset of nodes (i.e. those providing an acceptable signal level) can send information to the supervisor. The system composed by the supervisor and the sensor nodes can be seen as a multiple input multiple output scheme, where the number of transmitting antennas, i.e. the sensors nodes, is not fixed a priori but depends on the propagation conditions.

## 2.1 Notations and Scenario Description

The following notations are used throughout the Chapter:  $\mathbb{E}\{\cdot\}$  denotes expectation, and in particular  $\mathbb{E}_X\{\cdot\}$  indicates expectation with respect to the random variable  $X$ .  $\mathbb{P}\{\mathcal{A}\}$  denotes the probability of the event  $\mathcal{A}$ . In the case of i.i.d. unordered random variables (r.v's)  $X_1, \dots, X_n$ , we denote by  $f_X(x)$  the probability density function (pdf) of the generic term. We denote by  $X_{(1)}, \dots, X_{(n)}$ , with  $X_{(1)} \leq X_{(2)} \leq \dots \leq X_{(n)}$ , the ordered r.v's. Furthermore, we define

$f_{n,X}(x) \triangleq f_{X|N=n}(x)$ , and  $\mu_{n,X}^{(p)}$  the  $p^{th}$  moment of  $X$  conditioned on  $N = n$ . The cases  $\mu_{n,X}^{(1)}$  and  $\mu_X^{(1)}$  are commonly written as  $\mu_{n,X}$  and  $\mu_X$ , respectively.

In this Chapter we consider an infinite plane with uniformly distributed nodes (Poisson spatial distribution). With such model the probability to have one node in the infinitesimal area  $\delta A$  is  $\rho \delta A$ , where  $\rho$  denotes the density of nodes.

Let us consider the communication between a relay node and the receiver. As far as the propagation model is concerned, we assume that the ratio between the power transmitted ( $P_t$ ) by the  $j^{th}$  node and the power ( $P$ ) at the  $i^{th}$  receiving antenna is given by ( $i$  and  $j$  are omitted for the sake of conciseness)

$$G \triangleq \frac{P}{P_t} = \frac{1}{k \cdot D^\beta \cdot S} \quad (2.1)$$

where  $G$  and  $L \triangleq 1/G$  represent the channel gain and the power loss, respectively,  $k$  is a propagation coefficient,  $D$  is the distance from the transmitter to the receiver,  $\beta$  is the attenuation coefficient which commonly ranges from 2 to 5, finally,  $S$  is the long-term (shadowing) fading component, which is assumed to be log-normally distributed. We assume also that the shadowing samples coming from different links are independent. By introducing the logarithmic scale<sup>1</sup>, we obtain

$$\begin{aligned} \hat{L} &= 10 \log_{10} k + 10\beta \log_{10} D + 10 \log_{10} S \\ &= \hat{k} + k_\beta \ln D + \hat{S} \end{aligned} \quad (2.2)$$

where  $k_\beta \triangleq \beta \frac{10}{\ln 10}$ . Owing to the log-normal distribution of  $S$ ,  $\hat{S}$  is a Normal r.v. with zero mean and variance  $\sigma_S^2$ .

We assume that a node is in communication with another one when  $P > P_{Th}$  ( $P_{Th}$  is a suitable threshold that depends on the receiver sensitivity). We denote by  $N$  the number of nodes providing the receiver with  $P > P_{Th}$ , that is the r.v.  $N$  gives the number of nodes which are either in communication with the receiver (desired signals and/or interferers).

In the next section we derive the distribution of  $G$  under the hypothesis that the terminal is

---

<sup>1</sup>The notation  $\hat{X}$  will be used throughout the thesis to indicate  $10 \log_{10} X$ .

in communication with  $N$  nodes. From the distribution of  $G$  we can easily obtain that of the signal-to-noise ratio  $\gamma \triangleq \frac{P_t G}{\sigma_N^2}$ , where  $\sigma_N^2$  is the thermal noise power.

## 2.2 Statistic model for the received power

Several contributions have appeared in the past years to investigate connectivity effects in wireless systems when the position of nodes follows a PPP [21, 23, 39, 40]. The works of [23, 39] consider nodes which communicate with each other (i.e. the received power is larger than a given threshold) by assuming a propagation environment characterized by a distance-dependent loss and log-normal shadowing. They obtain the distribution of the distance between a pair of such points (see comments on this distribution in the Appendix) and of the number of nodes within the range of one such node, but do not address the distribution of the received power. In this Chapter we consider the propagation model given by (2.2) and derive the distribution of the received power when two nodes communicate the one each other.

Let us recall the following results, which are due to [23] and [39]:

- a) Let us consider a PPP and the propagation law given by (2.2), then  $N$  is a Poisson r.v. with distribution  $Q_{\mu_N}(n) = \frac{e^{-\mu_N} \mu_N^n}{n!}$  and mean

$$\mu_N = \pi \rho e^{2\frac{\hat{L}_T - \hat{k}}{k_\beta}} e^{2\frac{\sigma_S^2}{k_\beta^2}} = k_\rho e^{2\hat{L}_T/k_\beta}, \quad (2.3)$$

where  $k_\rho \triangleq \pi \rho e^{-2\hat{k}/k_\beta} e^{2\sigma_S^2/k_\beta^2}$ , and  $L_T \triangleq \frac{P_t}{P_{Th}}$  [23]. Note that  $L_T$  can be interpreted as the maximum loss which allows the communication between two nodes. As a consequence of this result,  $Q_{\mu_N}(0) = e^{-\mu_N}$  gives the probability that a node is isolated (probability that  $N=0$ ).

- b) Let us consider the power loss  $L$  of the nodes which are in communication with a given node (so  $L$  ranges from 0 to  $L_T$ ), and consider the ordered r.v.'s  $L_{(1)}, L_{(2)}, \dots$ . If  $T \triangleq e^{2\hat{L}/k_\beta}$ , then  $T_{(1)}$ , which ranges from 0 to  $e^{2\hat{L}_T/k_\beta} = L_T^{2/\beta}$ , has the following

exponential (truncated) distribution [39]

$$f_{T_{(1)}}(x) = \begin{cases} k_\rho \frac{e^{-k_\rho x}}{1 - e^{-\mu_N}} & x \in [0, e^{2\hat{L}_T/k_\beta}] \\ 0 & \text{otherwise} \end{cases}. \quad (2.4)$$

Note that in practical situations  $L_T^{2/\beta} \gg 1$  and  $\mu_N$  is larger than 3-4, which gives  $1 - e^{-\mu_N} \approx 1$ , and so  $f_{T_{(1)}}(x)$  can be well approximated as a (non truncated) exponential distribution.

In the next subsection, we use result b) to derive distribution of  $f_{n, T_1, \dots, T_n}(x_1, \dots, x_n)$ . Then, based on the simple relation between  $T$  and  $G$  we can obtain  $f_{n, G_1, \dots, G_n}(x_1, \dots, x_n)$ . Finally, by recalling that  $\gamma_i = \frac{P_i G_i}{\sigma_N^2}$ , we finally get  $f_{n, \gamma_1, \dots, \gamma_n}$ .

### 2.2.1 Distribution of $T$

Let us assume that a given node is in communication with exactly  $n$  nodes (case  $N = n$ ). Owing to the model used for the spatial distribution of nodes and to the hypothesis of independence of the shadowing samples, the r.v.'s  $T_1, \dots, T_n$  are mutually independent, therefore the distributions of  $T_1, \dots, T_n$  can be written as

$$f_{n, T_1, \dots, T_n}(x_1, \dots, x_n) = \prod_{i=1}^n f_T(x_i). \quad (2.5)$$

It is worth noting that  $f_T(x)$  represents the pdf of the unordered term  $T$  and does not depend on the number of nodes the receiver is in communication with. To derive  $f_T(x)$  we can use the following relation [41, pag. 10]

$$\begin{aligned} f_{n, T_{(1)}}(x) &= n[1 - F_{n, T_i}(x)]^{n-1} f_{n, T_i}(x) \\ &= n[1 - F_T(x)]^{n-1} f_T(x), \end{aligned} \quad (2.6)$$

where  $F_T(x)$  is the cumulative density function (cdf) of  $T$ .

Using the Total Probability Theorem we obtain the distribution of  $T_{(1)}$  given in (2.4)<sup>2</sup>

$$\begin{aligned} f_{T_{(1)}}(x) &= \sum_{i=1}^{\infty} \frac{\mathcal{P}\{N = n\}}{1 - e^{-\mu_N}} f_{n, T_{(1)}}(x) \\ &= \sum_{i=1}^{\infty} \frac{Q_{\mu_N}(n)}{1 - e^{-\mu_N}} n [1 - F_T(x)]^{n-1} f_T(x). \end{aligned} \quad (2.7)$$

Note that the scaling factor  $1 - e^{-\mu_N}$  accounts for the fact that the r.v.  $T$  is defined when at least one node is in communication with the receiver.

The evaluation of  $f_T(x)$  from (2.7) is quite cumbersome, however, we can easily check that the solution  $f_T(x) = 1/a$  for  $x \in [0, a]$  and zero otherwise satisfies (2.7). This can be proved by substituting  $f_T(x)$  and  $F_T(x)$  in (2.7) with  $1/a$  and  $x/a$ , in order to obtain

$$f_{T_{(1)}}(x) = \begin{cases} \frac{1}{a} \sum_{n=1}^{\infty} \frac{e^{-\mu_N} \mu_N^n}{n!(1 - e^{-\mu_N})} n \left[1 - \frac{x}{a}\right]^{n-1} & x \in [0, a] \\ 0 & \text{otherwise} \end{cases}. \quad (2.8)$$

Using the following identity

$$\sum_{i=1}^{\infty} n \frac{b^n}{n!} c^{n-1} = b e^{cb} \quad (2.9)$$

we finally get

$$f_{T_{(1)}}(x) = \begin{cases} \frac{\mu_N}{a} \frac{e^{-\mu_N x/a}}{1 - e^{-\mu_N}} & x \in [0, a] \\ 0 & \text{otherwise} \end{cases}, \quad (2.10)$$

which gives  $f_{T_{(1)}}(x)$ <sup>3</sup>.

Note that the propagation model (2.1) is valid only when the distance between the nodes is larger than some wavelengths. To account for this fact, we assume in the Chapter that attenuation cannot be smaller than  $k$ . In the absence of shadowing, this is equivalent to assume a "dead-zone" having a radius of 1 meter which is free from sensors [42]. Under the hypothesis that no node can be located in a circular area surrounding the receiver,  $N$  is still Poisson, but now its mean value is given by

$$\mu_N = \pi \rho \left[ e^{2 \frac{\hat{L}_T - \hat{k}}{k_\beta} + \frac{2\sigma_S^2}{k_\beta}} \Phi \left( \frac{\hat{L}_T - \hat{k}}{\sigma_S} + \frac{2\sigma_S}{k_\beta} \right) - \Phi \left( \frac{\hat{L}_T - \hat{k}}{\sigma_S} \right) \right], \quad (2.11)$$

<sup>2</sup>The r.v.  $T_{(1)}$  with distribution (2.4) is not conditioned on a particular value of  $N$ , it is averaged over all possible values of  $N$ .

<sup>3</sup>We obtain the exact expression for (2.4) by recalling that the upper limit of  $T$  is  $L_T^{2/\beta}$ .

where  $\Phi(x) = 1/\sqrt{2\pi} \int_{-\infty}^x e^{-u^2/2} du$ . On the other hand, we are considering a very small area (the radius is 1 meter) and the difference between the real value of  $\mu_N$  and the value given in (2.3) is negligible.

The pdf of  $T$  becomes

$$f_T(x) = \begin{cases} \frac{L_T^{2/\beta}}{1 - \left(\frac{k}{L_T}\right)^{2/\beta}} & x \in [k^{2/\beta}, L_T^{2/\beta}] \\ 0 & \text{otherwise} \end{cases}. \quad (2.12)$$

Using the typical values of  $L_T$  and  $\beta$  for a wireless environment, the term  $\left(\frac{k}{L_T}\right)^{2/\beta}$  is around  $10^{-4}$ , and therefore the normalizing factor in (2.12) is negligible.

## 2.2.2 Distribution of $G$

The results of the previous section can be used to derive the distribution of  $G_1, \dots, G_n$  when  $N = n$ . From (2.2), it is easy to show that

$$G = 10^{-\hat{L}/10} = e^{-\frac{\ln 10}{10} \hat{L}} = e^{-\frac{2\hat{L} \ln 10}{k\beta} \frac{k\beta}{10}} = T^{-\frac{k\beta}{2} \frac{\ln 10}{10}} = T^{-\beta/2} \quad (2.13)$$

which shows that  $T$  represents the power loss  $L$  when  $\beta = 2$ . The distribution of  $G$ , whose range is  $[1/L_T, 1/k]$ , can be derived using the general rule for the functions of random variables [43]

$$f_G(x) = \begin{cases} \frac{2}{\beta(L_T^{2/\beta} - k^{2/\beta})} \frac{1}{x^{1+2/\beta}} & x \in [1/L_T, 1/k] \\ 0 & \text{otherwise} \end{cases}, \quad (2.14)$$

and the cdf is given by

$$F_G(x) = \begin{cases} 0 & \text{otherwise} \\ \frac{1}{L_T^{2/\beta} - k^{2/\beta}} \left( L_T^{2/\beta} - \frac{1}{x^{2/\beta}} \right) & x \in [1/L_T, 1/k] \end{cases}. \quad (2.15)$$

The knowledge of  $F_G(x)$  allows us to derive  $f_{n, G_1, \dots, G_n}(x_1, \dots, x_n)$  and therefore  $f_{n, \gamma_1, \dots, \gamma_n}(x_1, \dots, x_n)$

$$f_{n, \gamma_1, \dots, \gamma_n}(x_1, \dots, x_n) = \left( \frac{P_t}{\sigma_N^2} \right)^{-n} \prod_{i=1}^n f_G \left( x_i \frac{\sigma_N^2}{P_t} \right). \quad (2.16)$$

The pdf of  $G$  can be used to derive the moments

$$\begin{aligned} \mu_G^{(p)} &\triangleq \mathbb{E} \{ G^p \} = \int_{1/L_T}^{1/k} x^p f_G(x) dx \\ &= \frac{2}{\beta (L_T^{2/\beta} - k^{2/\beta})} \frac{\left(\frac{1}{k}\right)^{p-2/\beta} - \left(\frac{1}{L_T}\right)^{p-2/\beta}}{p - 2/\beta}. \end{aligned} \quad (2.17)$$

Note that in case of  $p = 1$  (mean value of  $G$ ), the expectation exists only for  $\beta > 2$ .

Using [41, eq. (2.1.6) pp. 10] we can easily derive the distribution of  $f_{G(r)}(x)$ :

$$\begin{aligned}
f_{n,G(r)}(x) &= \frac{1}{B(r, n-r+1)} F_G^{r-1}(x) [1 - F_G(x)]^{n-r} f_G(x) \\
&= \frac{2L_T^{2(r-1)/\beta}}{B(r, n-r+1)\beta \left(L_T^{2/\beta} - k^{2/\beta}\right)^r} \\
&\quad \times \frac{1}{x^{1+2/\beta}} \left[1 - \frac{1}{(xL_T)^{2/\beta}}\right]^{r-1} \\
&\quad \times \left[1 - \frac{1}{L_T^{2/\beta} - k^{2/\beta}} \left(L_T^{2/\beta} - \frac{1}{x^{2/\beta}}\right)\right]^{n-r} \\
&\approx \frac{2}{\beta B(r, n-r+1)} \sum_{i=0}^{r-1} \left[ \binom{r-1}{i} \frac{(-1)^i}{L_T^{2(n-r+i+1)/\beta}} \right. \\
&\quad \left. \times \frac{1}{x^{1+2(n-r+i+1)/\beta}} \right],
\end{aligned} \tag{2.18}$$

where  $B(b, c) = \int_0^1 y^{b-1} (1-y)^{c-1} dy$  is the beta function [44] and the approximation has been obtained by assuming  $L_T^{2/\beta} - k^{2/\beta} \approx L_T^{2/\beta}$ .

To give an example, the distribution of the largest channel gain  $G_{max} = G_{(n)}$  can be written as

$$f_{n,G_{max}}(x) = \frac{2nL_T^{2(n-1)/\beta}}{\beta \left(L_T^{2/\beta} - k^{2/\beta}\right)^n} \frac{1}{x^{1+2/\beta}} \left[1 - \frac{1}{(xL_T)^{2/\beta}}\right]^{n-1}. \tag{2.19}$$

Finally, the moments of  $G(r)$  are given by

$$\begin{aligned}
\mu_{n,G(r)}^{(p)} &= \int_{1/L_T}^{1/k} x^p f_{G(r)}(x) dx \\
&= \frac{2}{\beta B(r, n-r+1) \left(L_T^{2/\beta} - k^{2/\beta}\right)^n} \sum_{i=0}^{n-r} \sum_{j=0}^{r-1} \\
&\quad \times \binom{n-r}{i} \binom{r-1}{j} (-1)^{(n-r-i+j)} k^{2/\beta(n-r-i)} L_T^{2/\beta(r-1-j)} \\
&\quad \times \begin{cases} \ln L_T - \ln k & p = 2(i+j+1)/\beta \\ \frac{k^{2/\beta(i+j+1)-p} L_T^{2/\beta(i+j+1)-p}}{p - \frac{2}{\beta}(i+j+1)} & \text{otherwise} \end{cases}.
\end{aligned} \tag{2.20}$$

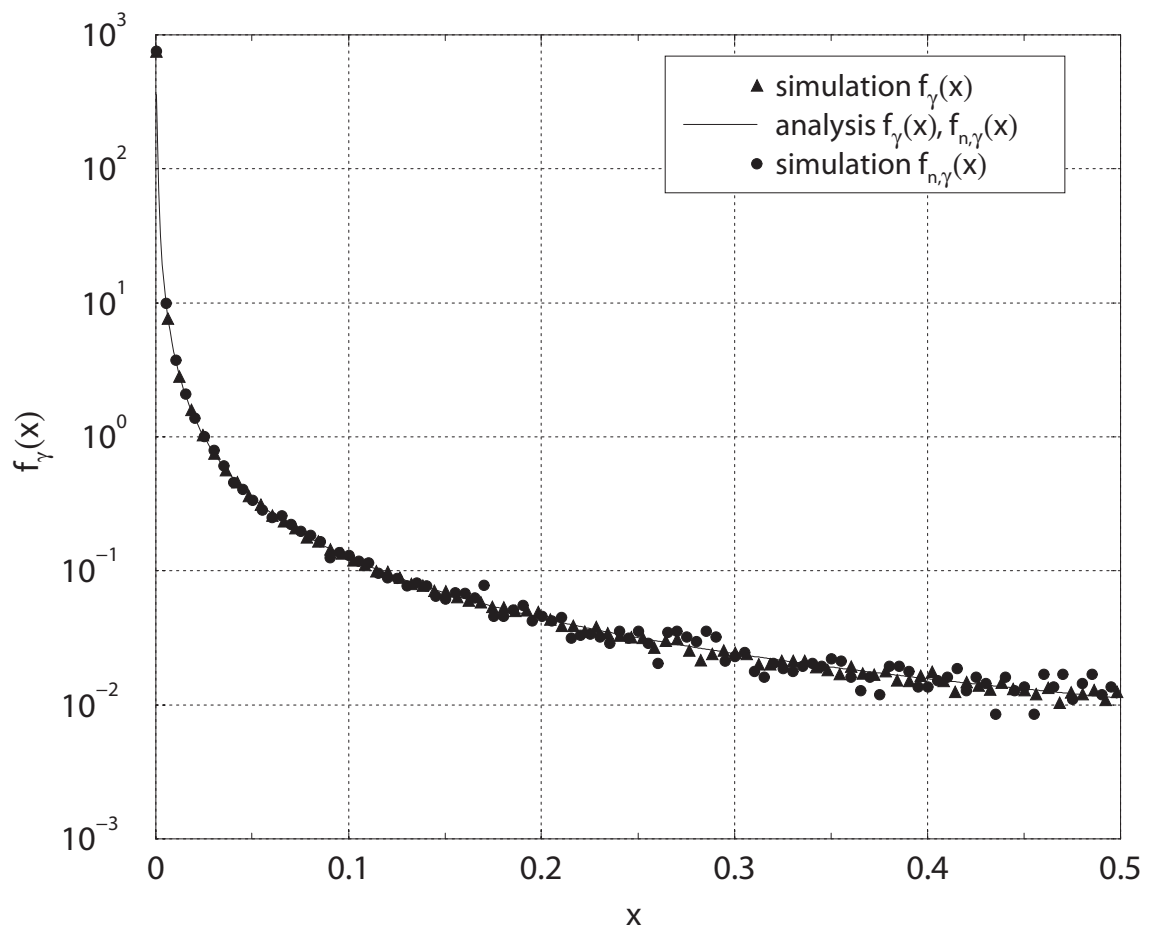
## 2.3 Distribution of the received power: comparison with simulations

The results on the distribution of the received power have been tested through Monte Carlo simulations. A squared area of  $A_S = 1000 \times 1000 \text{ m}^2$  is considered, the nodes are uniformly distributed in the area and their number follows a Poisson distribution with mean  $\rho A_S$ , where  $\rho = 5 \cdot 10^{-4} \text{ nodes/m}^2$ .  $10^6$  simulation trials have been carried out to obtain the results. The sink is located in the center of the area. The following parameters have been fixed:  $\hat{k} = 30 \text{ dB}$ ,  $\beta = 4$ ,  $\sigma_S = 5 \text{ dB}$ ,  $\hat{L}_T = 104 \text{ dB}$  and  $P_T/\sigma_T^2 = 0.158 \cdot 10^7$ . For each link, it has been examined the signal-to-noise ratio, given by the random variable  $\gamma = \frac{P_T G}{\sigma_n^2}$ .

Fig. 2.3 shows the comparison between the analytical expression for the pdf of  $\gamma$  and the distribution obtained through the simulations. The agreement is excellent, this confirms the accuracy of the model. The figure also shows the distribution of  $\gamma$  conditioned on  $N = 9$  (that is  $f_{9,\gamma}(x)$ ). As discussed in Section 2.2,  $f_{n,\gamma}(x)$  does not depend on  $n$  and therefore coincides with  $f_\gamma(x)$ . This behavior is confirmed by the simulations.

The comparison between analysis and simulation is also shown in Figs. 2.4 and 2.5, which report the distribution of some ordered elements of  $\gamma_1, \dots, \gamma_n$  conditioned on  $N = n$ . These distributions have been obtained using [41, pp. 10, eq. (2.1.6)].

Fig. 2.4 shows the distribution of the maximum signal-to-noise-ratio ( $\gamma_{\max} = \gamma_{(1)}$ ), whereas Fig. 2.5 plots the distribution of  $\gamma_{\min} = \gamma_{(9)}$ . Again, the comparison between analysis and simulation shows a perfect agreement. Finally, Fig. 2.6 gives the expectation of  $\gamma_{(r)}$ , for  $p = 1$  and  $n = 9$ , with  $r$  taking values from 1 to 9; as expected, the mean value of  $\gamma$  increases as  $r$  increases.

Figure 2.3: Probability density function of  $\gamma$ .

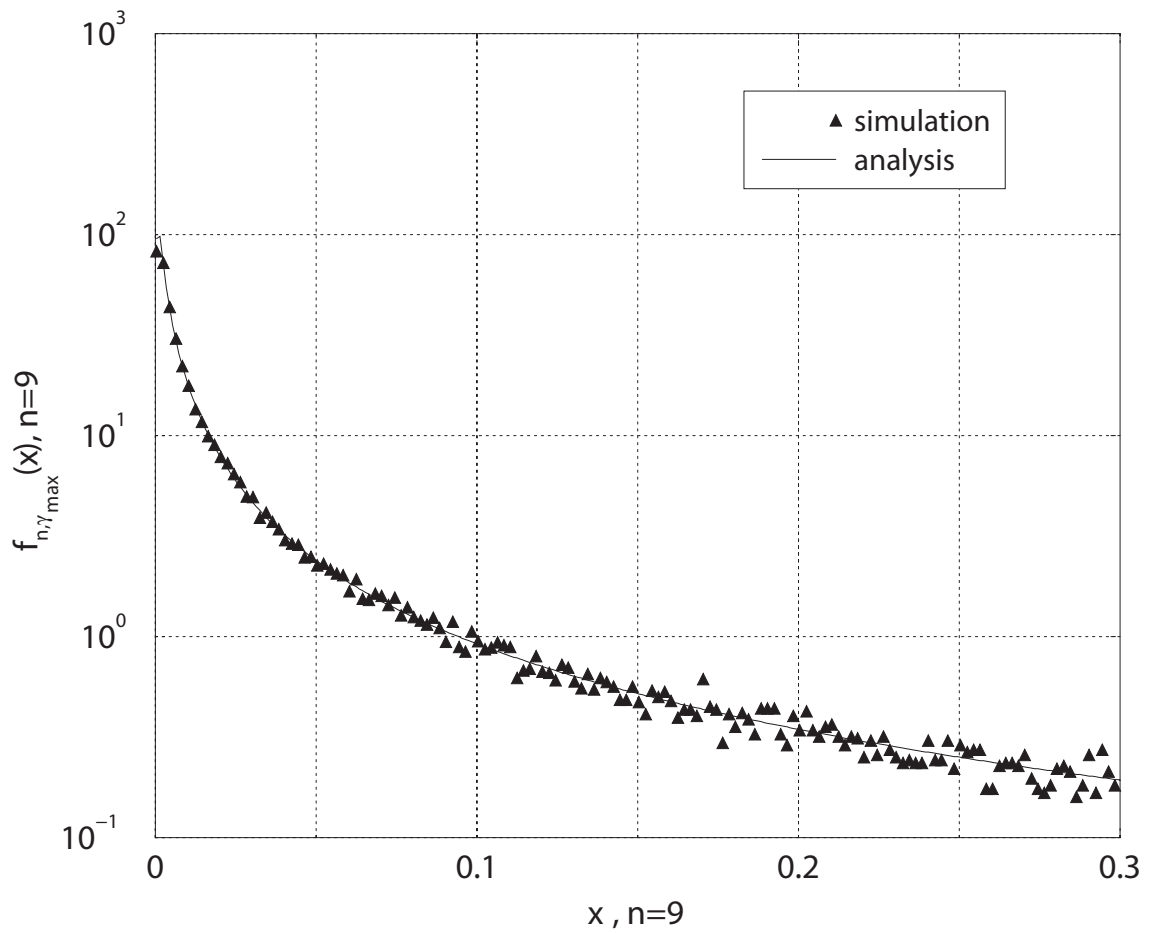


Figure 2.4: Probability density function of  $\gamma_{max} = \gamma_{(n)}$ ;  $n = 9$ .

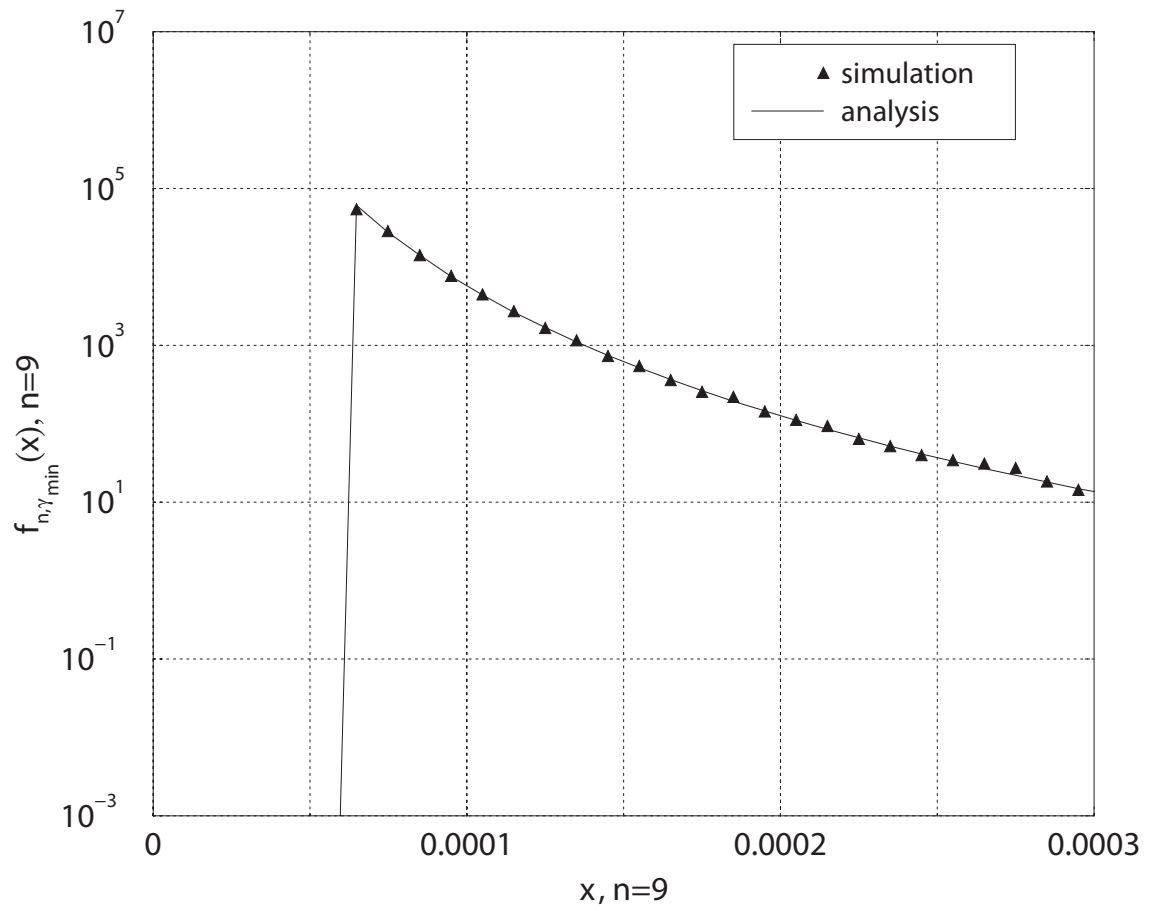


Figure 2.5: Probability density function of  $\gamma_{min} = \gamma_{(1)}$ ;  $n = 9$ .

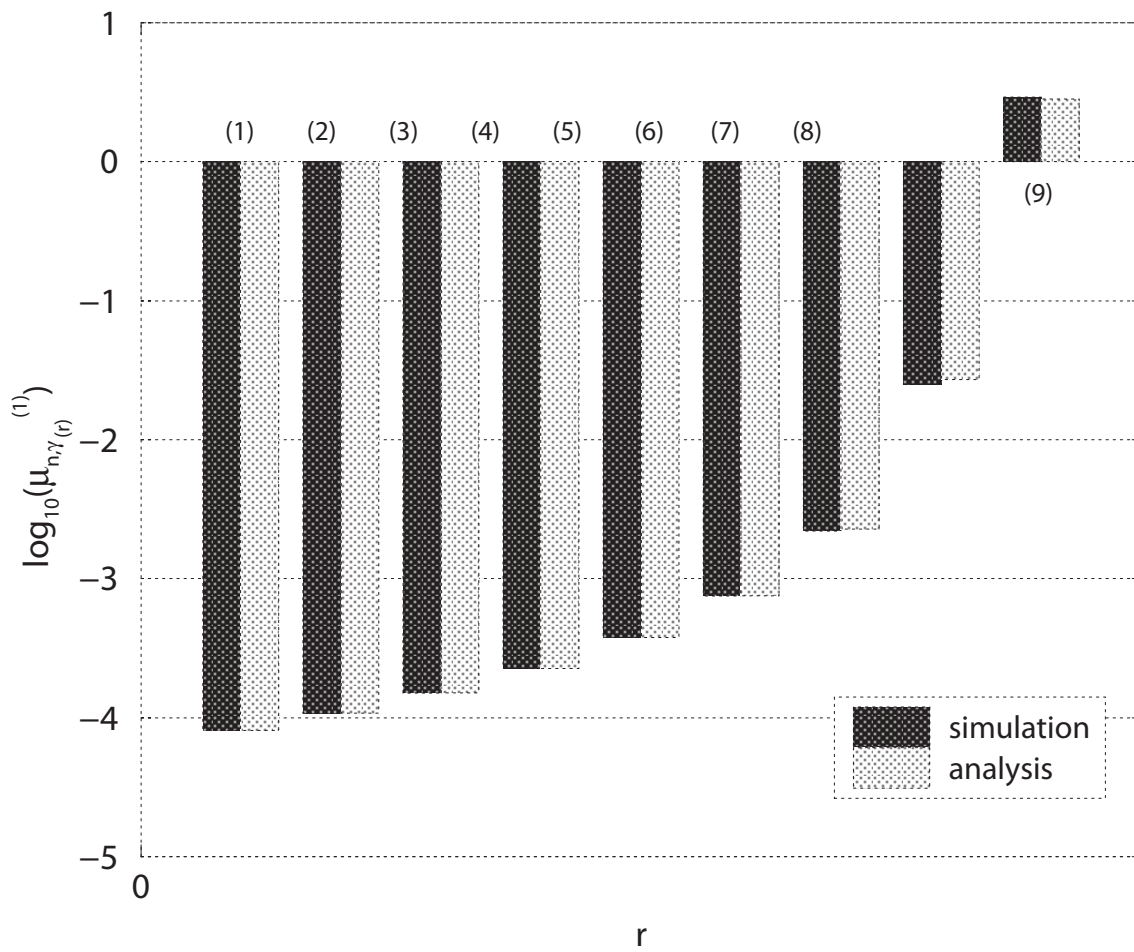


Figure 2.6: Moments of  $\gamma_{(r)}$ ;  $p = 1$  and  $n = 9$ , for  $r$  ranging from 1 to 9.

## **Chapter 3**

# **Connectivity models and Interference analysis for finite areas**

The majority of the papers which consider nodes' distribution based on PPP deal with infinite areas and with infinite nodes (see for instance [21,25,40]). The analysis of connectivity properties of decentralized networks operating in areas of limited extension would allow us to investigate the performance of wireless sensor networks employing clustered routing algorithms [45–47] or multi-stage distributed multiple-input-multiple-output (MIMO) [42, 48]. Unfortunately, this kind of analysis seems to be rather complex. In this Chapter we consider nodes located in a circular area and a propagation environment characterized by distance-dependent loss and log-normal shadowing. We derive an expression for the distribution of the power received by a given terminal when the other nodes are distributed according to a PPP. The results obtained in Chapter 2, valid for an infinite plane, can be seen as a particular case of the model proposed herein.

A few papers investigate interference effects in wireless ad hoc networks; to the authors' knowledge, the first attempt to characterize the distribution of the interference in a Poisson field of nodes is due to [49]. That paper, which considered a deterministic path-loss model and an infinite  $d$ -dimensional area, derived a closed form expression (although in terms of an infinite series expansion) for the probability density function (pdf) of the interference. That model was then extended in [50] to obtain the error performance in the case of spread spectrum for some modulation formats. A more realistic propagation environment was taken into account in [51] where both shadowing and Rayleigh fading were included. The presence of correlation among interferers was studied in [52] but the path loss model did not consider neither shadowing nor fast fading. The use of percolation theory to study the impact of interference in ad hoc networks was discussed in [37]. Owing to the peculiarities of percolation theory, a deterministic propagation model was considered in that paper. The performance of some routing schemes was investigated in [40] in a propagation environment characterized by deterministic path-loss and Rayleigh fading. Recently, the statistical model proposed in [51] was extended in [53] and [54]. These papers overcame the limitation of [50–52] about synchronicity of the interfering signals and applied their analysis to the error probability evaluation of linear modulated signals. The models proposed in [50–54] considered also the modulation format of the interfering signals.

Although the above mentioned papers are excellent tools for the characterization of the interference, they present a couple of disadvantages: i) most of them ([50–54]) make use of  $\alpha$ -stable distributions; ii) the interfering nodes are supposed to be located in an infinite (either bi- or  $d$ -dimensional) area. A disadvantage of  $\alpha$ -stable distributions is the absence of moments of order greater than or equal to the parameter  $\alpha$  [55]. Unfortunately, since  $\alpha$  is strictly related to the propagation law, no moment (i.e. mean and variance) can be evaluated in the case of wireless environments [52]. Furthermore, the hypothesis of nodes located in an infinite area is not realistic in the presence of personal and local area networks, which are commonly characterized by transmission ranges smaller than 100 – 200 m [56]. In such scenarios, interfering nodes are grouped in clusters of limited area, i.e. inside a building. Another limitation of some

existing works is the absence of a specific propagation model when the distance between the interfering and the reference node is less than some wavelengths [42, 50]. This results in an overestimate of the interference. In this Chapter we overcome these limitations. We propose an analytical framework for the statistical characterization of the amount of interference provided by nodes located on a given region of limited area in a propagation environment characterized by a deterministic path-loss and log-normal shadowing. Although our methodology is valid for areas of arbitrary dimension and shape (see Fig 3.1 a)), we focus the analysis on three simplified scenarios: i) nodes belonging to circular area whose distance from the receiver is arbitrary (Fig. 3.1 b)); ii) nodes located in a circular annulus around the receiver (Fig. 3.1 c)); iii) nodes located in a circular area around the receiver (Fig. 3.1 d)). Scenario b) can be used to characterize the interference received by an hot spot of nodes. Scenario c) finds application in the analysis of

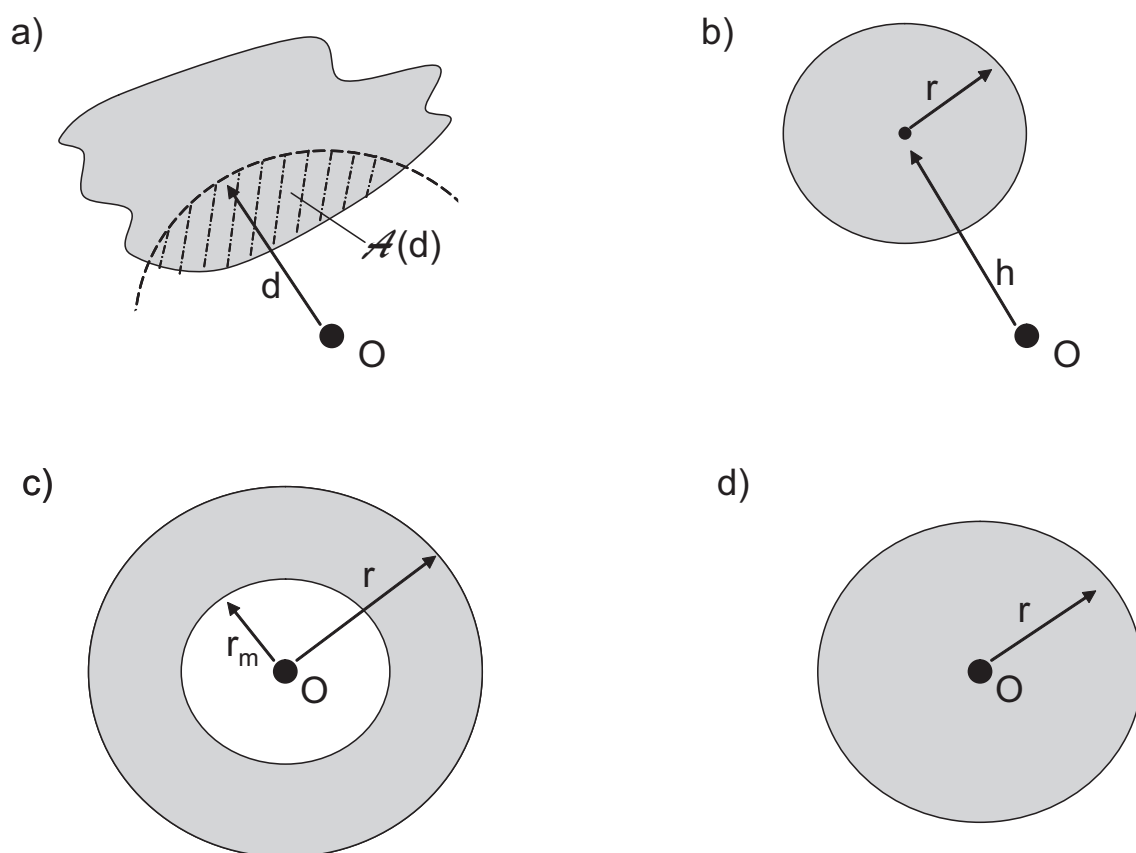


Figure 3.1: General case (a), external circular area case (b), circular annulus case (c) and circular area case (d).

networks which are completely surrounded by interferers. Finally, scenario d) can be used to characterize the amount of the self-interference, which is the interference received by nodes belonging to the same network. In the analysis of scenario d), we also consider a simple but more realistic path loss model to include the near field effects. The methodology proposed herein does not make use of the  $\alpha$ -stable distributions and allows the evaluation of any moment of the interference distribution. The present methodology can be used to provide a fast and accurate evaluation of the amount of interference in many practical situations.

The main contributions of this Chapter can be summarized as follows:

- We consider nodes located in an arbitrary area and derive the exact expression for the distribution of the channel gain.
- We obtain an expression for the derivation of any moment of the interference distribution.
- The expression for the moments of the interference requires the knowledge of the moments of the channel gain. To obtain closed form expressions, we consider some situation of interest in which the area occupied by the interfering nodes is regular (circular annulus and circular area around the receiver) and derive a closed form approximate expression for the moments of the interference. Numerical results will show that the agreement between approximated model and simulations is excellent.

### 3.1 Propagation environment

It is worth noting that in this chapter we use the same notations introduced in Section 2.1.

The scenario considered in this Chapter is characterized by a circular area with radius  $r_T$  and uniformly distributed nodes (Poisson spatial distribution) with density  $\rho$ . We assume that all the nodes in the area use the same value of transmitted power  $P_t$ . Let's consider the communication between a node ( $N_0$ ) located in the center of the area and another node  $N_1$ . We assume that the ratio between the power transmitted ( $P_t$ ) by  $N_1$  and the power ( $P$ ) received by  $N_0$  is given by

$$\frac{P_t}{P} = k \cdot D^\beta \cdot S \quad (3.1)$$

as in the previous Chapter. Again, we define  $L \triangleq kD^\beta S$  and  $G \triangleq 1/L$  (they represent the power loss in linear scale, and channel gain, respectively), and we also denote  $P \triangleq P_t G$ , where  $P$  is the received power. By introducing the logarithmic scale, we obtain  $\hat{L}$ , as described in the previous Chapter (see (2.2)).

## 3.2 Distribution of $G$

The aim of this Section is the derivation of the pdf of  $G$ , the channel gain between  $N_1$  and  $N_0$ , in the scenarios of Fig.3.1.

### 3.2.1 Distribution of $G$ : general case

Let's consider the scenario of Fig 3.1 a). We denote by  $\mathcal{A}$  the area of the grey surface identified by the intersection between the grey area and a circumference of radius  $d$  centered in  $O$ .

The probability that  $D \leq d$  is given by the expression

$$F_D(d) = \mathbb{P}\{D \leq d\} = \frac{\mathcal{A}(d)}{A}, \quad (3.2)$$

where  $A$  is the area of the grey surface of Fig. 3.1 a). The joint pdf of  $D$  and  $\hat{S}$  can hence be written as

$$f_{D,\hat{S}}(d, \hat{s}) = \frac{\mathcal{A}'(d) e^{-\hat{s}^2/(2\sigma_S^2)}}{A \sigma_S \sqrt{2\pi}}, \quad (3.3)$$

where  $\mathcal{A}'(x) \triangleq d\mathcal{A}(x)/dx$ . Note that  $\hat{s} \in (-\infty, \infty)$  and  $d$  ranges from the distance between the origin  $O$  and the closest point of the grey area of Fig. 3.1 a), and the distance between the origin and the farthest one. Let's make use of the following change of variable

$$\begin{cases} G = g_1(D, \hat{S}) = \frac{D^{-\beta}}{k} e^{-(\frac{\ln 10}{10})\hat{S}} \\ \hat{Y} = g_2(D, \hat{S}) = \hat{S} \end{cases}. \quad (3.4)$$

The Jacobian of the transformation is given by

$$J(d, \hat{s}) = \begin{pmatrix} \frac{\partial g_1}{\partial d} & \frac{\partial g_1}{\partial \hat{s}} \\ \frac{\partial g_2}{\partial d} & \frac{\partial g_2}{\partial \hat{s}} \end{pmatrix} = \begin{pmatrix} \frac{-\beta d^{-\beta-1}}{k} e^{-(\frac{\ln 10}{10})\hat{s}} & \frac{d^{-\beta}}{k} e^{-(\frac{\ln 10}{10})\hat{s}} \left(-\frac{\ln 10}{10}\right) \\ 0 & 1 \end{pmatrix}, \quad (3.5)$$

and the absolute value of its determinant is

$$|J(d, \hat{s})| = \frac{\beta d^{-\beta-1}}{k} e^{-(\frac{\ln 10}{10})\hat{s}}. \quad (3.6)$$

After some algebra, the joint distribution of  $G$  and  $\hat{Y}$  can be written as

$$f_{G,\hat{Y}}(g, \hat{y}) = \frac{\mathcal{A}'(\varphi(g, \hat{y}))}{A} \frac{e^{-\frac{\hat{y}^2}{2\sigma_S^2}}}{\sigma_S \sqrt{2\pi} \beta k^{1/\beta}} \frac{e^{-\frac{\ln 10}{10\beta} \hat{y}}}{g^{1+1/\beta}}, \quad (3.7)$$

where  $\varphi(g, \hat{y}) \triangleq e^{-\frac{\hat{y} \ln 10}{\beta 10}} / (kg)^{1/\beta}$ . Note that only the term  $\frac{\mathcal{A}'(\cdot)}{A}$  depends on the shape of the external area.

The general expression (3.7) will be specialized in the next subsections for some cases of interest.

### 3.2.2 Distribution of $G$ : external circular area

Let's consider the scenario b) of Fig. 3.1 which is composed by an external circular area. We denote by  $O'$  the center of the external circle having radius  $r$ ,  $h$  is the distance between  $O$  and  $O'$ , and  $Q, R$  are the intersection points between the circle and a circumference of radius  $d$  centered in  $O$  (see Fig. 3.2).

The overlapping area  $\mathcal{A}(d)$  is now given by

$$\mathcal{A}(d) = \theta(d, r, h)d^2 + \alpha(d, r, h)r^2 - d^2 \sin \theta(d, r, h) - r^2 \sin \alpha(d, r, h), \quad (3.8)$$

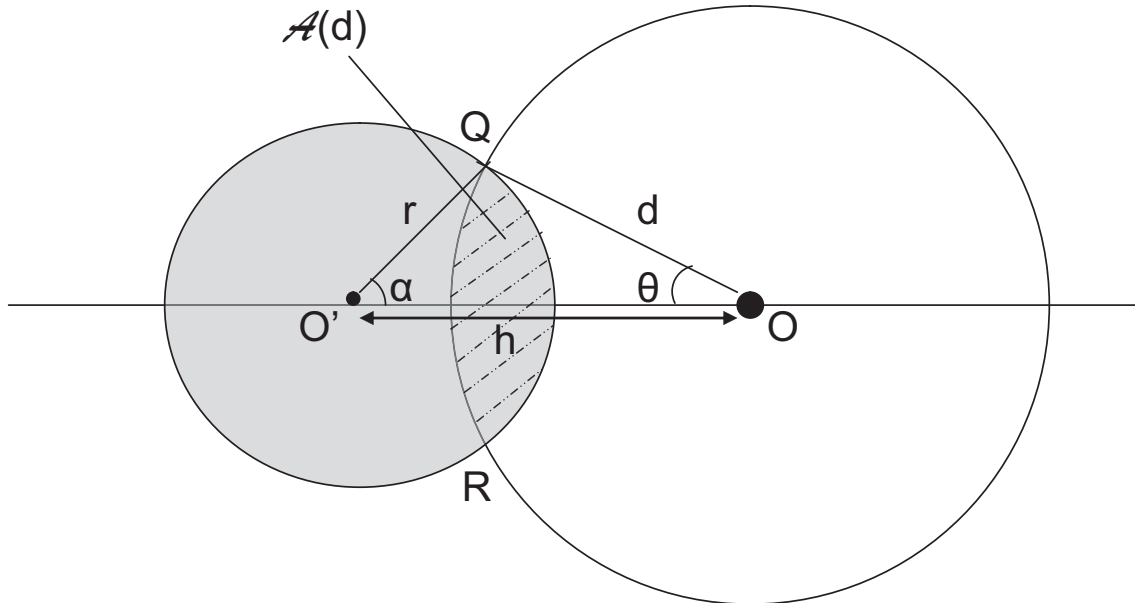


Figure 3.2: External circular area case: details.

where  $\theta(\cdot)$  and  $\alpha(\cdot)$  can be easily expressed in terms of  $d$ ,  $r$  and  $h$  through the Carnot theorem

$$\alpha(d, r, h) = \cos^{-1} \left( \frac{r^2 + h^2 - d^2}{2rh} \right), \quad (3.9)$$

$$\theta(d, r, h) = \cos^{-1} \left( \frac{d^2 + h^2 - r^2}{2dh} \right). \quad (3.10)$$

If we substitute the derivative of  $\mathcal{A}(d)$  (the expression is not given here for the sake of simplicity) in (3.7) we can easily obtain an expression for the joint distribution of  $G$  and  $\hat{Y}$ . Recalling that  $d$  ranges from  $h - r$  to  $h + r$ , the variables  $g$  and  $\hat{y}$  takes values in the intervals  $[0, \infty)$  and  $(-\hat{k} - 10 \log_{10} g - 10\beta \log_{10}(h + r), -\hat{k} - 10 \log_{10} g - 10\beta \log_{10}(h - r))$ , respectively. Finally, the marginal distribution  $f_G(\cdot)$  can be obtained by integrating  $f_{G\hat{Y}}(g, \hat{y})$  with respect to the variable  $\hat{y}$

$$f_G(g) = \frac{1}{\beta \sigma_S \sqrt{2\pi} k^{1/\beta} g^{1+1/\beta}} \int_{-(\hat{k}+10 \log_{10} g+10\beta \log_{10}(h+r))}^{-(\hat{k}+10 \log_{10} g+10\beta \log_{10}(h-r))} \frac{\mathcal{A}'(\varphi(g, \hat{y}))}{A} e^{-\frac{\hat{y}^2}{2\sigma_S^2}} e^{-\frac{\ln 10}{10\beta} \hat{y}} d\hat{y}. \quad (3.11)$$

Although closed form expressions for (3.11) do not appear to be obtainable, numerical integration of (3.11) allows a fast evaluation of  $f_G(g)$ .

### 3.2.3 Distribution of $G$ : the circular annulus case

Let's now consider again two nodes  $N_0$  and  $N_1$ , where  $N_0$  is located in  $O$ ,  $N_1$  is located in the annulus (Fig. 3.1 c)), and the distance between  $N_0$  and  $N_1$  ranges from  $r_m$  to  $r$ . The approach used to obtain the distribution of  $G$  is similar to that used in the previous cases. In such a scenario, the probability that the r.v.  $D \leq d$  is given by

$$F_D(d) = \mathbb{P}\{D \leq d\} = \frac{d^2 - r_m^2}{r^2 - r_m^2}, \quad (3.12)$$

therefore the joint pdf can be written as

$$f_{D,\hat{S}}(d, \hat{s}) = \frac{2de^{-\hat{s}^2/(2\sigma_S^2)}}{(r^2 - r_m^2)\sigma_S\sqrt{2\pi}} \quad (3.13)$$

for

$$r_m \leq d \leq r, \quad -\infty < \hat{s} < \infty.$$

If we make the change of variables (3.4), the joint pdf of the r.v.'s  $G$  and  $\hat{Y}$  can be written as

$$\begin{aligned}
f_{G,\hat{Y}}(g, \hat{y}) &= \frac{f_{D,\hat{S}}\left(\left[\frac{e^{-\left(\frac{\ln 10}{10}\right)\hat{y}}}{kg}\right]^{1/\beta}, \hat{y}\right)}{\left|J\left(\left[\frac{e^{-\left(\frac{\ln 10}{10}\right)\hat{y}}}{kg}\right]^{1/\beta}, \hat{y}\right)\right|} \\
&= \frac{2\left[\frac{e^{-\left(\frac{\ln 10}{10}\right)\hat{y}}}{kg}\right]^{1/\beta} e^{-\hat{y}^2/(2\sigma_S^2)}}{(r^2 - r_m^2)\sigma_S\sqrt{2\pi}\left(\frac{\beta}{k}\right)\left[\frac{e^{-\left(\frac{\ln 10}{10}\right)\hat{y}}}{kg}\right]^{-\frac{(\beta+1)}{\beta}} e^{-\left(\frac{\ln 10}{10}\right)\hat{y}}} \\
&= \frac{2k^{-2/\beta} e^{-\frac{2\hat{y}}{k\beta}} e^{-\frac{\hat{y}^2}{2\sigma_S^2}}}{(r^2 - r_m^2)\sigma_S\sqrt{2\pi}\beta g^{1+2/\beta}} \tag{3.14}
\end{aligned}$$

for

$$r_m < \frac{e^{-\frac{\ln 10}{10\beta}\hat{y}}}{(kg)^{1/\beta}} < r ,$$

which gives

$$-(\hat{k} + 10 \log_{10} g + 10\beta \log_{10} r) < \hat{y} < -(\hat{k} + 10 \log_{10} g + 10\beta \log_{10} r_m) .$$

The pdf of  $G$  can be derived by integrating  $\hat{Y}$  over its range of definition

$$\begin{aligned}
f_G(g) &= \int_{-(\hat{k}+10\log_{10}g+10\beta\log_{10}r)}^{-(\hat{k}+10\log_{10}g+10\beta\log_{10}r_m)} f_{G,\hat{Y}}(g, \hat{y}) d\hat{y} \\
&= \frac{2k^{-2/\beta} g^{-(1+2/\beta)}}{(r^2 - r_m^2)\sigma_S\sqrt{2\pi}\beta} \int_{-(\hat{k}+10\log_{10}g+10\beta\log_{10}r)}^{-(\hat{k}+10\log_{10}g+10\beta\log_{10}r_m)} e^{-\frac{\hat{y}^2}{(2\sigma_S^2)}} e^{-\frac{2\hat{y}}{k\beta}} d\hat{y} \\
&= \frac{e^{\frac{\sigma_S^2(\ln 10)^2}{50\beta^2}}}{(r^2 - r_m^2)\beta k^{2/\beta} g^{1+2/\beta}} \left[ \operatorname{erfc}\left(\frac{\hat{k} + 10 \log_{10} g + k\beta \ln r_m}{\sigma_S\sqrt{2}} - \frac{\sigma_S\sqrt{2}}{k\beta}\right) \right. \\
&\quad \left. - \operatorname{erfc}\left(\frac{\hat{k} + 10 \log_{10} g + k\beta \ln r}{\sigma_S\sqrt{2}} - \frac{\sigma_S\sqrt{2}}{k\beta}\right) \right] . \tag{3.15}
\end{aligned}$$

Equation (3.15) gives a closed form expression for the distribution of  $G$  for an interferer located in the circular annulus of Fig. 3.1 c). Note that in the case of annulus of infinite area ( $r \rightarrow \infty$ ), the distribution of  $G$  converges to zero. However, as it will be shown in subsection 3.3.2, the evaluation of the moments of the interference is still possible.

### 3.2.4 Distribution of $G$ : the circular area case

The circular area case depicted in Fig. 3.2 d) can be seen, in principle, as a special case of the circular annulus case discussed above. In particular, if now let  $r_m$  go to 0 in (3.15), the

distribution of  $G$  becomes

$$f_G(g) = \frac{e^{\frac{\sigma_S^2(\ln 10)^2}{50\beta^2}}}{r^2\beta k^{2/\beta}g^{1+2/\beta}} \left[ 2 - \operatorname{erfc} \left( \frac{\hat{k} + 10 \log_{10} g + k_\beta \ln r}{\sigma_S \sqrt{2}} - \frac{\sigma_S \sqrt{2}}{k_\beta} \right) \right]. \quad (3.16)$$

As discussed in Section 2.2, the propagation model in (3.1) is only valid when the distance between the nodes is larger than some wavelengths. A practical approach to overcome this limitation is to suppose the existence of a "dead-zone" around  $N_0$  having a radius of 1 meter which is free from nodes [42]. In this case, the expression for  $f_G(g)$  in the case of circular area is that given in (3.15) with  $r_m = 1$  m. A more realistic approach is based on the use of a two-slope propagation model [23]. The propagation model in (3.1) has to be modified as follows

$$G = \begin{cases} \frac{d^{-\beta}}{k_s} & d \geq 1 \text{ m} \\ \frac{1}{k} & d < 1 \text{ m} \end{cases}, \quad (3.17)$$

with this model we assume that the channel gain in a radius of 1 m around the reference is constant ( $1/k$ ) and we neglect the impact of shadowing<sup>1</sup>. Using the propagation model described in (3.17), the pdf of  $G$  becomes

$$\begin{aligned} f_G(g) &= \mathbb{P}\{D < 1 \text{ m}\} f_{G|D < 1}(g) + \mathbb{P}\{D \in [1, r]\} f_{G|D \in [1, r]}(g) \\ &= \frac{f_{G|D < 1}(g)}{r^2} + \left(1 - \frac{1}{r^2}\right) f_{G|D \in [1, r]}(g) \\ &= \frac{\delta\left(g - \frac{1}{k}\right)}{r^2} + \frac{e^{\frac{\sigma_S^2(\ln 10)^2}{50\beta^2}}}{r^2\beta k^{2/\beta}g^{1+2/\beta}} \left[ \operatorname{erfc} \left( \frac{\hat{k} + 10 \log_{10} g}{\sigma_S \sqrt{2}} - \frac{\sigma_S \sqrt{2}}{k_\beta} \right) \right. \\ &\quad \left. - \operatorname{erfc} \left( \frac{\hat{k} + 10 \log_{10} g + k_\beta \ln r}{\sigma_S \sqrt{2}} - \frac{\sigma_S \sqrt{2}}{k_\beta} \right) \right], \end{aligned} \quad (3.18)$$

where  $\delta(\cdot)$  is the Dirac delta function and we have used (3.15) with  $r_m = 1$  for the evaluation of  $f_{G|D \in [1, r]}(g)$ .

### 3.3 Interference analysis

To characterize the amount of interference received by the node located in  $O$ , we assume that all the nodes in the considered areas are source of interference [37, 40, 49–54]. This assumption

<sup>1</sup>This latter hypothesis is reasonable owing to the small distance between transmitter and receiver. However, the inclusion of shadowing for distances less than 1 meter in the proposed model is still possible.

is typical of multiple access schemes based on spread spectrum techniques where all the nodes transmit in the same frequency band. Other multiple access techniques could be considered but they are not taken into account here.

### 3.3.1 Evaluation of the Moments of the Interference

Owing to the PPP model considered for the nodes's positions, the number of terminals in the areas of Fig. 3.1, is a Poisson random variable with mean value  $\rho A$  [32]. If we assume that an interfering node transmits with probability  $p_A$ , the number of nodes that are really transmitting, say  $N$ , is still Poisson with mean  $\mu_N = \pi \rho p_A A$  [49]. Now, let's assume that there are  $n$  nodes in the considered area, and define the random variable  $I_n = P_T(G_1 + \dots + G_n)$ , where  $G_i$  represents the channel gain for the  $i^{\text{th}}$  interferer.  $I_n$  gives the amount of interference conditioned on the fact that the number of interferers is exactly  $n$ . The  $p^{\text{th}}$  moment of  $I$  (i.e. regardless the value of  $n$ ) can be written as

$$\begin{aligned} \mu_I^{(p)} \triangleq \mathbb{E}\{I^p\} &= \sum_{n=0}^{\infty} \mathbb{P}\{N = n\} \mu_{n,I}^{(p)} \\ &= \sum_{n=0}^{\infty} \frac{e^{-\mu_N} \mu_N^n}{n!} \mu_{n,I}^{(p)}. \end{aligned} \quad (3.19)$$

Recalling that  $\mu_{G_i}^{(p)} = \mu_G^{(p)}$  for each  $i$  and  $p$ , we get

$$\begin{aligned} \mu_{n,I}^{(p)} &\triangleq \mathbb{E}\{I^p | N=n\} \\ &= P_T^k \sum_{i_1=0}^p \dots \sum_{i_{n-1}=0}^{i_{n-2}} \binom{p}{i_1} \dots \binom{i_{n-2}}{i_{n-1}} \prod_{\ell=1}^n \mu_G^{(i_{\ell-1}-i_\ell)} \\ &= P_T^p p! \sum_{i_1=0}^p \dots \sum_{i_{n-1}=0}^{i_{n-2}} \frac{\prod_{\ell=1}^n \mu_G^{(i_{\ell-1}-i_\ell)}}{\prod_{m=1}^n (i_{m-1} - i_m)!}, \end{aligned} \quad (3.20)$$

with  $i_0 \triangleq k$ ,  $i_n = 0$ . If we substitute (3.20) in (3.19), we obtain a representation, in terms of an infinite series, of the interference received by a node located in the center of a circular area of radius  $r$ .

Although expression (3.20) is very concise and allows the evaluation of moments of any order, the presence of indexes  $i_1 \dots i_{n-1}$  does not allow us to simplify the infinite series in (3.19)

when evaluating the moments of  $I$ . To obtain closed form expressions for the first moments of  $I$ , we can define the ancillary r.v's  $Z = I/P_T$  and  $Z_n = G_1 + \dots + G_n$  and derive the moment generating function (m.g.f.) of  $Z_n$

$$\Phi_{Z_n}(s) \triangleq \mathbb{E} \{ e^{sZ_n} \} = \mathbb{E} \left\{ \prod_{i=1}^n e^{sG_i} \right\} = \Phi_G^n(s), \quad (3.21)$$

where we have used the fact that  $G_i$  (with  $i = 1, \dots, n$ ) are i.i.d. With the help of the total probability theorem, we can obtain the following expression for the m.g.f. of  $Z$ <sup>2</sup>

$$\begin{aligned} \Phi_Z(s) &= \sum_{n=0}^{\infty} \mathbb{P}\{N = n\} \Phi_{Z_n}(s) \\ &= \sum_{n=0}^{\infty} \frac{\mu_N^n e^{-\mu_N} \Phi_G^n(s)}{n!} \\ &= e^{\mu_N(\Phi_G(s)-1)}. \end{aligned} \quad (3.22)$$

By recalling that  $\mu_I^{(p)} = P_T^p \mu_Z^{(p)}$  and using the well-known relation between m.g.f. and moments [43] we get

$$\mu_I^{(p)} = P_T^p \left. \frac{d^p \Phi_Z(s)}{ds^p} \right|_{s=0} = P_T^p e^{-\mu_N} \left. \frac{d^p (e^{\mu_N \Phi_G(s)})}{ds^p} \right|_{s=0}. \quad (3.23)$$

A concise expression for the derivative in (3.23) can be obtained using the Faa-di Bruno's formula [57], which gives the  $p^{\text{th}}$  derivative of a composite function  $g(f(x))$

$$\frac{d^p g(f(x))}{dx^p} = \sum \frac{p!}{b_1! \dots b_p!} g^{(b)}(f(x)) \left( \frac{df(x)}{1! dx} \right)^{b_1} \dots \left( \frac{d^p f(x)}{p! dx^p} \right)^{b_p}, \quad (3.24)$$

where  $g^{(b)}(f(x))$  is the  $b^{\text{th}}$  derivative of  $g(\cdot)$  in the variable  $f(x)$ , the sum is over all different solutions in nonnegative integers  $b_1, \dots, b_p$  of  $b_1 + 2b_2 + \dots + p b_p = p$ , and  $b = b_1 + \dots + b_p$ .

By substituting (3.24) in (3.23) with  $g(x) = e^x$  and  $f(x) = \mu_N \Phi_G(x)$ , we obtain

$$\begin{aligned} \mu_I^{(p)} &= P_T^p \sum \frac{p!}{b_1! \dots b_p!} \left( \frac{\mu_N d\Phi_G(s)}{1! ds} \right)^{b_1} \bigg|_{s=0} \dots \left( \frac{\mu_N d^p \Phi_G(s)}{p! ds^p} \right)^{b_p} \bigg|_{s=0} \\ &= P_T^p \sum \frac{p! \mu_N^b}{b_1! \dots b_p!} \prod_{m=1}^p \left( \frac{\mu_G^{(m)}}{m!} \right)^{b_m}. \end{aligned} \quad (3.25)$$

<sup>2</sup>Note that (3.22) can be seen as the generalization of [49, eq. (14)] in the presence of shadowing.

To give some example, the first two moments of  $\mu_I$  are given below

$$\mu_I = P_T \mu_N \mu_G, \quad (3.26)$$

$$\mu_I^{(2)} = P_T^2 \mu_N \left( \mu_G^{(2)} + \mu_N \mu_G^2 \right), \quad (3.27)$$

other moments of  $I$  are listed in Table 3.1.

Expressions (3.20) and (3.25) are valid for any scenario and require only the knowledge of  $\mu_N$  and  $\mu_G^{(p)}$ . With regard to the scenarios in Fig. 3.1,  $\mu_N = \pi \rho p_A r^2$ ,  $\mu_N = \pi \rho p_A (r^2 - r_m^2)$  and  $\mu_N = \pi \rho p_A r^2$  in the scenarios b), c) and d), respectively. The moments of  $G$  can be obtained using the distributions given in (3.11) (scenario b)), (3.15) (scenario c)) and (3.16) (scenario d)), respectively. Closed form expressions for  $\mu_G^{(p)}$  will be given in subsections 3.3.2 and 3.3.3 for the cases of figures 3.1 c) and 3.1 d).

Finally, the knowledge of the first moments can be used to obtain an estimate of the distribution of  $I$  [58].

Table 3.1: The first five moments of  $\mu_I$ .

$p$	$\mu_I^{(p)}$
1	$P_T \mu_N \mu_G$
2	$P_T^2 \mu_N \left( \mu_G^{(2)} + \mu_N \mu_G^2 \right)$
3	$P_T^3 \mu_N \left( \mu_N^2 \mu_G^3 + 3 \mu_N \mu_G \mu_G^{(2)} + \mu_G^{(3)} \right)$
4	$P_T^4 \mu_N \left( \mu_G^{(4)} + 4 \mu_N \mu_G \mu_G^{(3)} + 3 \mu_N \mu_G^{(2)2} + 6 \mu_N^2 \mu_G^2 \mu_G^{(2)} + \mu_N^3 \mu_G^4 \right)$
5	$P_T^5 \mu_N \left( \mu_G^{(5)} + \mu_N^4 \mu_G^5 + 5 \mu_N \mu_G \mu_G^{(4)} + 10 \mu_N \mu_G^{(2)} \mu_G^{(3)} + 10 \mu_N^2 \mu_G^2 \mu_G^{(3)} + 10 \mu_N^3 \mu_G^3 \mu_G^{(2)} + 15 \mu_N^2 \mu_G \mu_G^{(2)2} \right)$

### 3.3.2 The moments of $G$ : circular annulus scenario

We here derive a closed form expression for the moments of  $G$  in the circular annulus case (scenario c) of Fig.3.1. By recalling (3.15), the  $p^{\text{th}}$  moment of  $G$  can be written as

$$\begin{aligned}
\mu_G^{(p)} &= \int_0^\infty g^p f_G(g) dg \\
&= \frac{e^{\frac{\sigma_S^2 (\ln 10)^2}{50\beta^2}}}{(r^2 - r_m^2)\beta k^{2/\beta}} \int_0^\infty g^{p-1-2/\beta} \left[ \operatorname{erfc} \left( \frac{\hat{k} + 10 \log_{10} g + k_\beta \ln r_m}{\sigma_S \sqrt{2}} - \frac{\sigma_S \sqrt{2}}{k_\beta} \right) \right. \\
&\quad \left. - \operatorname{erfc} \left( \frac{\hat{k} + 10 \log_{10} g + k_\beta \ln r}{\sigma_S \sqrt{2}} - \frac{\sigma_S \sqrt{2}}{k_\beta} \right) \right] dg \\
&= K_G \int_0^\infty g^A [\operatorname{erfc}(B \ln g + H(r_m)) - \operatorname{erfc}(B \ln g + H(r))] dg, \tag{3.28}
\end{aligned}$$

where

$$K_G = \frac{e^{\frac{\sigma_S^2 (\ln 10)^2}{50\beta^2}}}{(r^2 - r_m^2)\beta k^{2/\beta}},$$

$A = p - 1 - 2/\beta$ ,  $B = \frac{10}{\ln 10 \sigma_S \sqrt{2}}$ , and

$$H(x) = \frac{\hat{k} + k_\beta \ln x}{\sigma_S \sqrt{2}} - \frac{\sigma_S \sqrt{2}}{k_\beta}.$$

Owing to the presence of the  $\operatorname{erfc}$  function, the integral in (3.28) appears to be unsolvable in closed form. To obtain a closed form expression we need to find a tight approximation for  $\operatorname{erfc}(\cdot)$ . Recently, the following useful approximation has been proposed [59, eq. (14)]

$$\operatorname{erfc}(x) \simeq \frac{1}{6} e^{-x^2} + \frac{1}{2} e^{-4x^2/3}, \tag{3.29}$$

which has been proved to be tighter than the Chernoff-Rubin upper bound [59]. Unfortunately, this approximation (which becomes an upper bound in the interval  $[0.5, \infty)$ ) is tight only for  $x > 0.5$  [59], whereas the argument of the  $\operatorname{erfc}(\cdot)$  functions in (3.28) ranges from  $-\infty$  to  $\infty$ . To overcome this limitation we approximate  $\operatorname{erfc}$  with the function  $1 - x$  in the interval  $x \in [0, 1/2]$ . The extension to negative values of the argument is straightforward by exploiting the property that  $\operatorname{erfc}(x) = 2 - \operatorname{erfc}(-x)$ . Therefore, the approximation is given by

$$\operatorname{erfc}_{\text{approx}}(x) \triangleq \begin{cases} 2 - \frac{1}{6} e^{-x^2} - \frac{1}{2} e^{-4x^2/3} & x < -1/2 \\ 1 - x & |x| \leq 1/2 \\ \frac{1}{6} e^{-x^2} + \frac{1}{2} e^{-4x^2/3} & x > 1/2 \end{cases}, \tag{3.30}$$

the tightness of this approximation can be appreciated in Fig. 3.3.

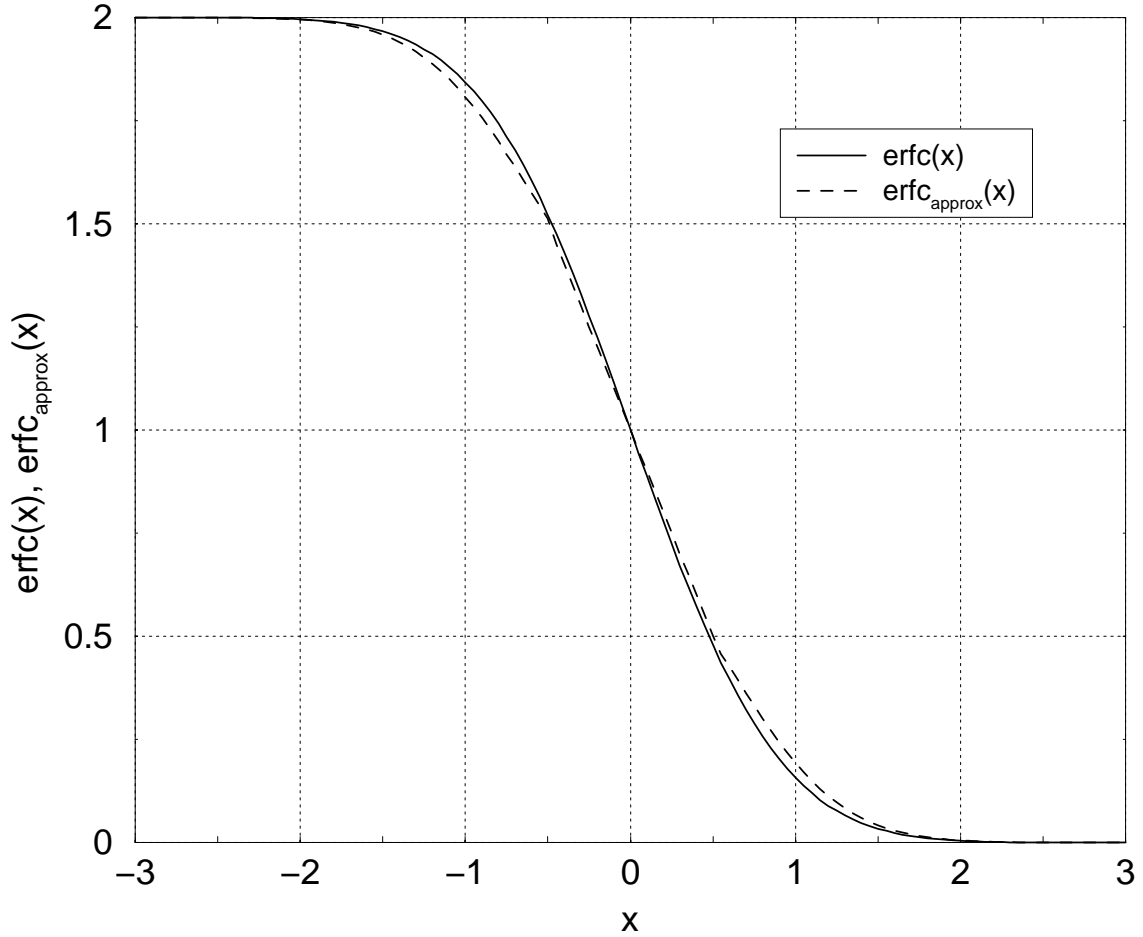


Figure 3.3: The comparison between the  $\text{erfc}(\cdot)$  function and its approximate expression.

By substituting (3.30) in (3.28), we obtain

$$\begin{aligned} \mu_G^{(p)} \approx & K_G \left[ \mathcal{F} \left( p-1-2/\beta, \frac{10}{\ln 10 \sigma_S \sqrt{2}}, \frac{\hat{k} + k_\beta \ln r_m}{\sigma_S \sqrt{2}} - \frac{\sigma_S \sqrt{2}}{k_\beta} \right) \right. \\ & \left. - \mathcal{F} \left( p-1-2/\beta, \frac{10}{\ln 10 \sigma_S \sqrt{2}}, \frac{\hat{k} + k_\beta \ln r}{\sigma_S \sqrt{2}} - \frac{\sigma_S \sqrt{2}}{k_\beta} \right) \right], \end{aligned} \quad (3.31)$$

where

$$\begin{aligned}
\mathcal{F}(x, y, z) &\triangleq \frac{2}{x+1} e^{-\frac{x+1}{y}(\frac{1}{2}+z)} - \frac{1}{6} e^{-z^2} \mathcal{I}\left(e^{-\frac{1}{y}(\frac{1}{2}+z)}, x-2yz, y^2\right) \\
&- \frac{1}{2} e^{-4z^2/3} \mathcal{I}\left(e^{-\frac{1}{y}(\frac{1}{2}+z)}, x-8yz/3, 4y^2/3\right) + \frac{1}{(1+x)^2} \\
&\times \left[ e^{-\frac{1+2z}{2y}} \left( e^{\frac{2+x-2xz}{2y}} \left( 1+y+x(1+z) - z - (1+x)y \ln\left(e^{\frac{1-2z}{2y}}\right) \right) + e^{-\frac{x(1+2z)}{2y}} \right. \right. \\
&\times \left. \left. \left( -1-y+x(1+z) + z(1+x)y \ln\left(e^{-\frac{1+2z}{2y}}\right) \right) \right) \right] \\
&+ \frac{1}{6} e^{-z^2} \mathcal{J}\left(e^{\frac{1}{y}(\frac{1}{2}-z)}, x-2yz, y^2\right) + \frac{1}{2} e^{-4z^2/3} \mathcal{J}\left(e^{\frac{1}{y}(\frac{1}{2}-z)}, x-8yz/3, 4y^2/3\right).
\end{aligned} \tag{3.32}$$

The functions  $\mathcal{I}(\cdot)$  and  $\mathcal{J}(\cdot)$  in (3.32) are given by

$$\mathcal{I}(a, e, f) \triangleq \int_0^a g^{e-f \ln g} dg = \frac{e^{\frac{(1+e)^2}{4f}} \sqrt{\pi} [1 + \operatorname{erf}(-\frac{1+e-2f \ln a}{2\sqrt{f}})]}{2\sqrt{f}}, \tag{3.33}$$

and

$$\mathcal{J}(a, e, f) \triangleq \int_a^\infty g^{e-f \ln g} dg = \frac{e^{\frac{(1+e)^2}{4f}} \sqrt{\pi} [1 - \operatorname{erf}(-\frac{1+e-2f \ln a}{2\sqrt{f}})]}{2\sqrt{f}}. \tag{3.34}$$

As already discussed in subsection 3.2.3, when  $r \rightarrow \infty$  (the area of the annulus tends to infinite)  $\mu_G$  tends to zero. However, the moments of the interference are still finite. This behavior can be explained by observing that, as shown in (3.25), the expression for  $\mu_I^{(p)}$  for an arbitrary (and finite) value of  $r$  is given by a sum of terms  $\mu_N^b \mu_G^{(p)b_1} \cdots \mu_G^{(p)b_p}$ ; each term can be rearranged as

$$\left[ \pi \rho (r^2 - r_m^2) \right]^b \left[ \frac{e^{\frac{\sigma_S^2 (\ln 10)^2}{50\beta^2}}}{(r^2 - r_m^2) \beta k^{2/\beta}} \right]^{b_1 + \cdots + b_p} \Psi^{b_1}(1, r, r_m) \cdots \Psi^{b_p}(p, r, r_m) \tag{3.35}$$

where  $\Psi(p, r, r_m) = \int_0^\infty g^{p-1-2/\beta} [\operatorname{erfc}(B \ln g + H(r_m)) - \operatorname{erfc}(B \ln g + H(r))] dg$ . If  $r \rightarrow \infty$ , (3.35) becomes

$$\left[ \frac{\pi \rho e^{\frac{\sigma_S^2 (\ln 10)^2}{50\beta^2}}}{\beta k^{2/\beta}} \right]^b \Psi^{b_1}(1, \infty, r_m) \cdots \Psi^{b_p}(p, \infty, r_m), \tag{3.36}$$

which is a finite quantity for all values of  $p$  (provided that  $\beta > 2$ ).

### 3.3.3 The moments of $G$ : circular area scenario

In the circular area scenario, we use the expression for  $f_G(\cdot)$  given in (3.18) jointly with approximation (3.30), to obtain

$$\begin{aligned} \mu_G^{(p)} &= \frac{1}{r^2 k^p} + \frac{e^{\frac{\sigma_S^2 (\ln 10)^2}{50\beta^2}}}{r^2 \beta k^{2/\beta}} \int_0^\infty g^{p-1-2/\beta} [\operatorname{erfc}(B \ln g + H(1)) - \operatorname{erfc}(B \ln g + H(r))] dg \\ &\approx \frac{1}{r^2 k^p} + \frac{e^{\frac{\sigma_S^2 (\ln 10)^2}{50\beta^2}}}{r^2 \beta k^{2/\beta}} \left[ \mathcal{F} \left( p-1-2/\beta, \frac{10}{\ln 10 \sigma_S \sqrt{2}}, \frac{\hat{k}}{\sigma_S \sqrt{2}} - \frac{\sigma_S \sqrt{2}}{k_\beta} \right) \right. \\ &\quad \left. - \mathcal{F} \left( p-1-2/\beta, \frac{10}{\ln 10 \sigma_S \sqrt{2}}, \frac{\hat{k} + k_\beta \ln r}{\sigma_S \sqrt{2}} - \frac{\sigma_S \sqrt{2}}{k_\beta} \right) \right]. \end{aligned} \quad (3.37)$$

Note that also in the case of circular area, when  $r \rightarrow \infty$  the moments of  $g$  tend to zero, but the moments of interference are finite.

## 3.4 Numerical results

In all the numerical results shown here the transmit power  $P_T$  has been fixed at  $10^{-3} W$  and  $p_A = 1$ .

### 3.4.1 External Circular Area Case: Scenario b)

Some examples of result for the external circular area case are given in Fig. 3.4, which shows the mean value of the overall interference  $I$ , as a function of  $r$ , for different values of  $\beta$ . The other parameters are  $h = 150 m$  (the distance between the center of the circular area and the receiver),  $\hat{k} = 30 dB$ ,  $\sigma_S = 5 dB$  and  $\rho = 5 \cdot 10^{-4} nodes/m^2$ . The curves have been obtained by calculating  $f_G(g)$  in (3.11) and  $\mu_G$  numerically.

### 3.4.2 Circular Annulus Case: Scenario c)

Figs. 3.5 and 3.6 show the mean value and the variance of  $I$  as functions of  $r_m$  in the circular annulus case. Three different values of  $\beta$  (ranging from 3 to 5) are considered, with  $\hat{k} = 30 dB$ ,  $r = 200 m$ ,  $\sigma_S = 5 dB$  and  $\rho = 5 \cdot 10^{-4} nodes/m^2$ . The expression used to obtain  $\mu_G^{(1)}$  and

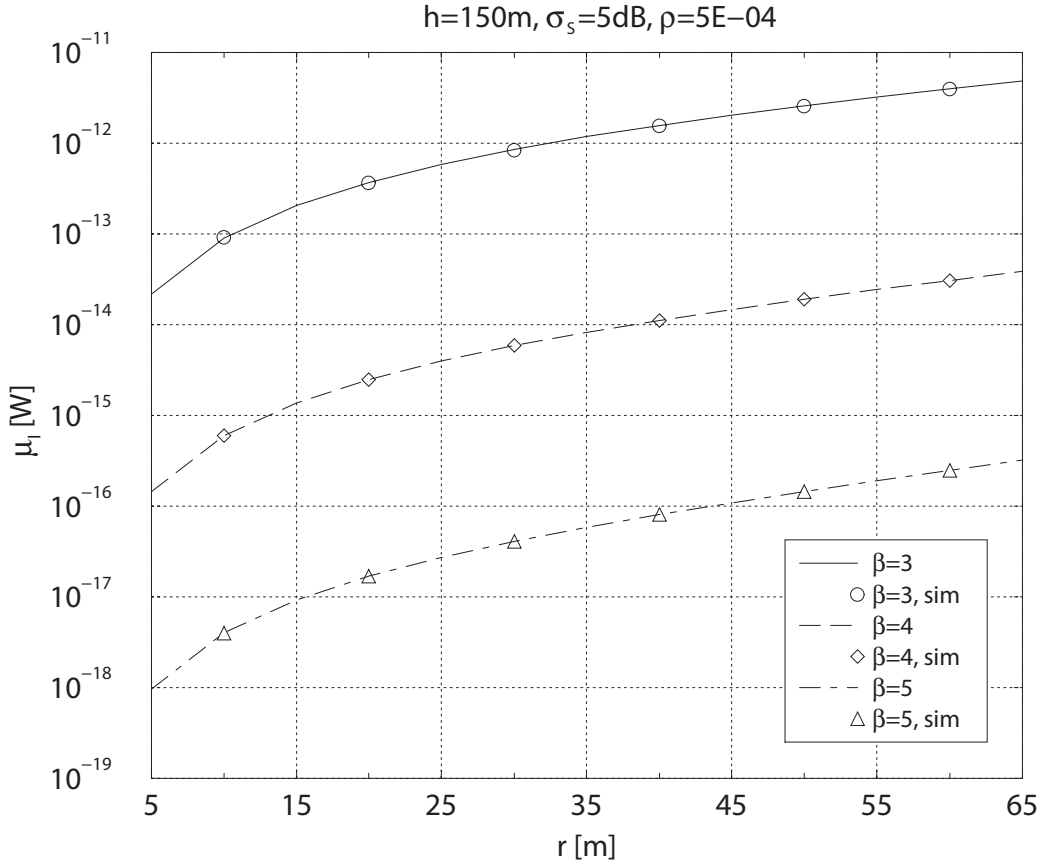


Figure 3.4: Scenario b):  $\mu_I$  as a function of  $r$  for different values of the propagation parameter  $\beta$ .

$\mu_G^{(2)}$  is given in (3.31). As expected, an increase in the value of  $r_m$  decreases the mean value of the interfering nodes by reducing the total amount of interference. The figures shows that the approximation is very tight. Finally, we observe that the behavior of mean value and variance of  $I$  as a function of  $r_m$  is quite similar.

### 3.4.3 Circular area case: Scenario d)

Figs. 3.7 and 3.8 show the role played by shadowing on the first two moments of the interference for different values of the nodes' density  $\rho$  (ranging from  $5 \cdot 10^{-3}$  to  $5 \cdot 10^{-5}$  nodes/m<sup>2</sup>). The expression used to obtain  $\mu_G^{(1)}$  and  $\mu_G^{(2)}$  is given in (3.37). The following parameters have been considered:  $\beta = 4$ ,  $\hat{k} = 30$  dB and  $r = 50$  m. As expected, shadowing and nodes' density have a significant influence on the overall interference. In particular, the shadowing increases

the moments of the interference. As far as the role of  $\rho$  is concerned, it is straightforward to observe that (3.37) does not depend on  $\rho$ , and so the moments of  $I$  are linearly dependent on  $\rho$ . We can also observe that the agreement between simulations and analysis (we recall that eq. (3.37) is an approximate expression) is still excellent.

Fig. 3.9 shows the mean value of  $I$  as a function of the radius  $r$  of the circular area for different values of the propagation parameter  $\hat{k}$ . The other parameters are  $\beta = 4$ ,  $\rho = 5 \cdot 10^{-4}$  nodes/m<sup>2</sup> and  $\sigma_S = 5$  dB. It is interesting to observe that values of  $r$  larger than 5 m have no impact on  $\mu_I$ . This can be explained by observing that if we increase the radius, the average number of interferers in the circular area grows with a quadratic (with respect to  $r$ ) behavior,

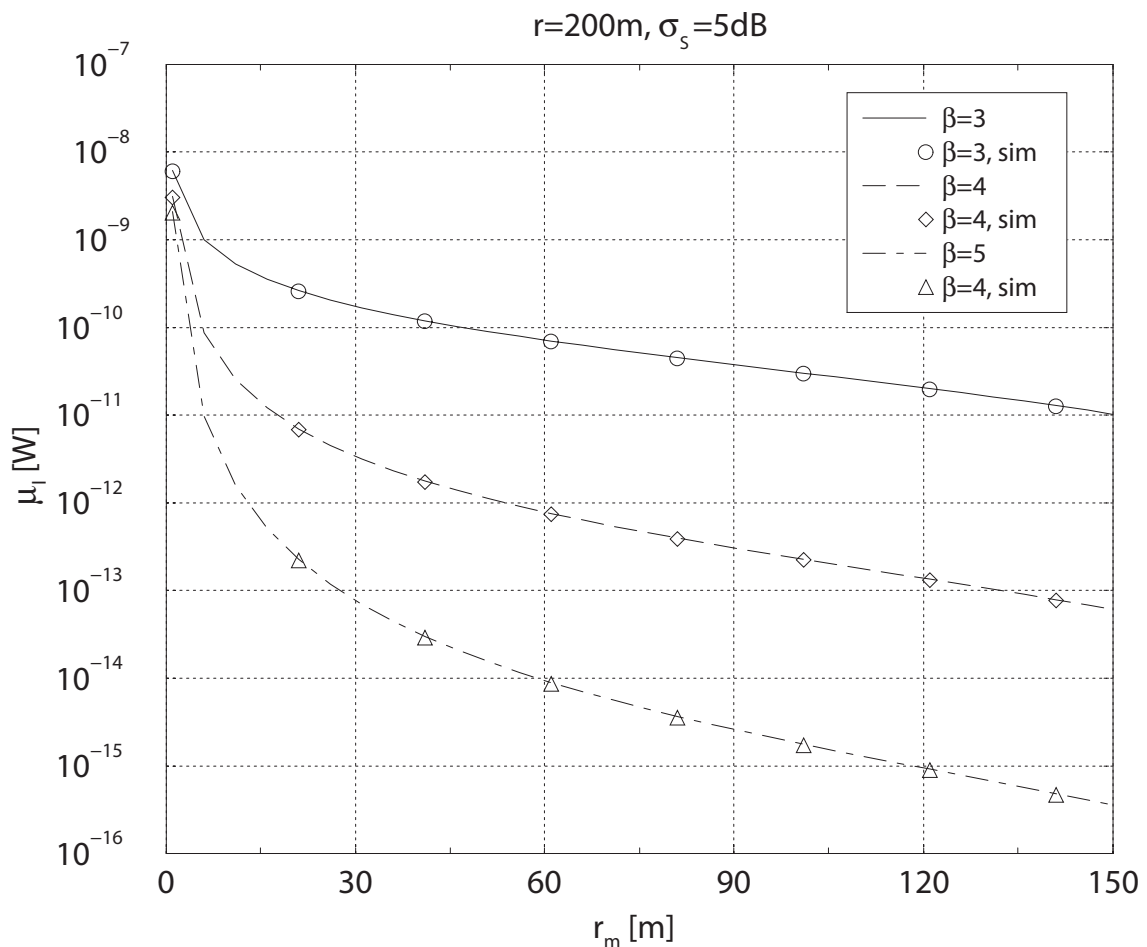


Figure 3.5: Scenario c):  $\mu_I$  as a function of  $r_m$  for different values of the coefficient propagation  $\beta$ .

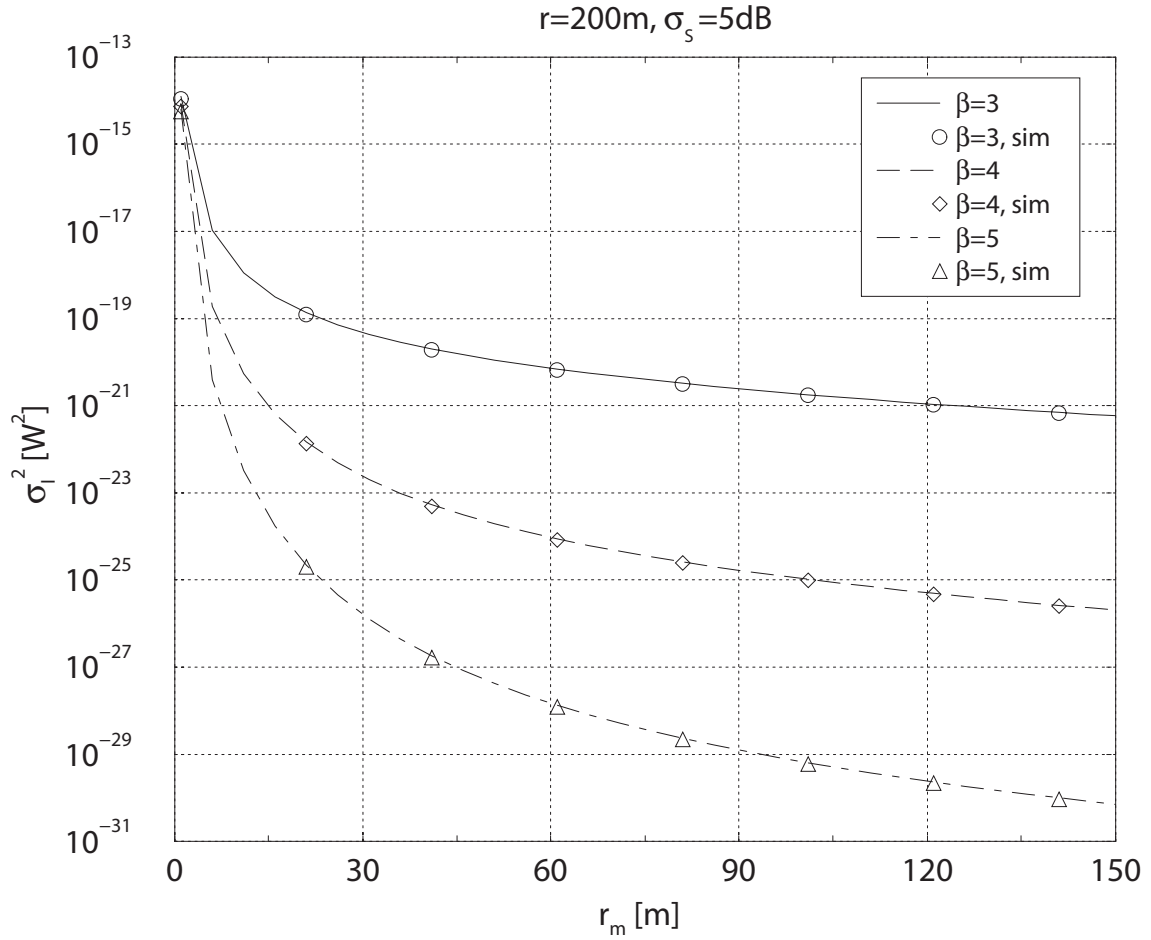


Figure 3.6: Scenario c): the variance of  $I$  as a function of  $r_m$  for different values of the coefficient propagation  $\beta$ .

while the power they provide, given the value of  $\beta$  considered ( $\beta = 4$ ), decreases quickly with the distance. From the analytical point of view, we can easily observe that  $r$  appears in equation (3.37) in the constant term and inside the  $\text{erfc}(\cdot)$  argument. To obtain  $\mu_I$  we multiply the mean value of  $G$  by  $\mu_N$ , this operation eliminates the term  $r$  from the constant. The only term where  $r$  appears is in the argument of the second  $\text{erfc}(\cdot)$  in (3.18). On the other hand, it is well known that  $\text{erfc}(x) - \text{erfc}(y) \approx \text{erfc}(x)$  if  $y \gg x$  (and  $x, y > 0$ ), therefore, when  $r \gg 1$ , the value of the second  $\text{erfc}(\cdot)$  is negligible compared to the first one (which does not contains  $r$ ). The comparison between the assumption of "dead-zone" and the "two-slope" model considered in (3.17) reveals that, although the behavior of the two models is similar, the assumption about the

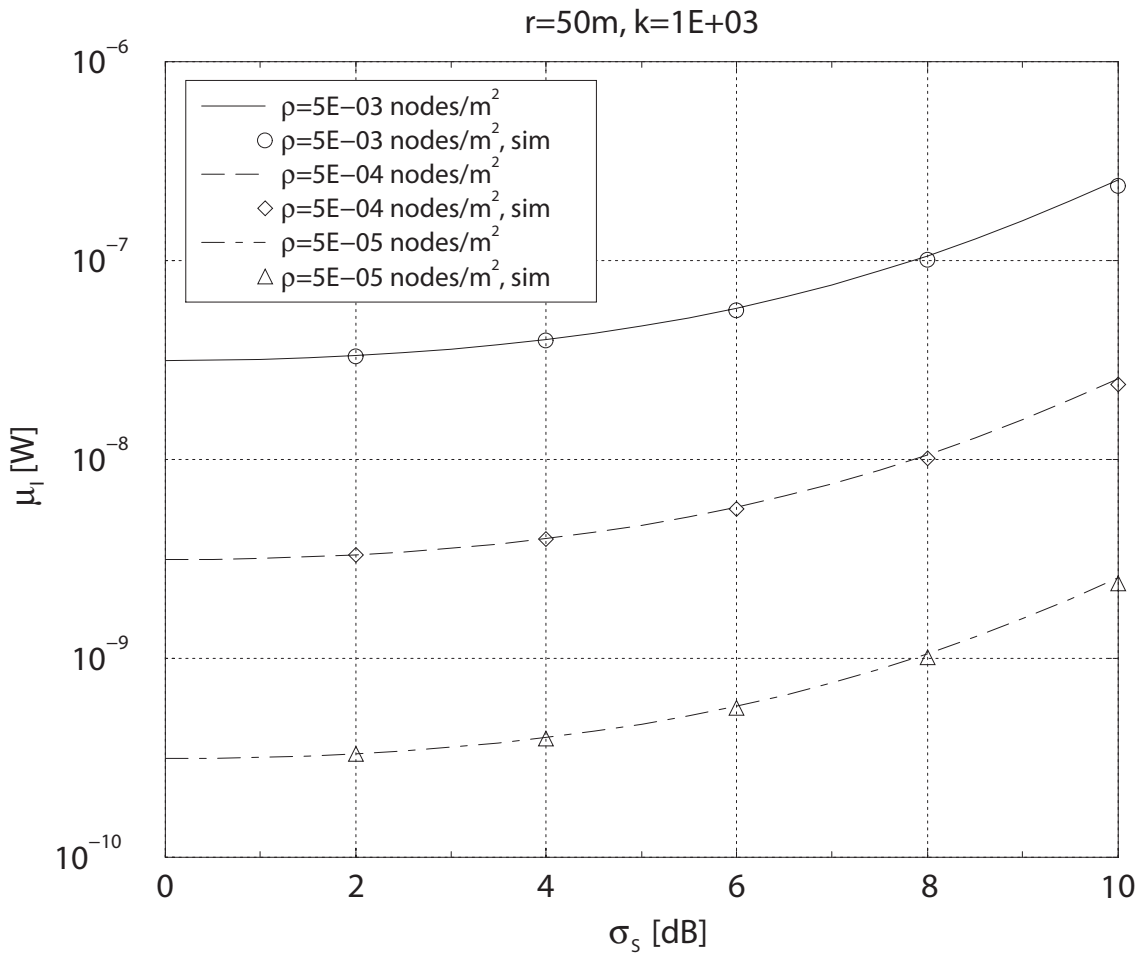


Figure 3.7: Scenario d):  $\mu_I$  as a function of  $\sigma_S$  for different values of the nodes' density  $\rho$ .

existence of a "dead zone" provides an underestimate of the real amount of interference.

Note that in the case the propagation model is given by (3.1) and  $r \rightarrow \infty$ , the moments of  $I$  do not exist. This is true also in the absence of shadowing<sup>3</sup>.

<sup>3</sup>It is easy to show that the pdf expression for  $I$  obtained in [49] (shadowing is neglected) does not allow the evaluation of the moments.

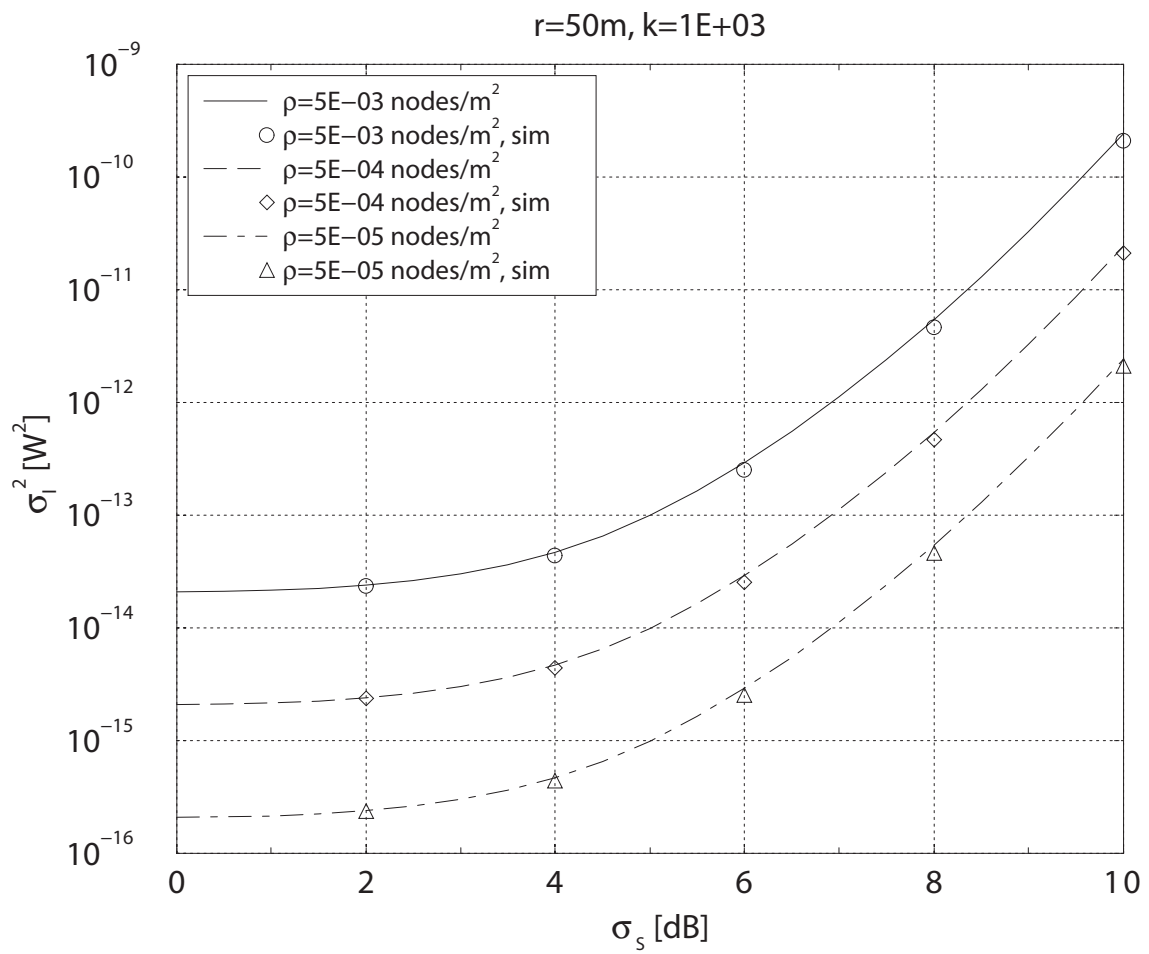


Figure 3.8: Scenario d): the variance of  $I$  as a function of the standard deviation of shadowing ( $\sigma_S$ ) for different values of the nodes' density  $\rho$ .

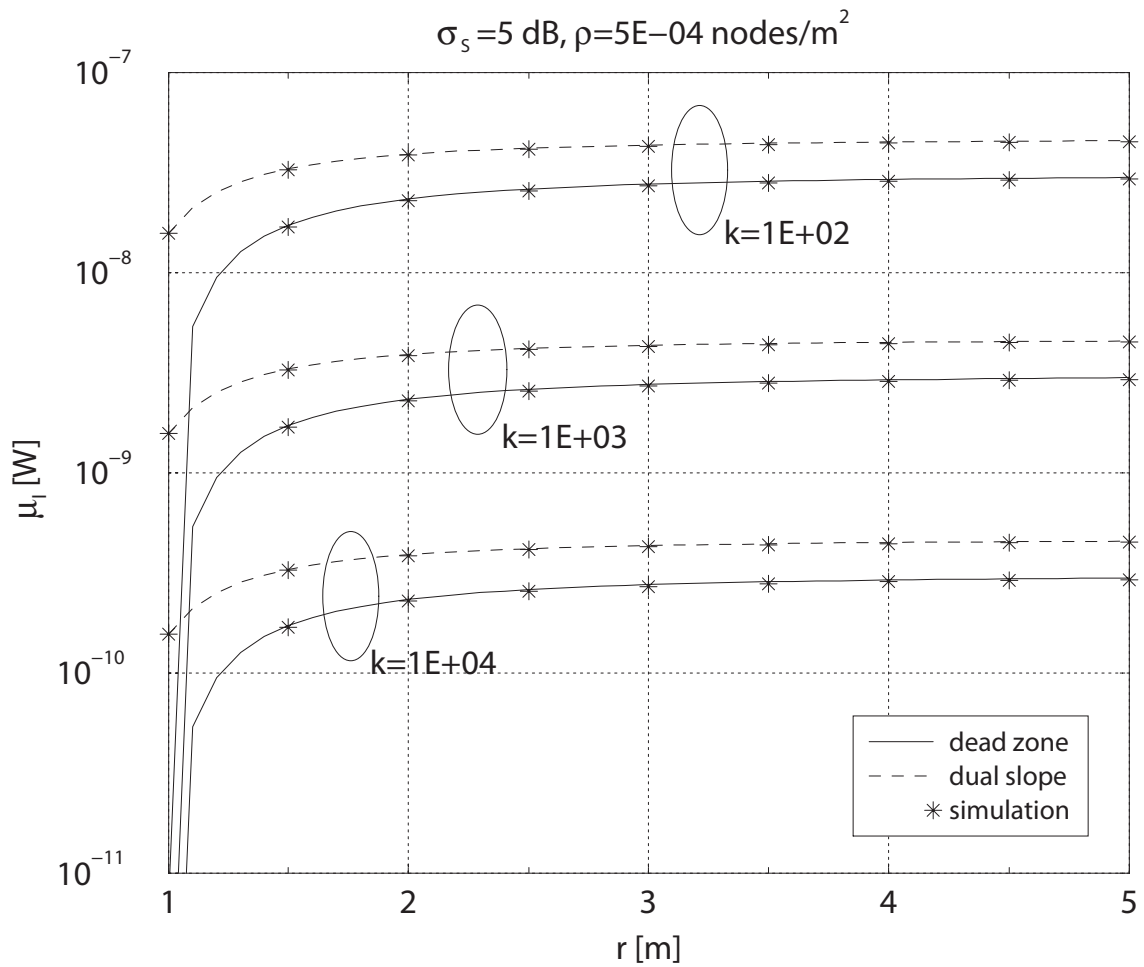


Figure 3.9: Scenario d):  $\mu_I$  as a function of  $r$  for different values of  $k$ . Comparison between *dead-zone* and *dual-slope* model.

## Chapter 4

# Achievable Rate of networks with multiple-antenna sinks

The increasing need for spectrally efficient techniques in decentralized wireless architectures (such as Ad Hoc and Sensor Networks) has led to the investigation of multiple antenna systems where the spectral efficiency is obtained exploiting spatial diversity [60, 61].

Bounds on the theoretical capacity achievable by wireless ad hoc networks have been recently obtained in [62] when the node location is known and in [63] when nodes are uniformly distributed in a  $d$ -dimensional region. The cooperation between nodes to obtain a *virtual* multiple-input-multiple-output (MIMO) relay network has been studied in [64].

The use of multiple antennas in these wireless networks has been also investigated in [42] where upper and lower bounds on the overall system capacity are given. In [42], the received power (averaged over fast fading fluctuations) on the antennas of the terminals is assumed to be random and i.i.d. The bounds given in [42], which become tight when the number of relaying

nodes approaches infinity, do not consider the specific statistical distribution of the received signal (only the hypothesis of i.i.d. is requested). In the case of wireless sensor networks (WSNs), the capacity of a sink in the presence of different tiers of sensors has been investigated in [65] but the final expression is written in terms of the mean (averaged over the fast fading) power received by the sensors which depends, in the absence of power control, by the sensors' location. The results in [42] and [65] reveal that the position of nodes and the connectivity aspects play an important role on the system performance. Several investigations have been carried out in the past years to address connectivity issues in wireless systems (see for instance [22–26, 66, 67]). Some of the previous papers (i.e. [22, 26, 66]), require that the channel gain has to be modelled as a deterministic distance-dependent function. With this model the random terms, such as shadowing and fast fading, which appear in many practical applications, cannot be taken into account. A different approach is used in [23–25, 67] where both shadowing and distance-dependent loss are considered.

In this Chapter we consider the WSN scenario illustrated in Fig.4.1, where the sink is equipped with multiple antennas and receives data from sensors whose position is distributed according to a Poisson point process (PPP) and derive the average (over the fading fluctuations and node position) achievable rate. A similar scenario is also considered in [68, 69].

We investigate a propagation environment characterized by a distance-dependent loss and lognormal shadowing. Rayleigh fading is also considered [65, 70, 71]. Under these assumptions, the number of sensors which communicate with the sink is not fixed a priori but depends on their location and on the propagation conditions. Similarly to the scenario considered in [47], we assume that the sink aims at collecting data from a specific region around it, so that no routing aspects have to be considered. In such a scenario only a subset of nodes (that is, those providing an acceptable signal level) can send information to the sink. The system made up by the sink and the sensor nodes can be seen as a multiple input multiple output scheme, where the number of transmitting antennas, in this case the sensors devices, is a random variable. Also, since sensors do not usually implement power control, in this equivalent MIMO system the values

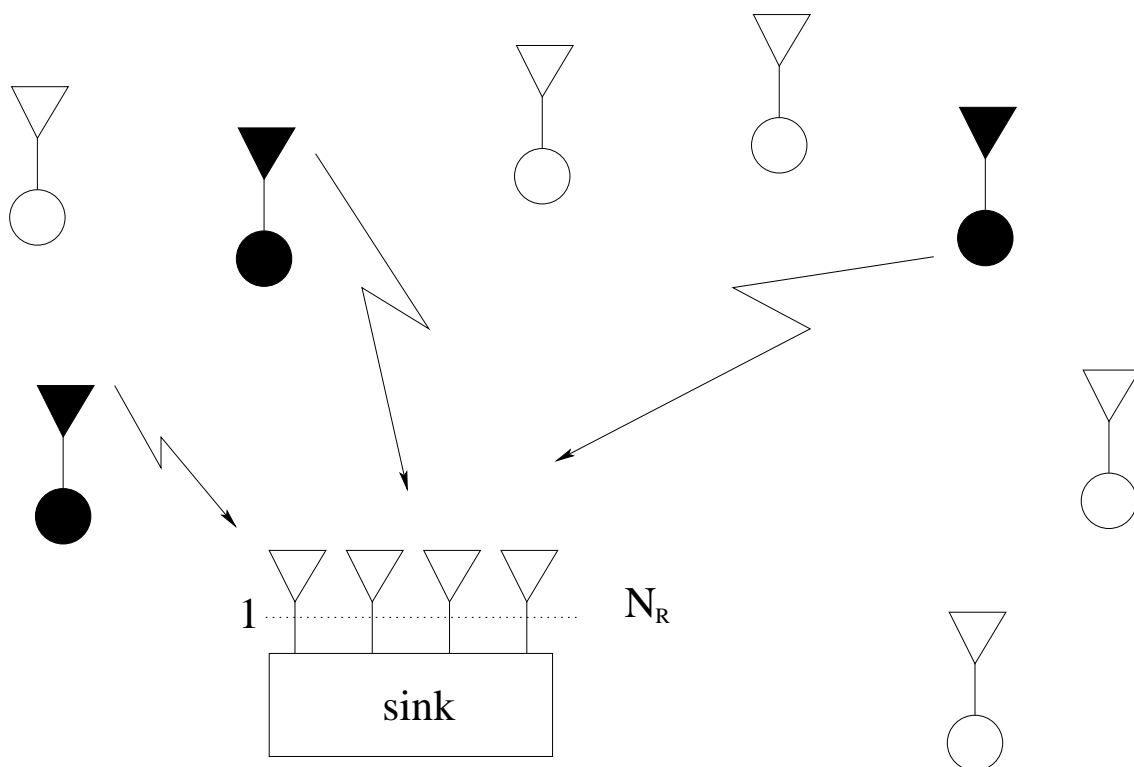


Figure 4.1: Scenario wireless sensor network with multi-antenna sink. Black sensors are those providing a power larger than a certain threshold.

of the received power (averaged over fast fading fluctuations) at the antennas of the sink is not deterministic owing to the randomness of the sensors' position and the presence of shadowing.

The main contributions of this Chapter can be summarized as follows:

- We give an expression for the achievable rate of a WSN in case the sink is equipped with multiple antennas and the position of sensors is random.
- We derive an expression for the distribution of the power (averaged over fast fading) received by the antennas of the sink when the position of the sensors is distributed according to a PPP.
- We obtain an expression for the average (over fast and slow fading fluctuations and sensors' position) achievable rate and investigate the impact on the performance of nodes' density, propagation parameters and correlation of the data emitted by the sensors.

The Chapter is organized as follows: in Section I we introduce the notation used in the Chapter and formalize the expression for the achievable rate. In Section II we derive an expression for the achievable rate conditioned on a given realization of the received powers at the sink, and discuss the role played by the correlation among data on the performance. Finally, in Section III we show some result.

## 4.1 System Description

### 4.1.1 Notations

Throughout the Chapter vectors and matrices are indicated by bold,  $\mathbf{A} > 0$  represents a positive-definite matrix,  $|\mathbf{A}|$  denotes the determinant of  $\mathbf{A}$ ,  $\{a_{i,j}\}_{i,j=1,\dots,M}$  is an  $M \times M$  matrix with elements  $a_{i,j} = \{\mathbf{A}\}_{i,j}$  and  $diag[\mathbf{a}]$  is a matrix whose elements are  $a_{i,i} = a_i$  for  $i = 1, \dots, M$  and 0 otherwise. The superscript  $\dagger$  denotes conjugation and transposition. Moreover, all the notations described in Chapter 2, Section 2.1, are assumed.

### 4.1.2 The scenario

The WSN scenario we consider in this Chapter is the same described in Chapter 2: it is characterized by an infinite plane where sensors are distributed according to a PPP with density  $\rho$ .

Let's consider communication between a single-antenna sensor and the sink (supervisor), which is supposed to be equipped with  $N_R$  antennas (see Fig. 4.1). As far as the propagation model is concerned, we assume that the ratio between the power transmitted by the  $j^{th}$  sensor ( $P_{T,j}$ ) and the power on the  $i^{th}$  receiving antenna of the sink ( $P_i$ ) is given by

$$\frac{P_{T,j}}{P_i} = k \cdot D_j^\beta \cdot S_j \cdot f_{i,j} \quad (4.1)$$

where  $k$  is a propagation coefficient,  $D_j$  is the distance between the sensor  $j$  and the sink<sup>1</sup>,  $\beta$  is the attenuation coefficient. Finally,  $S_j$  and  $f_{i,j}$  are the long-term (shadowing) and the short-term

---

<sup>1</sup>We assume that the distance between the antenna elements of the sink is negligible compared to the distance between the sensors and the sink.

(fast) fading components, respectively. Shadowing is assumed to be log-normally distributed, with  $S_j = 10^{\hat{S}_j/10}$  and  $\hat{S}_j \sim N(0, \sigma_S^2) \forall j$ . Rayleigh fading is considered, so  $f_{i,j}$  is exponentially distributed with unit mean. We assume also that shadowing coefficients are independent across transmitters, while fading coefficients (which depend upon both  $i, j$ ) are assumed independent across transmitters and receivers. Sensor networks do not usually implement power control, so even in this Chapter we assume that  $P_{T,j} = P_T \forall j$ . As in the previous we define  $L_j \triangleq kD_j^\beta S_j$  and  $G_j \triangleq 1/L_j$ ; they represent the averaged (with respect to the fast fading) power loss (in linear scale) and channel gain, respectively, in the link between the  $j^{\text{th}}$  sensor and the sink. We also define  $\bar{P}_j \triangleq P_T G_j$ , where  $\bar{P}_j$  represents the power received by the sink related to the  $j^{\text{th}}$  sensor averaged with respect to the fast fading. By introducing the logarithmic scale, we obtain (the index  $j$  is omitted for the sake of conciseness)

$$\begin{aligned} \hat{L} &= 10 \log_{10} k + 10\beta \log_{10} D + 10 \log_{10} S \\ &= \hat{k} + k_\beta \ln D + \hat{S} \end{aligned} \quad (4.2)$$

where  $k_\beta \triangleq \beta \frac{10}{\ln 10}$ .

Bit rate of the data streams emitted by sensors are usually quite low so that the fast fading components vary during the transmission period (i.e. the time spent to transmit a message). To obtain a reliable communication, the average (over the fast fading) power received by the sink has to be larger than the receiver sensitivity of the sink. So, when  $\bar{P}_j > P_{\text{Th}}$  (where  $P_{\text{Th}}$  is a suitable threshold as in the previous Chapters), we say that the sensor  $j$  communicates with the sink. We denote again by  $N$  the number of nodes providing the receiver with  $\bar{P} > P_{\text{Th}}$ , that is the r.v.  $N$  gives the number of nodes that can communicate with the receiver. The maximum number of nodes that the receiver can actually handle is obviously limited by the hardware equipment of the sink, we denote this number by  $N_E$ . For the sake of simplicity, in this Chapter we investigate the case  $N_E \leq N_R$ , however, the results presented herein can be easily extended to the case  $N_E > N_R$ . If  $N > N_E$  we assume the receiver selects  $N_E$  nodes (providing  $\bar{P} > P_{\text{Th}}$ ) regardless of their position with respect to the receiver. We therefore assume that the sink has the same probability to receive the acknowledgement message by the far and the close nodes.

As an example, a possible criterion for the choice of the sensors could be the following: only the first  $N_E$  nodes that send an acknowledgement message, regardless their position or the value of power received by the sink, are chosen. Note that, although this criterion does not consider the specific value of received power  $\bar{P}$  (which depends on the node's position), only the sensors providing  $\bar{P} > P_{Th}$  are taken into account. Other choices could be considered, for instance the receiver could select the  $N_E$  sensors providing the largest power among all the available. This latter choice may provide a better achievable rate but its analysis appears to be rather complicated and is left to subsequent studies.

### 4.1.3 System Model

The signal vector  $\mathbf{y}$  received by the sink can be written as

$$\mathbf{y} = \mathbf{H}\mathbf{P}\mathbf{b} + \mathbf{n} \quad (4.3)$$

where  $\mathbf{P} = \text{diag}[\bar{P}_1, \dots, \bar{P}_{N_{\min}}]$  with  $N_{\min} = \min\{N, N_E\}$ , the vector  $\mathbf{b}$  represents the symbols emitted by the  $N_{\min}$  sensors with  $\mathbb{E}\{b_j\} = 0$  and  $\mathbb{E}\{|b_j|^2\} = 1 \forall j = 1, \dots, N_{\min}$ . Correlation among the information carried by the sensors is taken into account by the covariance matrix  $\mathbf{B} = \mathbb{E}\{\mathbf{b}\mathbf{b}^\dagger\}$ .  $\mathbf{H}$  is an  $(N_R \times N_{\min})$  matrix whose complex element  $h_{i,j}$  represents the fast fading contribution ( $f_{i,j} = |h_{i,j}|^2$ ) in the link between the  $j^{\text{th}}$  node and the  $i^{\text{th}}$  receiving antenna. Based on the hypothesis of independence of the fast fading contributions, the elements of  $\mathbf{H}$  are modelled as i.i.d. Gaussian r.v.'s with zero-mean, independent real and imaginary parts with  $\mathbb{E}\{|h_{i,j}|^2\} = 1$ .  $\mathbf{n}$  is the thermal noise vector whose elements are modelled as zero-mean Gaussian r.v.'s with  $\mathbb{E}\{\mathbf{n}\mathbf{n}^\dagger\} = \sigma_n^2 \mathbf{I}$  and  $\mathbf{I}$  is the identity matrix.

Sensors are characterized by a reduced computation capability and the feedback between sink and sensors is generally minimized. Therefore we assume that channel state information is available only on the sink site (i.e. sensors transmit pilot sequences before the data stream). Under this conditions, the achievable rate  $R$  at the sink can be evaluated using the following well-known relation which gives the capacity of a MIMO system with  $N_{\min}$  transmitting and

$N_R$  receiving antennas [72]

$$R = \log_2 |\mathbf{I} + \mathbf{H}\mathbf{\Gamma}\mathbf{B}\mathbf{H}^\dagger| \quad (4.4)$$

where  $\mathbf{\Gamma} = \text{diag}[\bar{\gamma}]$ ,  $\bar{\gamma} = [\bar{\gamma}_1, \bar{\gamma}_2, \dots, \bar{\gamma}_{N_{\min}}]^T$  is the received signal-to-noise vector (averaged over the fast fading), where  $\bar{\gamma}_j = \bar{P}_j/\sigma_n^2$  is the average signal-to-noise ratio due the  $j^{\text{th}}$  sensor.

It is worth noting that the  $N_{\min}$  elements of  $\bar{\gamma}$  are randomly chosen over the ensemble of  $N$ .

#### 4.1.4 The Achievable Rate

After some algebra the expression for the achievable rate can be written as [72]

$$R = \sum_{i=1}^{N_{\min}} \log_2 (1 + \lambda_i) \quad (4.5)$$

where  $\lambda_1, \dots, \lambda_{N_{\min}}$  are the nonzero eigenvalues of  $\mathbf{H}\mathbf{E}\mathbf{H}^\dagger$ , with  $\mathbf{E} = \mathbf{\Gamma}\mathbf{B}$ . Starting from (4.5), the mean achievable rate (averaged over the position of the nodes and of the fading value) becomes

$$\begin{aligned} \mu_R &= \mathbb{E}_{N_{\min}, \lambda} \left\{ \sum_{i=1}^{N_{\min}} \log_2 (1 + \lambda_i) \right\} \\ &= \mathbb{E}_{N_{\min}} \left\{ \mathbb{E}_{\lambda} \left\{ \sum_{i=1}^{N_{\min}} \log_2 (1 + \lambda_i) \right\} \right\} \\ &= \mathbb{E}_{N_{\min}} \left\{ \mathbb{E}_{\mathbf{E}} \left\{ \mathbb{E}_{\lambda_{|\mathbf{\Gamma}}} \left\{ \sum_{i=1}^{N_{\min}} \log_2 (1 + \lambda_{i|\mathbf{\Gamma}}) \right\} \right\} \right\} \\ &= \mathbb{E}_{N_{\min}} \left\{ N_{\min} \mathbb{E}_{\mathbf{E}} \left\{ \mathbb{E}_{\lambda_{|\mathbf{E}}} \left\{ \log_2 (1 + \lambda_{|\mathbf{E}}) \right\} \right\} \right\} \end{aligned} \quad (4.6)$$

where  $\lambda_{|\mathbf{E}}$  represents an unordered eigenvalue of  $\mathbf{H}\mathbf{E}\mathbf{H}^\dagger$  for a given realization of the random matrix  $\mathbf{E}$  and of  $N_{\min}$ .

Expression (4.6) shows that the mean achievable rate in the scenario of Fig.4.1 can be obtained by means of the average over the fast fading channel ensemble, followed by the average over the matrix  $\mathbf{E}$ , which takes distance-dependent loss and shadowing into account. Furthermore, as the number of nodes that communicate with the receiver is a r.v. too, the expression for the achievable rate has to be averaged over this number.

Expression (4.6) can be further simplified to obtain

$$\begin{aligned} \mu_R &= \sum_{n=1}^{N_E-1} \mathbb{P}\{N = n\} n \mathcal{E}(n) \\ &+ N_E \mathcal{E}(N_E) \left( 1 - \sum_{n=0}^{N_E-1} \mathbb{P}\{N = n\} \right) \end{aligned} \quad (4.7)$$

where  $\mathcal{E}(n) \triangleq \mathbb{E}_{\mathbf{E}}\{\Upsilon(n, \mathbf{E})\}$ ,  $\Upsilon(n, \mathbf{E}) \triangleq \mathbb{E}_{\lambda_{|\Gamma}}\{\log_2(1 + \lambda_{|\Gamma})\}$ ,  $\mathbf{E}$  is now a  $(n \times n)$  matrix with  $\Gamma = \text{diag}[\bar{\gamma}_1, \bar{\gamma}_2, \dots, \bar{\gamma}_n]^T$ .

Note that, since  $\mathbf{E} = \Gamma \mathbf{B}$  and  $\mathbf{B}$  is deterministic,  $\mathbb{E}_{\mathbf{E}}\{\Upsilon(n, \mathbf{E})\} = \mathbb{E}_{\Gamma}\{\Upsilon(n, \Gamma \mathbf{B})\}$ . This means that, to evaluate  $\mathcal{E}(n)$  we do not need the distribution of  $\mathbf{E}$ , but we can use the joint distribution of  $\bar{\gamma}_1, \bar{\gamma}_2, \dots, \bar{\gamma}_n$  conditioned on  $N = n$ .

To summarize, the evaluation of  $\mu_R$ , requires the investigation of the following terms:

- $\Upsilon(n, \mathbf{E})$ , which will be addressed in Section II.
- $\Pr\{N = n\}$ , and the joint distribution of  $\bar{\gamma}_1, \bar{\gamma}_2, \dots, \bar{\gamma}_n$  conditioned on  $N = n$ , which have been discussed and derived in Section 2.2.

## 4.2 Evaluation of the Achievable Rate

### 4.2.1 Evaluation of $\Upsilon(n, \mathbf{E})$

In the case of Rayleigh fading channel, the elements of  $\mathbf{H}$  are i.i.d Gaussian rv's and the distribution of the eigenvalues of  $\mathbf{H}\mathbf{E}\mathbf{H}^\dagger$  can be obtained by using the theory of the Wishart matrices (see for instance [73, 74]). In particular, the distribution of the ordered nonzero eigenvalues  $\zeta_{(1)}, \dots, \zeta_{(q)}$  (with  $\zeta_{(1)} > \dots > \zeta_{(q)}$ ) of  $\mathbf{Z} = \mathbf{X}\mathbf{A}\mathbf{X}^\dagger$ , when  $\mathbf{X}$  is a  $(p \times q)$  matrix, with  $q \leq p$ , whose elements are i.i.d complex Gaussian samples, and  $\mathbf{A}$  is a deterministic  $(q \times q)$  matrix with distinct nonzero eigenvalues  $\alpha_{(1)}, \dots, \alpha_{(q)}$  (with  $\alpha_{(1)} > \dots > \alpha_{(q)}$ ) can be written as [75]

$$f_{\zeta}(\mathbf{x}) = K |\mathbf{E}(\mathbf{x}, \boldsymbol{\alpha})| \cdot |\mathbf{V}_q(\mathbf{x})| \prod_{i=1}^q x_i^{p-q} \quad (4.8)$$

where

$$K = \frac{|\mathbf{A}|^{-p}}{\Gamma_q(p) |\mathbf{W}_q(\boldsymbol{\alpha})|} \quad (4.9)$$

$\mathbf{V}_q(\mathbf{x}) = \{x_j^{i-1}\}_{i,j}$  is a  $(q \times q)$  Vandermonde matrix,  $\mathbf{W}_q(\boldsymbol{\alpha}) = \{(-\alpha_j)^{1-i}\}_{i,j}$ ,  $\mathbf{E}(\mathbf{x}, \boldsymbol{\alpha}) = \{e^{-x_j/\alpha_i}\}_{i,j}$ ,  $\Gamma_q(p) \triangleq \prod_{i=1}^q (p-i)!$ .

The pdf of the generic unordered eigenvalue  $\zeta$  can be derived starting from the joint pdf of the eigenvalues

$$f_\zeta(x_1) = \int_0^\infty \int_0^\infty \dots \int_0^\infty \frac{f_\zeta(\mathbf{x})}{q!} dx_q \dots dx_3 dx_2. \quad (4.10)$$

The previous expression seems to be cumbersome but can be simplified by using the following Theorem:

**Theorem 4.1**

Let  $\Phi(\mathbf{x}) = \{\phi_i(x_j)\}_{i,j}$  and  $\Psi(\mathbf{x}) = \{\psi_i(x_j)\}_{i,j}$  be two  $(M \times M)$  matrices and  $\xi(x)$  a generic function.

The following identity holds

$$\int_a^b \dots \int_a^b \int_a^b |\Phi(\mathbf{x})| \times |\Psi(\mathbf{x})| \prod_{l=1}^M \xi(x_l) dx_M dx_{M-1} \dots dx_2 = (M-1)! \sum_{s=1}^M \sum_{m=1}^M (-1)^{s+m} \phi_s(x_1) \psi_m(x_1) \xi(x_1) \left| \left\{ \int_a^b \phi_{r_{i,s}}(x) \psi_{r_{j,m}}(x) \xi(x) dx \right\}_{i,j} \right|, \quad (4.11)$$

where  $a$  and  $b$  are two arbitrary numbers, the matrices in (4.11) are  $(M-1 \times M-1)$  and

$$r_{s,m} \triangleq \begin{cases} s & \text{if } s < m \\ s+1 & \text{if } s \geq m \end{cases}. \quad (4.12)$$

*Proof:* See [76].

Since the joint pdf of the eigenvalues of  $\mathbf{Z}$  in (4.8) is in the form

$$f_\zeta(\mathbf{x}) = K |\Phi(\mathbf{x})| \times |\Psi(\mathbf{x})| \prod_{l=1}^q \xi(x_l), \quad (4.13)$$

the application of Theorem 4.1 with  $a = 0$  and  $b \rightarrow \infty$  gives

$$f_\zeta(x) = (q-1)! K \sum_{s=1}^q \sum_{m=1}^q (-1)^{s+m} \phi_s(x) \psi_m(x) \xi(x) \left| \left\{ \int_0^\infty \phi_{r_{i,s}}(u) \psi_{r_{j,m}}(u) \xi(u) du \right\}_{i,j} \right| \quad (4.14)$$

Expression (4.14) can be specialized to the case of interest by substituting  $q = n$ ,  $p = N_R$ ,  $\phi_i(x_j) = x_j^{i-1}$ ,  $\psi_i(x_j) = e^{-x_j/\eta_i}$ , where  $\eta_i$  (with  $i = 1, \dots, n$ ) are the unordered nonzero eigenvalues of the matrix  $\mathbf{E}$ , and  $\xi(x) = x^{N_R-n}$ , to obtain

$$f_{\lambda|\mathbf{E}}(x_1) = \frac{K}{n} \sum_{s=1}^n \sum_{m=1}^n \left| \left\{ (\eta_{r_{j,m}})^{N_{\mathbf{R}}-n+r_{i,s}} (N_{\mathbf{R}} - n + r_{i,s} - 1)! \right\}_{i,j} \right| (-1)^{s+m} x_1^{N_{\mathbf{R}}-n+s-1} e^{-x_1/\eta_m}. \quad (4.15)$$

By using (4.15) to calculate  $\mathbb{E}_{\lambda|\Gamma} \{ \log_2 (1 + \lambda|\Gamma) \}$ , we obtain

$$\begin{aligned} \Upsilon(n, \mathbf{E}) &= \frac{K}{n} \sum_{s=1}^n \sum_{m=1}^n \left| \left\{ \eta_{r_{j,m}}^{N_{\mathbf{R}}-n+r_{i,s}} (N_{\mathbf{R}} - n + r_{i,s} - 1)! \right\}_{i,j} \right| (-1)^{s+m} \quad (4.16) \\ &\times \int_0^{\infty} \log_2(1+x) x^{N_{\mathbf{R}}-n+s-1} e^{-x/\eta_m} dx \\ &= \frac{K}{n \ln 2} \sum_{s=1}^n \sum_{m=1}^n \left| \left\{ \eta_{r_{j,m}}^{N_{\mathbf{R}}-n+r_{i,s}} (N_{\mathbf{R}} - n + r_{i,s} - 1)! \right\}_{i,j} \right| (-1)^{s+m} \\ &\times (N_{\mathbf{R}} - n + s - 1)! e^{1/\eta_m} \sum_{k=1}^{N_{\mathbf{R}}-n+s} \eta_m^k \Gamma(k - N_{\mathbf{R}} + n - s, 1/\eta_m), \end{aligned}$$

where

$$K = \frac{(-1)^{n(n-1)/2}}{\Gamma_n(N_{\mathbf{R}}) |\mathbf{W}_n(\boldsymbol{\eta})| \left( \prod_{i=1}^n \eta_i^{N_{\mathbf{R}}} \right)}, \quad (4.17)$$

with  $\boldsymbol{\eta} = [\eta_1, \dots, \eta_n]^T$ . To simplify the integral in (4.16), we have used the following identity [77, eq. (78)]

$$\int_0^{\infty} \ln(1+x) x^{a-1} e^{-dx} dx = (a-1)! e^d \sum_{k=1}^a \frac{\Gamma(-a+k, d)}{d^k}, \quad (4.18)$$

where  $\Gamma(\alpha, x)$  is the incomplete Gamma function [44, pp. 949, 8.350.2]. Eq. (4.16) gives the achievable rate averaged over fast fading of the system depicted in Fig.4.1 when the number of sensors able to communicate with the sink is  $n$  ( $n \leq N_{\mathbf{R}}$ ) with signal-to-noise ratios given by  $[\bar{\gamma}_1, \bar{\gamma}_2, \dots, \bar{\gamma}_n]^T$ . Note that the previous expression gives also the achievable rate of a  $n \times N_{\mathbf{R}}$  MIMO system with arbitrary transmission power and can be seen as an alternative expression for [75, eq. (36)], which gives the achievable rate of a MIMO system with equal power transmission but correlated fading among the received antennas.

In the case of  $N_{\mathbf{E}} < N_{\mathbf{R}}$ , the distribution of the eigenvalues of  $\mathbf{H}\mathbf{E}\mathbf{H}^\dagger$  is related to that of a singular Wishart matrix [78]. The use of the expression for the joint pdf of the eigenvalues of a singular Wishart given in [78, eq. (23)], jointly with the results given in Theorem 1 leads to an

expression for  $\Upsilon(n, \mathbf{E})$  for the case  $N_E < N_R$ . The expression is not given here for the sake of conciseness.

In the case  $N_E = 1$ , that is when only one sensor can communicate with the sink,  $\Upsilon(1, \mathbf{B}\Gamma)$  can be simplified as

$$\Upsilon(1, \mathbf{B}\Gamma) = \frac{1}{\eta_1^{N_R} \ln 2} e^{1/\eta_1} \sum_{k=1}^{N_R} \eta_1^k \Gamma(k - N_R, 1/\eta_1).$$

### 4.2.2 Evaluation of $\mathcal{E}(n)$

As discussed previously, the evaluation of the expectations in (4.7) requires the knowledge of the distribution of  $N$  (to evaluate  $\mathbb{P}\{N = n\}$ ) and the joint distribution of  $\bar{\gamma}_1, \bar{\gamma}_2, \dots, \bar{\gamma}_n$  conditioned on  $N = n$ .

The distribution of  $N$  in the scenario of interest has been already obtained in [67], and it has been discussed in Section 2.2 (see equations (2.3) and (2.11)).

By recalling some result from Chapter 2, remembering that  $\bar{\gamma} = \left(\frac{P_T}{\sigma_n^2}\right) T^{-\beta/2}$ , and using the general rule for the distribution of functions of r.v.'s [43], we get the distribution of  $f_{\bar{\gamma}}(x)$

$$f_{\bar{\gamma}}(x) = \begin{cases} \frac{2}{\beta(L_T^{2/\beta} - k^{2/\beta})} \left(\frac{P_T}{\sigma_n^2}\right)^{2/\beta} \frac{1}{x^{1+2/\beta}} & x \in \left[\frac{P_T}{\sigma_n^2 L_T}, \frac{P_T}{\sigma_n^2 k}\right] \\ 0 & \text{otherwise} \end{cases} \quad (4.19)$$

whose cdf is given by

$$F_{\bar{\gamma}}(x) = \begin{cases} 0 & \text{otherwise} \\ \frac{\left(\frac{P_T}{\sigma_n^2}\right)^{2/\beta}}{L_T^{2/\beta} - k^{2/\beta}} \left(\frac{P_T}{\sigma_n^2 L_T}^{-2/\beta} - \frac{1}{x^{2/\beta}}\right) & x \in [1/L_T, 1/k] \end{cases}, \quad (4.20)$$

and the distributions of  $\bar{\gamma}_1, \dots, \bar{\gamma}_n$  conditioned on  $N = n$ :

$$f_{n, \bar{\gamma}_1, \dots, \bar{\gamma}_n}(x_1, \dots, x_n) = \prod_{i=1}^n f_{\bar{\gamma}}(x_i). \quad (4.21)$$

Using (4.21), we can write  $\mathcal{E}(n)$  as a function of  $f_{\bar{\gamma}}(x)$  as follows

$$\begin{aligned} \mathcal{E}(n) &= \mathbb{E}_{\Gamma}\{\Upsilon(n, \mathbf{B}\Gamma)\} \\ &= \int_{\frac{P_T}{\sigma_n^2 L_T}}^{\frac{P_T}{\sigma_n^2 k}} \int_{\frac{P_T}{\sigma_n^2 L_T}}^{\frac{P_T}{\sigma_n^2 k}} \dots \int_{\frac{P_T}{\sigma_n^2 L_T}}^{\frac{P_T}{\sigma_n^2 k}} \Upsilon(n, \mathbf{B}\Gamma) \prod_{i=1}^n f_{\bar{\gamma}}(x_i) dx_1 \dots dx_{n-1} dx_n, \end{aligned} \quad (4.22)$$

where  $\Upsilon(n, \mathbf{E})$  and  $f_{\bar{\gamma}}(x)$  are given by (4.16) and (2.14), respectively. To evaluate the achievable rate  $\mu_R$ , we substitute (4.22) in (4.7) and recall that  $\mathbb{P}\{N = n\} = \frac{e^{-\mu_N} \mu_N^n}{n!}$  (where  $\mu_N$  is given by (2.11)).

### 4.2.3 Spatial Correlation model

Several models could be considered to characterize the spatial correlation among sensors [79], generally correlation tends to be a decreasing function of the inter-sensor distance [80]. As shown in the previous Sections, in this Chapter we consider sensors having a random position and without a specific indexing based on their reciprocal position. With this model, the distance between sensors 1 and 2 could be larger than that between sensors 1 and 4. This justifies the use of the following correlation model

$$\{\mathbf{B}\}_{i,j} = \begin{cases} 1 & i = j \\ \rho_C & i \neq j \end{cases} \quad (4.23)$$

where the coefficient  $\rho_C$ , ranging from 0 to 1, does not depend on the specific value of the indexes  $i$  and  $j$  (except, obviously, in the case  $i = j$  whose value is 1). Note that equation (4.16) holds only when the coefficients  $\eta_1, \dots, \eta_n$  are all distinct, in the case two (or more) coefficients are identical we can use the general methodology proposed in [81] to obtain the specific expression for (4.8). On the other hand, when  $N_E = 2$  (the case  $N_E = 1$  is trivial as correlation does not play any role), the model described by (4.23) leads to

$$\begin{aligned} \eta_1 &= \frac{1}{2} \left( \bar{\gamma}_1 + \bar{\gamma}_2 + \sqrt{(\bar{\gamma}_1^2 - \bar{\gamma}_2^2)^2 + 4\bar{\gamma}_1\bar{\gamma}_2\rho_C} \right) \\ \eta_2 &= \frac{1}{2} \left( \bar{\gamma}_1 + \bar{\gamma}_2 - \sqrt{(\bar{\gamma}_1^2 - \bar{\gamma}_2^2)^2 + 4\bar{\gamma}_1\bar{\gamma}_2\rho_C} \right). \end{aligned} \quad (4.24)$$

In that case, the condition  $\eta_1 = \eta_2$  is satisfied only if

$$\bar{\gamma}_1 = \bar{\gamma}_2 \left( 1 - 2\rho_C \left( \rho_C \pm \sqrt{\rho_C^2 - 1} \right) \right), \quad (4.25)$$

but since  $\rho_C \leq 1$ , eq. (4.25) does not have any solution (with the only exception of the case  $\rho_C = 0$ ) in the set of the nonnegative real numbers. Note also that if  $\bar{\gamma}_1$  and  $\bar{\gamma}_2$  take nonnegative values,  $\eta_1$  and  $\eta_2$  are also nonnegative for any value of  $\rho_C \in [0, 1)$ . In the case  $\rho_C = 1$  we have  $\eta_2 = 0$  and the methodology proposed in [81] can be applied.

### 4.3 Achievable Rate analysis: numerical results

To obtain the results about the achievable rate of the scenario of Fig. 4.1, we have fixed  $N_E = 2$  and  $\sigma_n^2 = 6.3 \cdot 10^{-11}W$  and evaluated (4.22) numerically. As a matter of fact, this expression is exact and valid for arbitrary numbers of receiving antennas but requires the evaluation of nested  $N_E$ -fold integrals that appear to be unsolvable in closed-form. To give an idea of the amount of time needed for  $N_E=2$ , the computation of (4.22) on a 1.7 GHz Personal Computer requires a few seconds. Obviously, the case  $N_E = 3$  requires more computational time (about 10 minutes).

Fig. 4.2 shows the mean achievable rate ( $\mu_R$ ) as a function of the transmitted power ( $P_T$ ) for different values of the receiving antennas, ranging from 1 to 6. The density of sensors is equal to  $5 \cdot 10^{-4}node/m^2$ ,  $\sigma_S = 5dB$  and  $\rho_C = 0.5$ . As expected, large values of  $P_T$  increase the mean achievable rate, the same behavior can be observed when more antennas are added to the receiver. The spread between the curves corresponding to  $N_R = 1$  and  $N_R = 6$  increases for large values of  $P_T$ . Note that, since we are considering the condition  $N_R \geq N_E$ , in the case  $N_R = 1$  we have fixed  $N_E = 1$ .

Fig. 4.3 shows the mean achievable rate as a function of the density of the sensors ( $\rho$ ) for different values of  $N_R$ ,  $P_T = 0.1 W$ ,  $\rho_C = 0.7$  and again  $\sigma_S = 5 dB$ . The figure shows that the mean value of the achievable rate tends to saturate for large values of  $\rho$ . This can be explained by recalling that the pdf of the signal-to-noise ratio  $\bar{\gamma}$  does not depend on  $\rho$  (as shown in Section 2.2 it depends only on  $\beta$ ,  $k$  and  $L_T$ ), so  $\rho$  has an impact only on the probabilities that  $N = 1$  and  $N \geq 2$ , these values do not change significantly for large values of  $\rho$ .

Fig. 4.4 shows the mean achievable rate as a function of  $P_T$  for different values of the standard deviation of shadowing with  $\rho = 5 \cdot 10^{-5}nodes/m^2$  and  $\rho_C = 0.7$ . We can observe that the effect of the standard deviation of shadowing is negligible for small values of  $P_T$ . This is due to the fact that  $\sigma_S$  has an impact only on  $\mathcal{P}\{N = n\}$  and with a density of  $\rho = 5 \cdot 10^{-5}nodes/m^2$  the probabilities that  $N = 1$  and  $N \geq 2$  are only partially effected by a variation of  $\sigma_S$ . As shown in [23],  $\sigma_S$  increases the average number of nodes that can communicate with the receiver, this justifies the largest value of  $\mu_R$  when  $\sigma_S$  increases.

Finally, the role played by the correlation coefficient  $\rho_C$  is investigated in Fig.4.5, which shows  $\mu_R$  as a function of  $\rho_C$  for different values of  $P_T$ . As expected, increasing values of  $\rho_C$  cause a reduction in terms of  $\mu_R$ . However, this effect is limited to small values of  $P_T$ . This can be justified by observing (4.25) which shows that, in the case  $N_E = 2$ ,  $\eta_1$  and  $\eta_2$  are weakly dependent on  $\rho_C$  (for values of  $\rho_C$  ranging from 0 to 1).

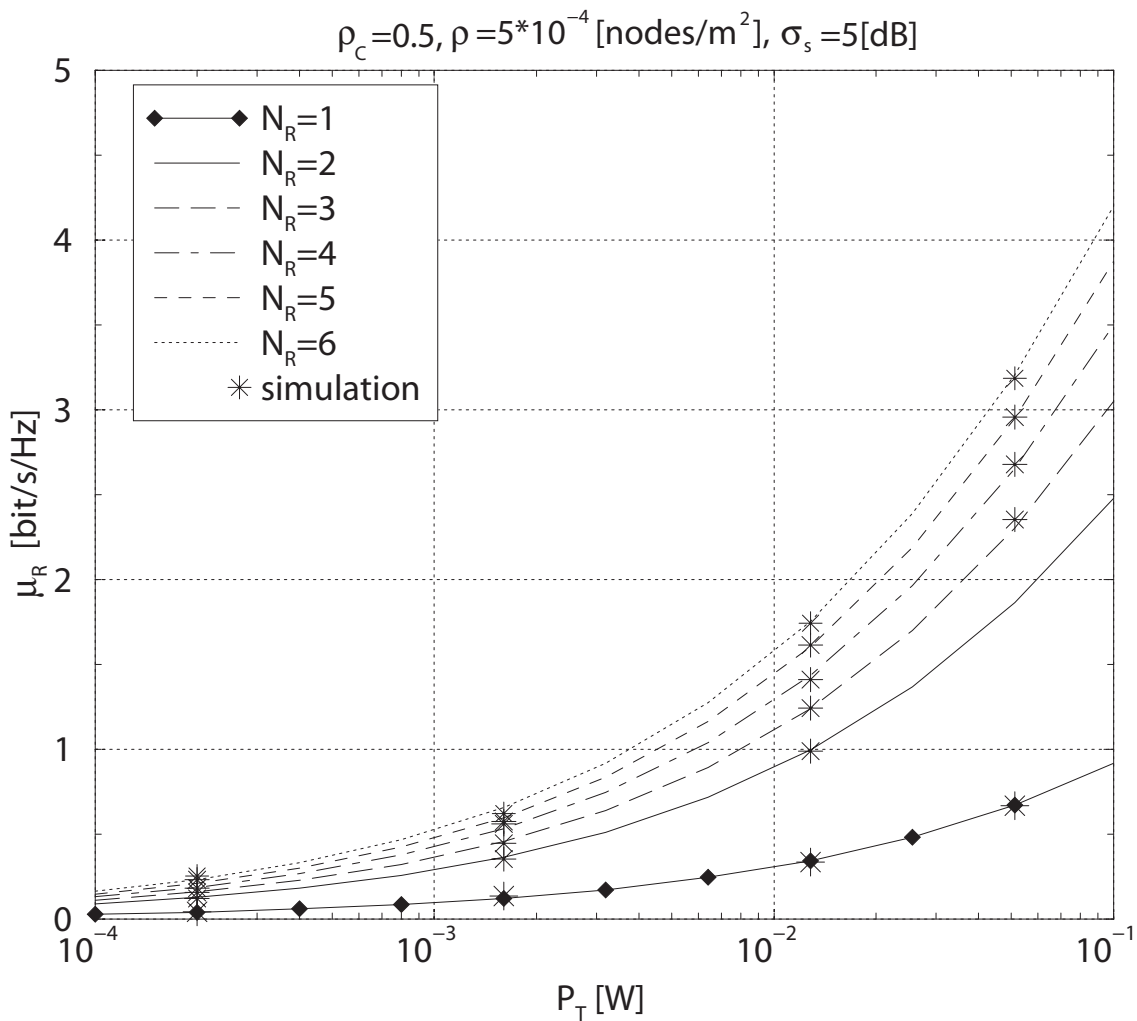


Figure 4.2:  $\mu_R$  as a function of  $P_T$  for different values of  $N_R$ :  $\rho = 5 \cdot 10^{-4} \text{ nodes/m}^2$ ,  $\rho_C = 0.5$ ,  $\sigma_s = 5 \text{ dB}$ .

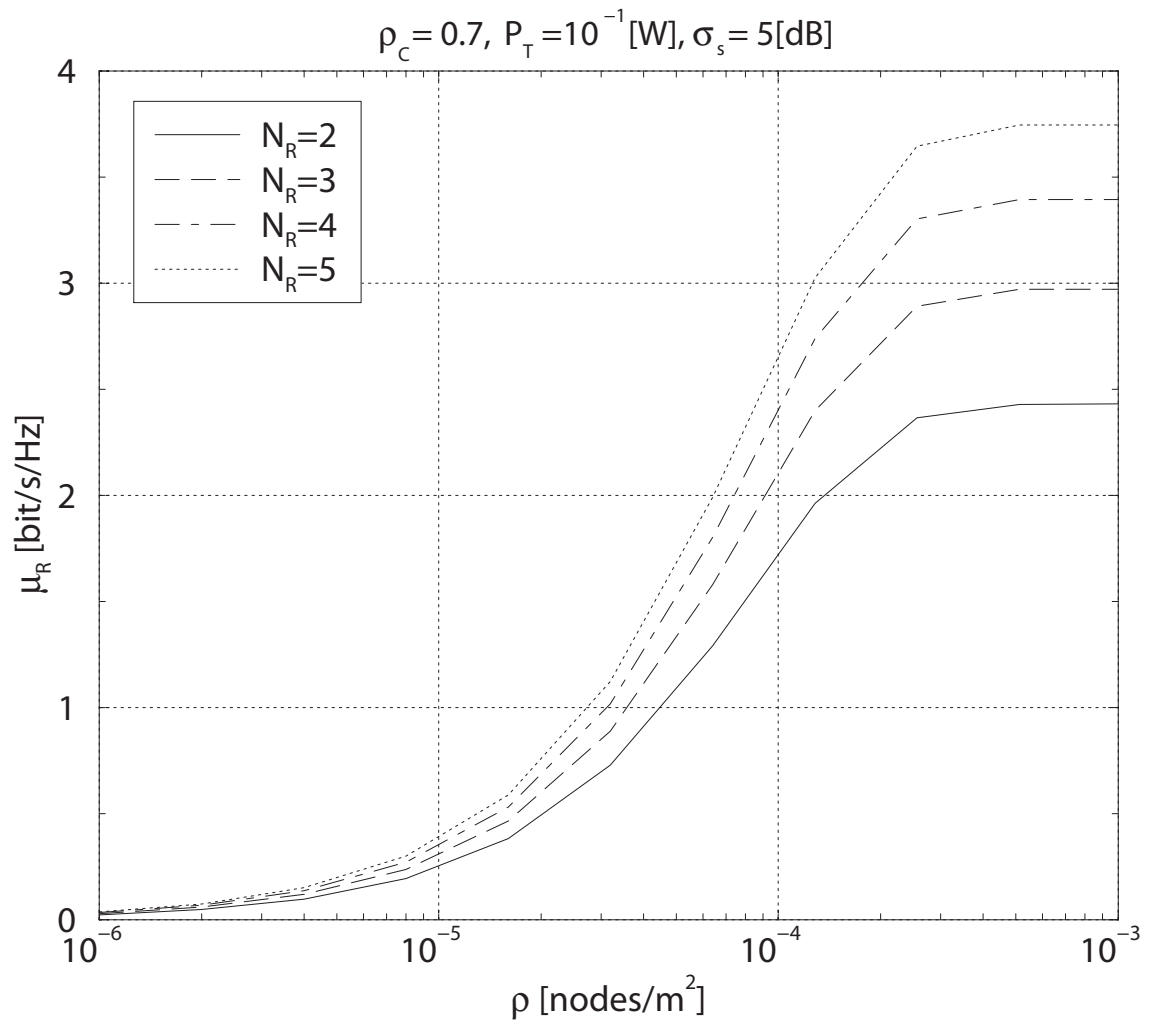


Figure 4.3:  $\mu_R$  as a function of  $\rho$  for different values of  $N_R$ :  $P_T = 10^{-1} \text{W}$ ,  $\rho_C = 0.7$ ,  $\sigma_S = 5 \text{dB}$ .

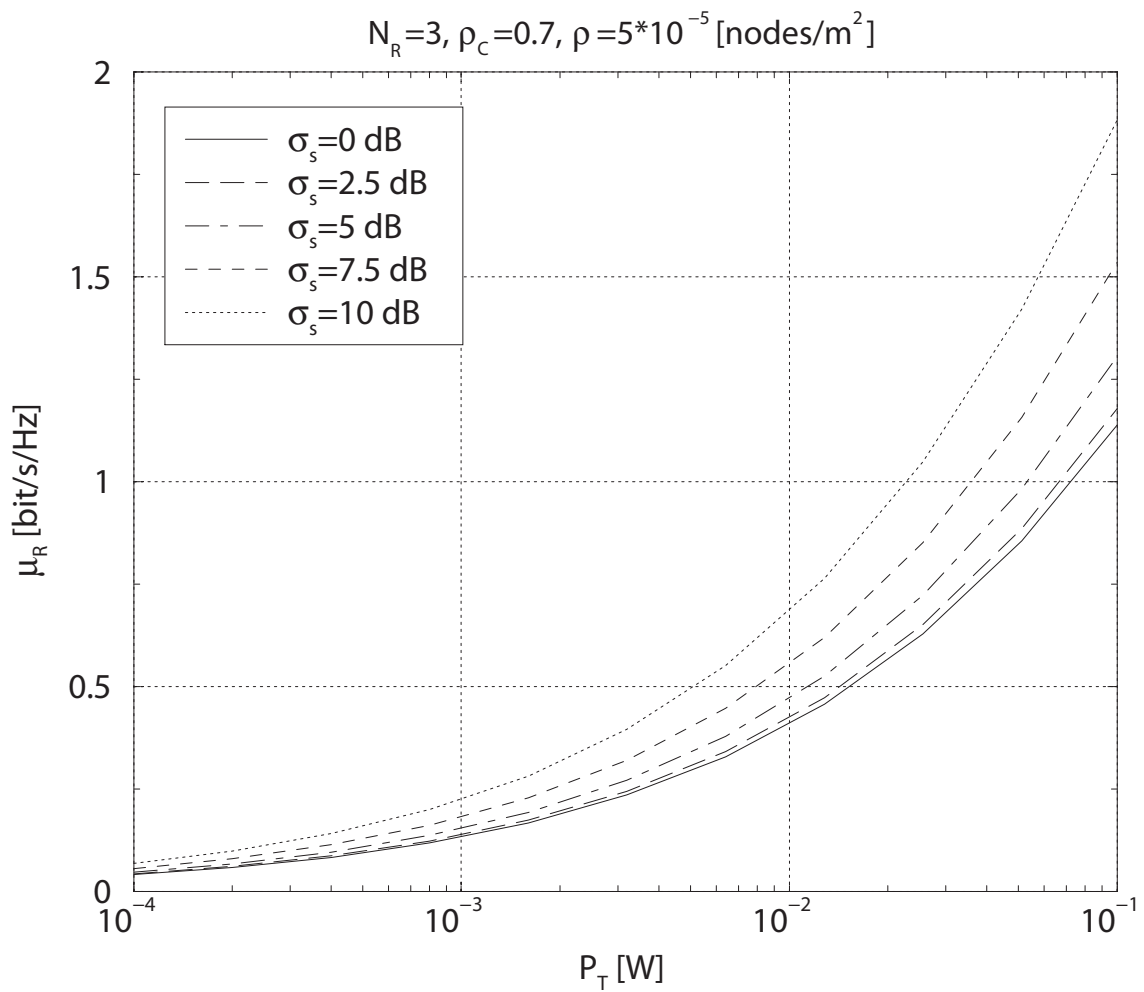


Figure 4.4:  $\mu_R$  as a function of  $P_T$  for different values of  $\sigma_S$ :  $\rho = 5 \cdot 10^{-5} \text{nodes}/\text{m}^2$ ,  $\rho_C = 0.7$ ,  $N_R = 3$ .

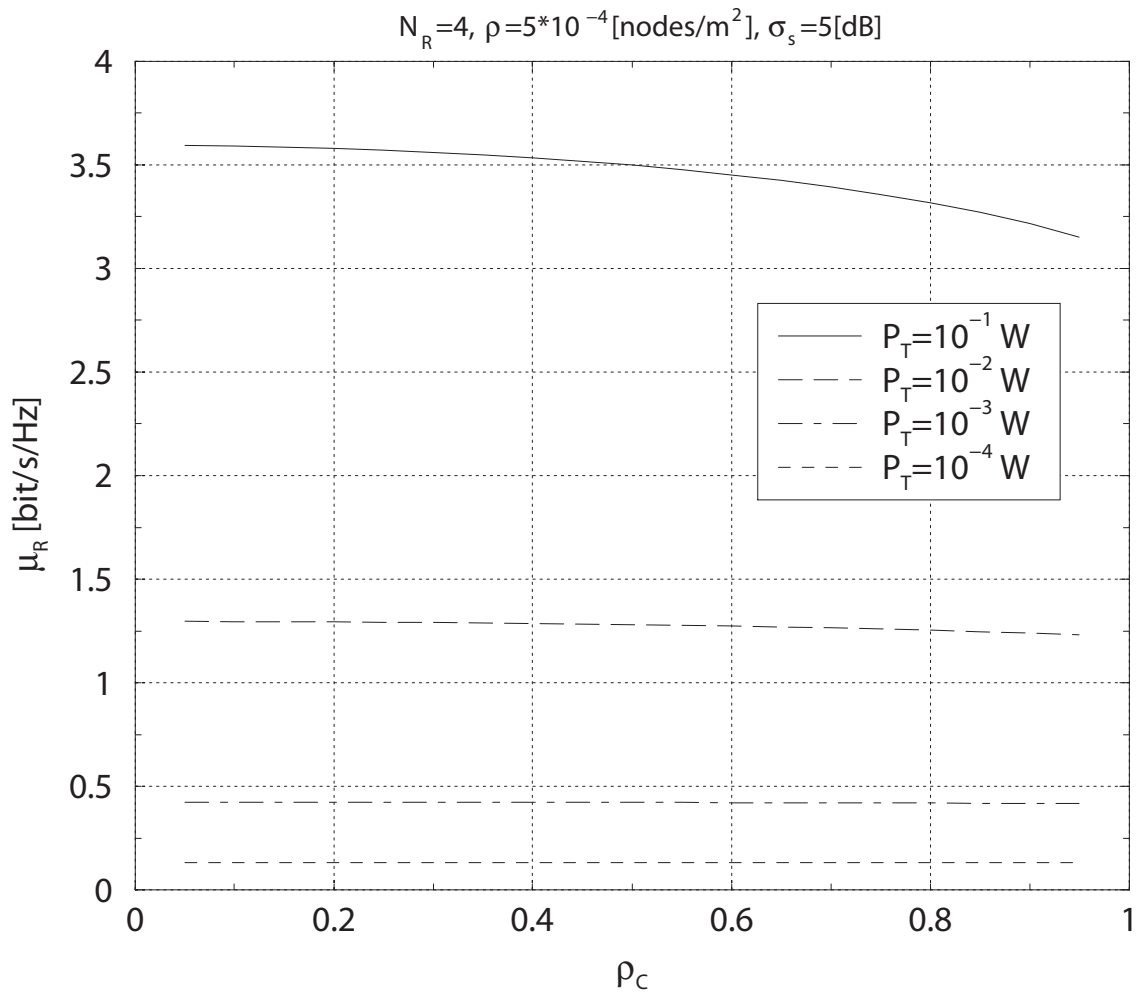


Figure 4.5:  $\mu_R$  as a function of  $\rho_C$  for different values of  $P_T$ :  $\rho = 5 \cdot 10^{-4} \text{nodes}/\text{m}^2$ ,  $N_R = 4$ ,  $\sigma_s = 5\text{dB}$ .



## **Chapter 5**

# **Experimental Activity: development and performance evaluation of a Multi-Hop IEEE802.15.4 Wireless Sensor Network**

This Chapter is dedicated to a case study: performance evaluation of a real-world applications of WASNs. Within the Project carried out since June 2005 for two years at Wilab in cooperation with the Italian SME (Small Medium Enterprise) SADEL, an application scenario denoted as TCS (Tracking and Communication System) was investigated. IEEE802.15.4 at 2.4 GHz ([82]) was considered a candidate technology, owing to the requirement of low cost devices and the need to transmit few bytes per second from each source, a condition that can be met with IEEE802.15.4 devices.

## 5.1 TCS Application Scenario

### 5.1.1 Description and Requirements

The application scenario includes:

- a large number (in the order of tens) of IEEE802.15.4 nodes deployed in a bounded environment (such as an airport, or a railway station) and connected to a backbone network using separate techniques, possibly wired (e.g. Ethernet),
- a large number of mobile devices (in the order of hundreds) equipped with several types of sensors, transmitting through multiple hops their data, taken with a frequency of 1 Hz, to any infrastructure node.

The TCS application scenario includes nodes that move in an environment whose geometry is well known, at low speed, and whose location needs to be continuously tracked. To this purpose, the mobile nodes are equipped with self-localization techniques (such as GPS, Global Positioning System, if outdoor) and they need to report their current position to the infrastructure every second. The nodes might also measure some physical properties of the environment they are travelling, such as temperature, etc, also reporting every second the data measured. Examples of this scenarios are railway stations, where the nodes to be tracked are trolleys used by passengers to carry their own luggage, or the external part of airports, where the mobile nodes are the vehicles carrying food, gasoline, people, etc to the aircraft from the buildings and viceversa; in the airport case, the mobiles might reach speed of around 75 Kmh.

The infrastructure is composed of wireless nodes, located in fixed and properly planned positions in the environment; they all forward the data gathered to a single server, through a separate backbone network. As a result, the mobile nodes can report their data to any sinks in the area. A mobile node might reach the infrastructure through direct links, or multiple hops. However, apart from the data received from the mobile nodes, the infrastructure nodes do not exchange information about their configurations with the other nodes through the backbone

network. Therefore, all radio resource management issues are completely distributed, as there is no global or even local knowledge of the network configuration at each node.

In summary, the requirements posed by the application were set as follows:

- frequency of sample generation by each source: 1 Hz;
- number of bytes per sample: 20 Bytes;
- maximum delay between sample collection and delivery to the infrastructure: 5 s;
- coverage of the area to be monitored: 90 %;
- maximum speed of mobile nodes: 75 Km/h;
- environment to be covered: a rectangular area of no less than  $0.5 \cdot 0.2$  square meters;
- ability of the network to work even in the presence of interference caused by Wi-Fi hot spots.

The hardware platform selected by the SME was provided by Freescale, and was composed of boards equipped with a battery, some sensors, a RAM with 64 Kbytes, a MC9s08GT60 microcontroller and a MC1319x ( $x = 1$  or  $2$  or  $3$ ) radio transceiver with maximum transmit power of 3.6 dBm.

### 5.1.2 Tests

The above description of the scenario provides indication on the main issues to be considered in order to verify whether IEEE802.15.4 is a suitable candidate to realize the network. These issues are listed below.

One of the main issues concerns the mobility. IEEE802.15.4 Physical layer was designed for stationary nodes (see [82]), therefore, the ability of the air interface to work in mobile conditions, even if at low speed (up to 75 Km/h), must be checked. Moreover, the association procedure in IEEE802.15.4 devices requires some time to be completed, and this is a very relevant step to be taken for each link before the true exchange of data from the mobile node to the

sink can take place. Owing to the fact that the topology of the network changes very frequently because of the movements of mobile nodes, the time needed to complete the association procedure must be checked. Another important issue concerns the network Throughput. According to IEEE802.15.4 nomenclature ([82]), the infrastructure nodes will play the role of the PAN (Personal Area Network) coordinators, while the mobile nodes are Full Function Devices able to forward data transmitted by other nodes. Each PAN coordinator uses one of the 16 carrier frequencies available at 2.4 GHz, according to a proper planning, or to a self-organizing distributed channel selection procedure. Many devices might be simultaneously connected to a given infrastructure node, in the order of tens. So, even if few bytes per second are transmitted by each node, the sinks (the coordinators) might gather a significant amount of data every second. IEEE802.15.4 has a channel bit rate of 250 Kbit/s when used at 2.4 GHz, and this seems to promise that no throughput problems will be encountered. However, owing to the protocol overhead, at application layer the throughput can be significantly lower. So, this is also one of the aspects that needs to be checked.

If all the above checks are passed by the technology, then it is proven that IEEE802.15.4 is a suitable candidate and the software to prepare the application can be completed.

### **Mobility Test**

It was decided to start by testing the technology on the field in mobility conditions. The IEEE802.15.4 physical layer was designed for stationary nodes. The effects of mobility can play a significant role on the performance of a digital receiver. The node movement can determine a Doppler shift of the carrier frequency with respect to the transmitted signal, proportional to the speed. Multipath components can also produce signal distortion in the presence of a Doppler shift. The overall effects of such phenomena on the performance of a digital link can not be predicted easily with theoretical tools. A field trial can show whether they represent a significant limit for the performance.

It was then decided to test the IEEE802.15.4 nodes under mobility conditions, with one node acting as PAN coordinator (denoted as C in the following) located in a fixed position,



Figure 5.1: PAN coordinator C and device D

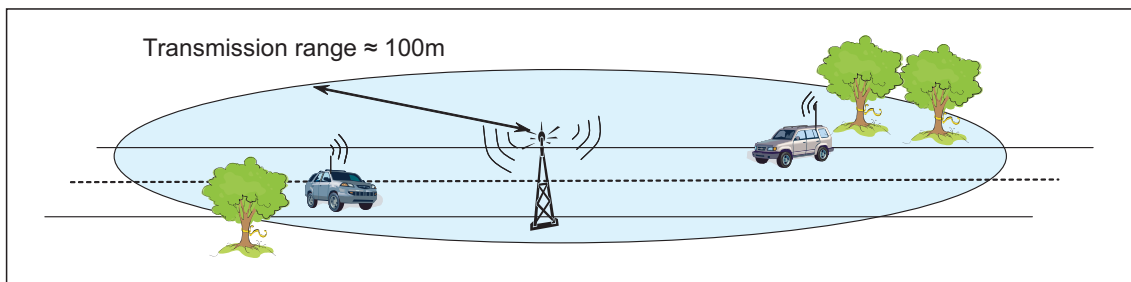


Figure 5.2: Field trial geometry

and a device (denoted as D) running over a vehicle at different speeds, trying to associate to the PAN, and sending data. The field trial was built as follows. A large and empty street was considered as environment for the measurements. The node C was located on side of the street, about 70 cm above ground, and the node D was placed inside a car (at about 100 cm above ground) running at constant speed along the empty street. Both nodes were equipped with omnidirectional antennas. Pictures of both nodes are shown in Fig. 5.1.

The maximum transmission range of the coordinator was measured, setting the transmit power of nodes at the nominal level of 0 dBm: received power was found to be above the receiver sensitivity for distances below about 100 m, generating a coverage length of about 200 m owing to the use of an omnidirectional antenna mounted on node C. The car was run along the street at speed  $v$  which was kept constant for about 300 meters, 150 before and 150 after the

point where the node C was located. Fig. 5.2 sketches the field trial geometry.

The following steps were then taken:

1. before launching the car, the coordinator performed a frequency scan procedure to select the least interfered channel among the 16 available in the ISM (Industrial, Scientific and Medical) band at 2.4 GHz;
2. the best carrier was selected and the coordinator was set in a status waiting for association requests, based on the non-beacon enabled mode of IEEE802.15.4 MAC, with acknowledge;
3. the device in the car was set in a status of cyclic search for a coordinator; basically, the node D was trying each frequency sending a packet and waiting for an acknowledgement by C; if no packet was sent back before a time out set at 0.5 s, the next channel was tried; once an acknowledgement on a channel was received, the node D started immediately the transmission of data with packets having a payload of 20 bytes, counting the acknowledgements received from the coordinator;
4. the car was launched at constant speed  $v$  and all packets transmitted and received by both nodes were recorded.

The experiment was repeated several times (only 5 for practical reasons) in order to generate average values of the measurements.

Scope of the field trial was to check whether the association procedure was successful and the data transfer efficient at various speeds.

Fig. 5.3 shows the association time measured at different speeds. The association time is defined as the time interval between reception of the first packet from C and the transmission of the first data packet sent by D to C. The Figure shows that the association time is shorter for larger speeds. The reason for this stands in the fact that at very low speed the car keeps close to the border of the transmission range of the coordinator for some seconds; in such conditions, even if a first packet transmission was successful, a large packet error rate is experienced and

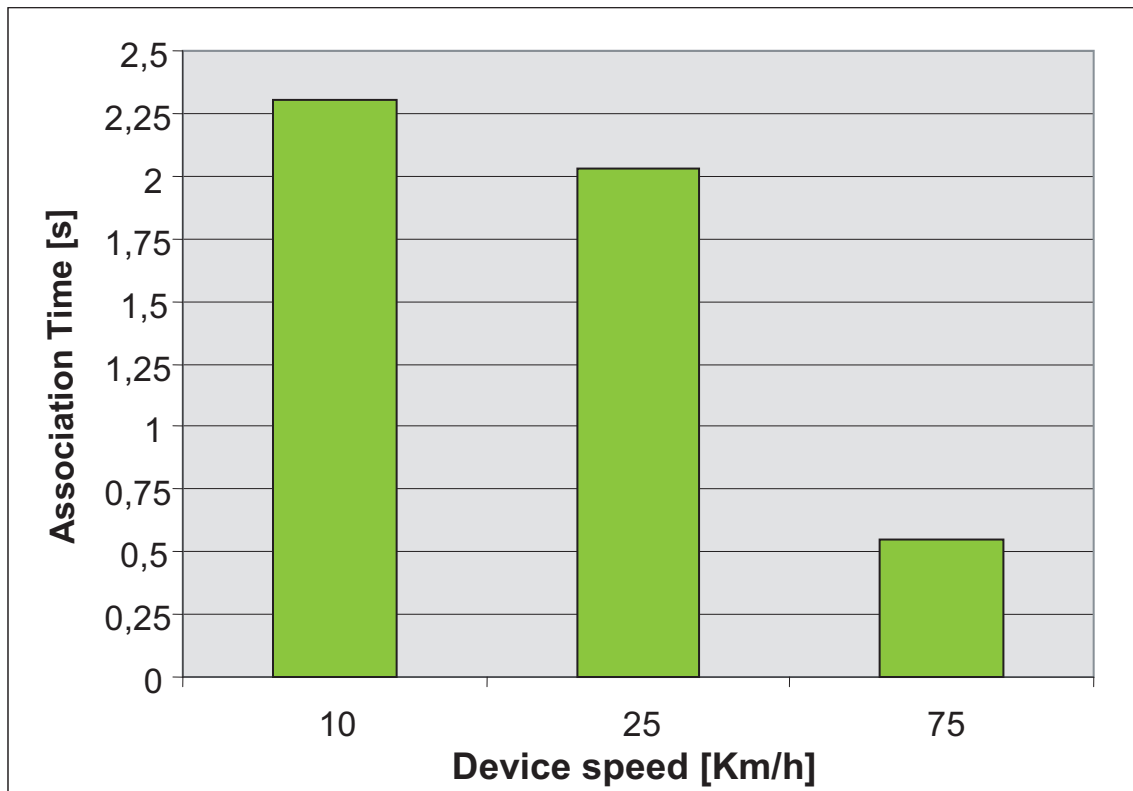


Figure 5.3: Association time measured at different speeds

some packets can be lost. Since the association procedure requires the transmission in both directions of the link of several packets, the loss of some of them determines an increased time needed to complete the procedure. When the speed was larger (above 25 Km/h in our experiments), the car moved quickly towards the coordinator, finding better channel conditions and low packet error rates after the first packet was received, thus bringing the association time to a value which is the minimum possible according to the IEEE802.15.4 MAC procedure: about 0.5 s. From the viewpoint of the distance traveled by node D during the association procedure, the case at 25 Km/h was the worst encountered (with measures performed at 10, 25, 50, 75 Km/h): about 14 meters were run before the procedure was concluded. In other words, 14 out of 200 meters of coverage were lost (that is, 7 %) to complete the association to the coordinator, before data transmission could take place.

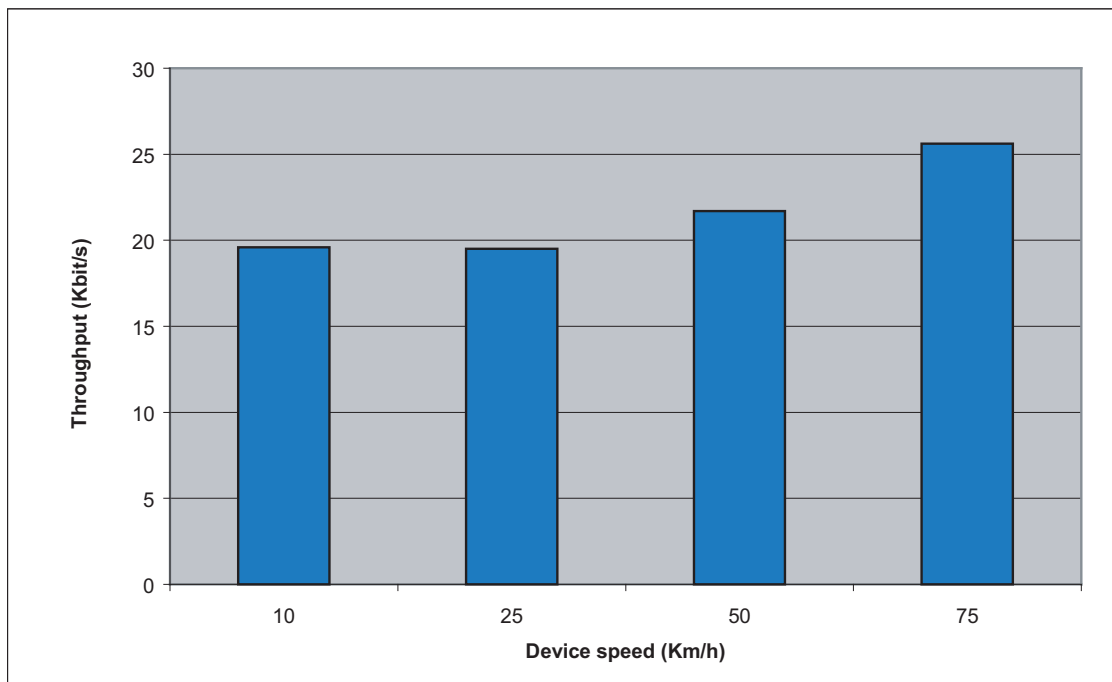


Figure 5.4: Throughput measured at different speeds

Fig. 5.4 reports the throughput measured during the data transmission phase at various speeds. The throughput was computed as the ratio between the amount of data transmitted successfully (packets sent by D and acknowledged by C) and the time the node D was associated to the coordinator. Both numerator and denominator of such ratio can depend on  $v$ : in fact, the amount of data successfully transmitted depends on the packet error rate which might increase for larger speeds, and the time the node D was associated is shorter when increasing the speed of the car. The Figure shows that the throughput does not change significantly with  $v$  ranging from 10 to 75 Km/h, with the maximum value obtained for larger speeds. The reason for this might stand in the fact that at 75 Km/h the time the device was associated to the coordinator was shorter. Indeed, a better figure to be considered is the amount of data successfully transmitted by node D during the time it was associated.

Fig 5.5 shows such figure as a function of speed. As expected, at 75 Km/h a smaller amount of data was delivered, owing to a shorter time available for transmission.

The data throughput ranges from about 18 to 25 Kbit/s, values that are significantly below the throughput of 38 Kbit/s that can be measured with both transmitting and receiving nodes being still, with link distance equal to 1 m; Fig. 5.6 shows the values of throughput measured, both in acknowledged and unacknowledged mode for the non beacon enabled mode of IEEE802.15.4, in such ideal conditions when the payload size is changed. The reason for the lower throughput (18-25 instead of 38 Kbit/s) clearly can be found in the non ideal channel conditions of mobile environments.

In all cases, however, transmission of significant amount of data was possible. This proves that IEEE802.15.4 can be efficiently used even in a mobile environment, at least at speed no larger than 75 Km/h.

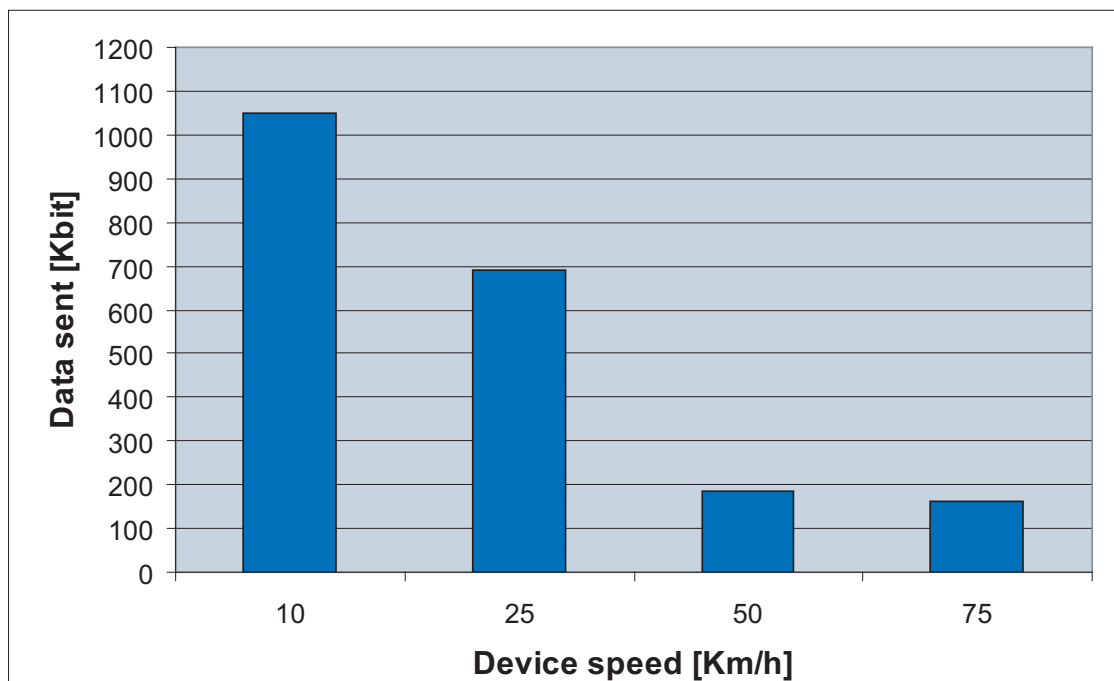


Figure 5.5: Amount of data successfully transmitted at different speeds

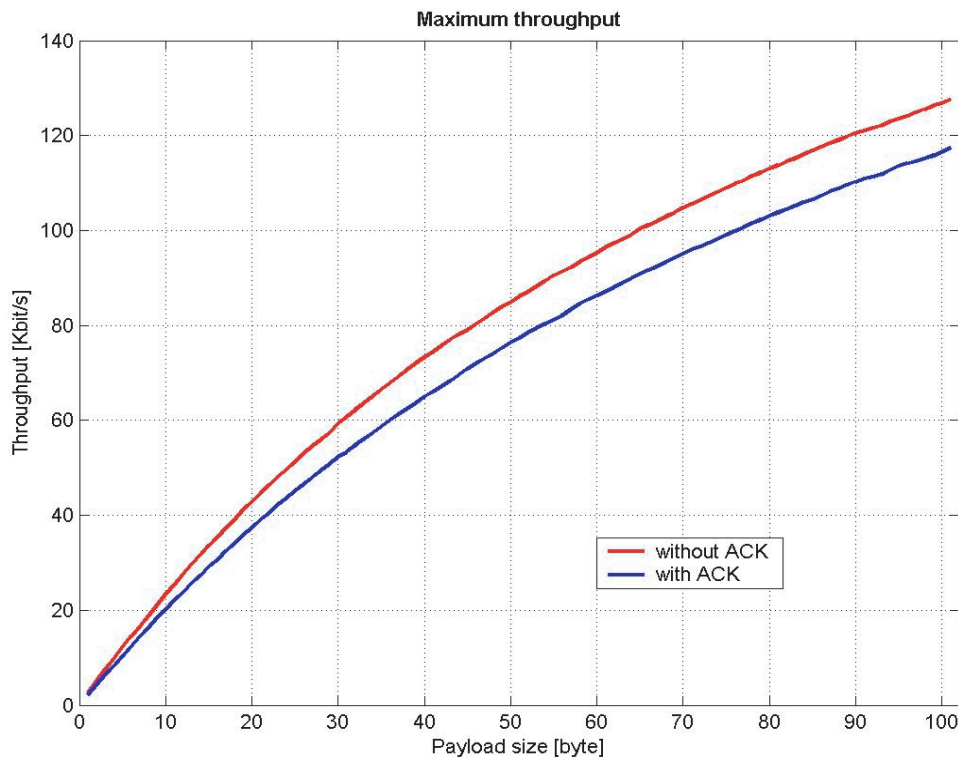


Figure 5.6: Throughput measured in ideal conditions, as a function of the payload size

### Throughput Test with Multiple Hops

Even if the channel bit rate of IEEE802.15.4 links at 2.4 GHz is 250 Kbit/s, the application layer throughput is significantly smaller because of the protocol overhead, mainly due to the MAC (sub)layer. Fig. 5.6 reported above has shown that even if the payload size is maximum (about 100 Bytes), the application layer throughput can not go above around 130 Kbit/s for point-to-point links. However, in the presence of multi-hop links, the throughput can be significantly lowered owing to the potential interference among the separate hops disturbing each other.

Fig. 5.7 reports measures performed with one, two or three routers located in between a transmitter and a receiver. With one router, two hops form the link between source and destination. With two routers, three hops, etc. The Figure refers to the beacon-enabled mode of IEEE802.15.4. It clearly shows that the throughput can be significantly lowered when multiple

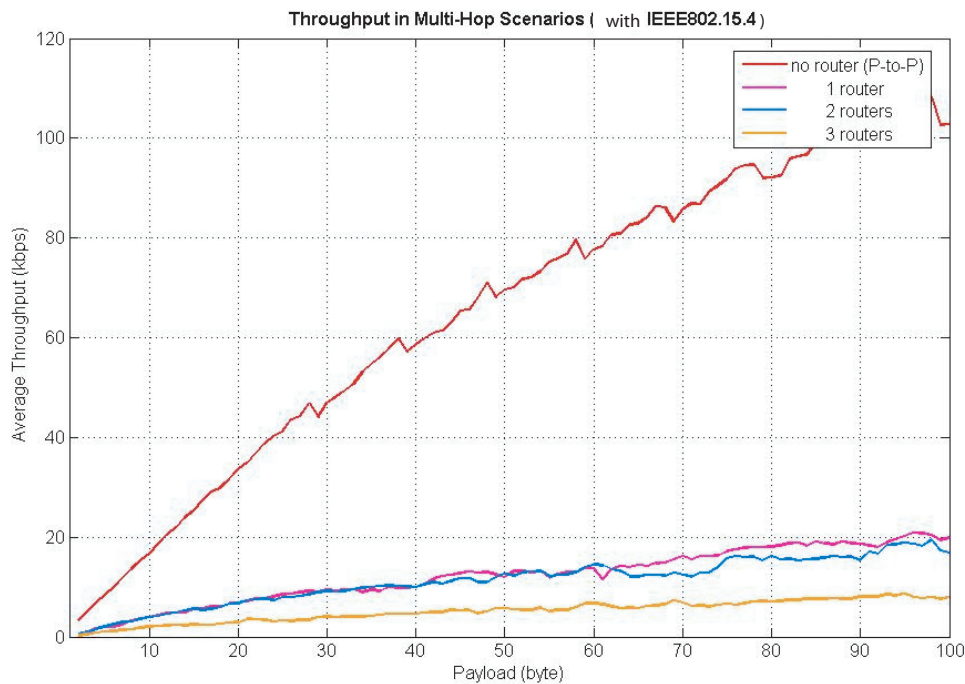


Figure 5.7: Throughput measured with one, two or three routers

hops are included. With a payload size of 20 bytes, the throughput lowers from about 35 Kbit/s to about 7 Kbit/s with two routers, and even worse with three routers.

## 5.2 TCS with IEEE802.15.4: Interference and Selection of the Transmission Modes

IEEE802.15.4 uses ISM frequency bands that can also be occupied by other wireless systems, like e.g. Bluetooth devices or IEEE802.11a/b/g/... hot spots. Since the network to be deployed under the TCS specifications needs to work in environments like railway stations, where Wi-Fi hot spots might exist, it was important to check the ability of the IEEE802.15.4 network to work in the presence of such sources of interference. An IEEE802.11 hot spots transmits a signal whose spectrum approximately spans over a bandwidth of 20 MHz. Since the IEEE802.15.4 signal occupies a frequency channel of 5 MHz and the entire ISM band at 2.4 GHz is 80 MHz

large, it is expected that even in the presence of a few hot spots, the IEEE802.15.4 network can efficiently work, provided that a suitable channel is selected by the PAN coordinator.

Moreover, in the TCS application scenario a cellular architecture is considered. Therefore we could have several 802.15.4 nodes transmitting in the same area, and the analysis of how to choose the transmitting frequency (with the aim of limiting the amount of interference in the network) becomes an important issue.

According to the description of the application scenario, multiple sinks are deployed in the rectangular area. Each of them will play the role of PAN coordinator, serving all devices traveling the sub-area (in the following denoted as cell) they cover. Concerning the frequency channel used by coordinators, the following options can be considered:

- they all use the same channel, manually selected during their configuration;
- they use different channels, suitably re-used, manually selected during their configuration;
- they all start a frequency scan procedure and autonomously select the least locally interfered channel.

With the third option, the mobile nodes have no knowledge of the frequency re-use pattern, as there is no a priori information on the channel frequencies used by the coordinators, and they do not exchange such information through the backbone network. As a result, once the devices de-associate from a PAN coordinator because they are leaving the cell, they need to start a new frequency scan procedure in order to find the next channel, used by the coordinator they are reaching. With the second option, the same is true unless only two frequencies are re-used in the area. In fact, if only two channels are used in an alternate way (e.g. channels 4 and 8, like 4-8-4-8-4-...) when moving from one coordinator towards the next one, the mobile nodes can be made aware of the fact that then when they de-associate from a coordinator using channel 4, then the next channel used is 8. No frequency scan is needed, and this reduces the time needed for associating to the next coordinator in the line. With the first option, no frequency scan or

re-selection is needed and this simplifies the development of the software to be implemented over the IEEE802.15.4 nodes.

However, if all nodes use the same channel, then a strong co-channel interference is present. Even if two channels are re-used alternatively, the interference can be severe. Moreover, when using multiple channels, also adjacent interference can play a significant role.

To assess the ability of IEEE802.15.4 to work in such conditions, a simulation tool was developed. It considers a rectangle having sides  $a$  and  $b$  with coordinators uniformly distributed along the perimeter, with a distance  $D$  separating each other. Then a mobile node is placed along the perimeter, in all possible positions, and the carrier-to-interference,  $\gamma$ , for the mobile-to-infrastructure link is computed for all positions. The power loss law is given by  $L = k_0 + k_1 \log(d) + s$  where  $d$  is link distance and  $s$  is a Gaussian r.v. with zero mean and standard deviation  $\sigma$ ; the power loss is expressed in logarithmic scale; A point over the perimeter is assumed to be covered if  $\gamma$  is above a given threshold set at 6 dB.

Adjacent and co-channel interference were taken into account. Concerning the co-channel interference, we simply evaluated the power that the device receives from the coordinators transmitting on the carrier's same channel. For what concern the adjacent one, we started from the analysis of the power spectrum of the signal generated by ZigBee devices, that is equivalent to an MSK spectrum; than, the percentage of spectrum that overlaps the adjacent channel (and that generates interference) was evaluated.

The coverage probability of the scenario is then assessed as the ratio between the number of covered points and the total number of positions considered. We denote as outage probability the complementary of the coverage probability; the target values for outage probability are below 10 %. The evaluation is done for various re-use patterns, with one or more channels used.

The following set of Figures shows some simulation results, obtained by fixing  $a = 1000$  m,  $b = 500$  m,  $D = 100$  m,  $k_0 = 15$ ,  $k_1 = 20$ ,  $\sigma = 5$ , transmit power set at 0 dBm, receiver sensitivity of -85 dBm. Fig. 5.8 shows results for the SIR (Signal to Interference Ratio) over

200 meters of perimeter when using a single channel. The outage probability value is about 0.33. In Fig. 5.9 the case with two frequencies (channels 0 and 8) is shown; in these conditions, the outage probability is about 5.5 %, a value which fulfils the requirements.

By using four frequencies (channels 0, 4, 8, 12) the outage probability falls below 0.01. Fig. 5.10 shows the values of  $\gamma$  in this case.

These results show that with two channels alternatively re-used, interference effects can be kept under control and only about five percent of the scenario suffers from excessive interference. Therefore, option two, above, is a viable solution. On the other hand, the carrier-to-interference is too low in one third of the scenario if the same channel is used by all coordinators; therefore, the first option can not be implemented.

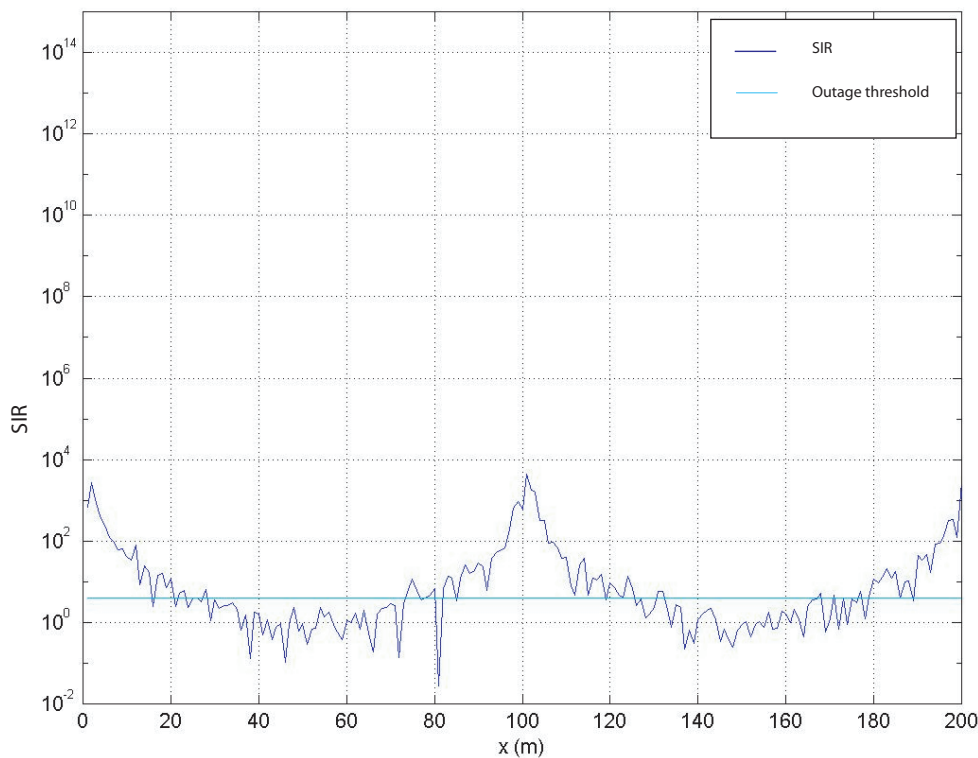


Figure 5.8: SIR over 200 m of perimeter, case with single frequency

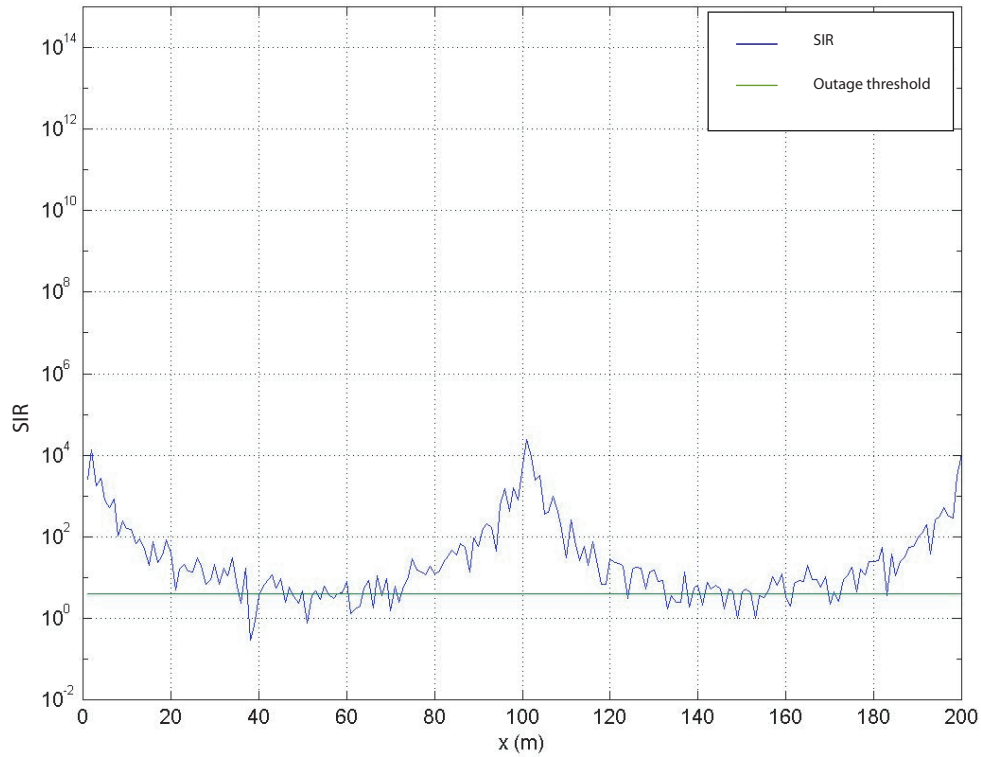


Figure 5.9: SIR over 200 m of perimeter, case with two frequencies

According to these discussions, a situation with two channels used alternatively seems to be the best option, and will be considered as the final choice in the remainder of the case study.

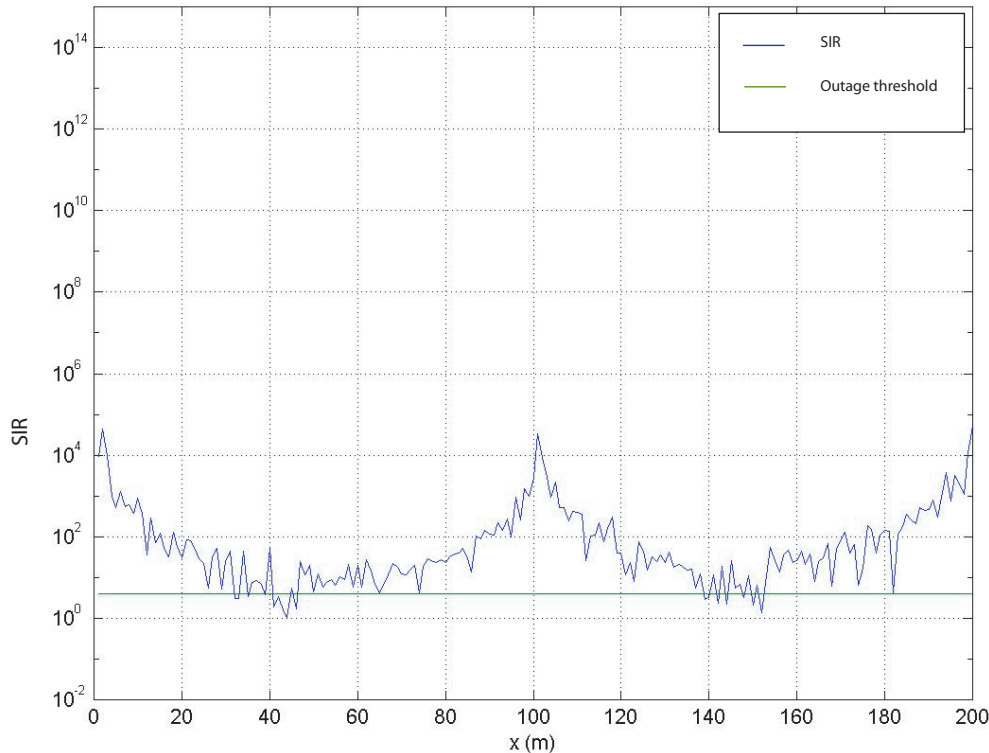


Figure 5.10: SIR over 200 m of perimeter, case with four frequencies

## 5.3 TCS with IEEE802.15.4: System Design

### 5.3.1 Possible implementations: Beacon Enabled or Non Beacon Enabled; Static or Dynamic

A step by step methodology has been used to develop the TCS project; initially the features of a communication on a mobile network based on IEEE802.15.4 have been studied, then the possible problems related to the cellular architecture have been analyzed. In particular, some network characteristics have been examined in detail, to study and theoretically compare several possible implementations of the project:

- Beacon Enabled (BE) Network (see [82], [83]);
- Non Beacon Enabled (NBE) Network (see [82], [83]);

- **Dynamic Scenario:** the position of the PAN coordinators can change, they can move through the scenario (for instance, they could be located on moving vehicles);
- **Static Scenario:** the PAN coordinators are fixed.

Concerning the coordinators' dynamism, a Dynamic Scenario implies that the coordinators involved in the cellular architecture needs to communicate among themselves to collect information on their neighbors. Unfortunately the coordinators will be probably distributed in the area in such a way that they cannot communicate with each other using 802.15.4, but they will need a different technology (e.g. WiFi, Ethernet, ...) to exchange information. Therefore, we focus the attention on the Static Scenario.

For what concern the choice between the two different IEEE802.15.4 MAC protocol modes (BE and NBE), we need to take some of their characteristics into consideration:

- **NBE:**

It is not possible to use the beacon packet as a synchronization signal, therefore the devices are not synchronized. If they are not associated to any coordinator, they need to scan the frequencies till they find a coordinator that hears the device's packets and starts the association procedure.

- **BE:**

A synchronization signal (given by the beacon packet) is available, and, thanks to the periodic beacon sent by the PAN coordinators, a non associated device will easily hear a PAN coordinator during its scan phase. Moreover, some existing MAC procedure that points out an error after three lost beacon packets are available, and they could be used to realize the de-association.

Concerning the association times, through some straightforward calculation it can be shown that they (inclusive of both scan times in the worse case and decision times) are very similar for the BE and NBE case. So, it can be concluded that the BE solution seems better than the

NBE, since it allows the use of existing MAC procedures and simplifies association and de-association. Moreover, it has another advantage from the traffic point of view (the NBE case involves one more packet in the initial phase, and this implies more overhead).

Before implementing the whole application, some preliminary tests have been taken to verify the reliability of the above theoretical conclusions. The experiments confirmed the drawn conclusions, but the tests with the BE mode showed one crucial software problem, which was not present with the NBE mode. When a device is associate to a PAN coordinator and the link quality lowers, if the communication falls down the device starts sending association requests and the coordinator stops working. Owing to this problem, the NBE MAC mode was chosen for the implementation of the TCS in a Static Scenario.

### **5.3.2 Leacky Bucket**

The TCS scenario foresees several coordinators deployed in the area where de mobile devices can run. As soon as the quality of the communication between the devices and its PAN coordinator starts decreasing, probably the device is moving away from the coordinator, approaching the boundaries of its coverage area. In this situation, the device needs to get some actions to discover if there is any coordinator capable to provide it a higher received power in its neighborhood, in order to associate to it.

To realize it, a Leaky Bucket algorithm has been introduced to determine the moment in which the device is forced to a scan procedure, in order to found a possible new coordinator. If the device, through the scan, finds an available coordinator, it de-associates from its previous coordinator and try to associates with the new one.

A counter (whom value cannot go down zero) has been introduced to implement the Leaky Bucket; it increases by one at each lost packet, while decreases by one for every successfully transmitted packet (that is, when the device receives the coordinator's Acknowledge). As soon as the counter exceeds a certain threshold (N lost packets), we can assume that the losses are not related to brief signal attenuations (due for instance to fast fading), but they are caused by the fact that the device is near to the end of the coverage area, and a new scan phase is forced.

The application requirements foresee that the devices generate and send one packet each second; but a moving vehicle takes smaller than a second to go across a zone strongly affected by fading (it has been calculated about 20 ms at a 10 Km/h speed). Therefore, the Leaky Bucket threshold for our application will not be fixed as a consequence of the mean width of an area of maximum fading attenuation, but it will be related to the mean vehicles' speed, to the mean coverage area dimension, and to the mean distance among the coordinators.

To give an example, let us consider several PAN coordinators distributed along a street (separated by a distance of 100 m) characterized by a coverage length of about 100 m, and a vehicle, equipped with an IEEE802.15.4 device, that moves along the street with a speed of 50 Km/h. The device sends to its coordinator one packet every second, and let us suppose that in a certain instant it is communicating with the coordinator C1. If we fix the Leaky Bucket threshold  $N$  to 4, and the device is approaching the end of the coverage area, the device will take 5 seconds (that is 5 consecutive lost packets) before understanding it is outside the C1 range, and starting the de-association procedure. In 5 seconds the device will cover about 70 m, at it risks to go out the next coordinator coverage area without having the time to associate with it.

To avoid this situation, there are three possibilities: reduce the Leaky Bucket threshold, increase the frequency of the samples generation and transmission, or increase the distance between the coordinators. By appropriately choosing the values of these three parameters according to the particular scenario specifications, the optimum Leaky Bucket threshold for the desired application can be obtained.

### 5.3.3 Final Test: Scenarios

The first mobility test, described above in Section 5.1.2, shows that IEEE802.15.4 can be efficiently used to build up a mobile sensor network. Starting from that test's results, it was decided to make another measures campaign to examine the actual system performance in the TCS cellular scenario (see Fig. 5.11) and to test the association and de-association procedures in three different realistic situations. The experiments have been realized in a large street characterized

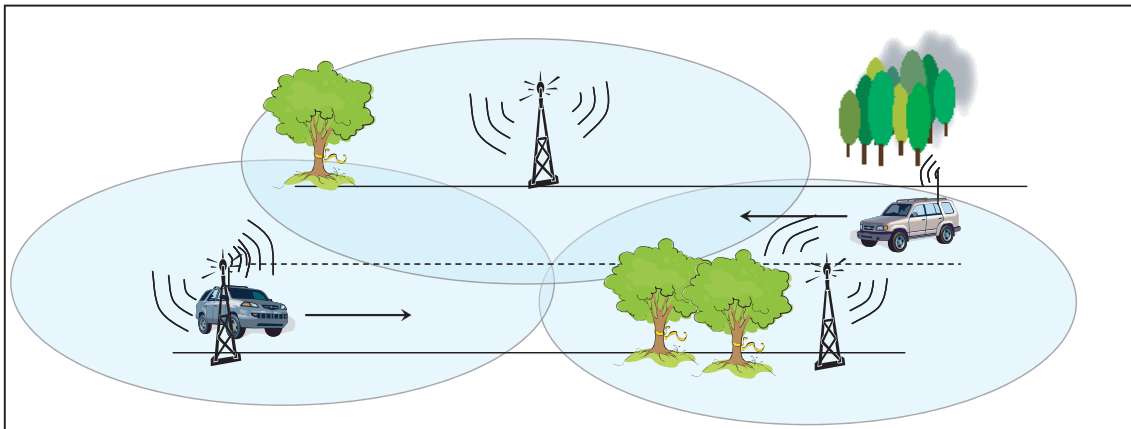


Figure 5.11: Final test phase, field trial geometry



Figure 5.12: PAN coordinator C and device D, final test phase

by some natural obstacles (trees) and bordered by warehouses.

In the three tested scenarios, an IEEE802.15.4 device (D), generating one sample each 0.5 s, is positioned inside a vehicle (about 150 cm above ground, see Fig. 5.12), and the vehicle runs the street alternately in both directions. The device speed has been fixed to 50 kmh in each test session, because the goal of this second test phase was to verify the impact of some parameters (for instance the Leaky Bucket threshold, or the transmitted power) on the system performance, having us previously tested the feasibility of the communication in mobility conditions up to 75 kmh.

In the first of the three tested scenarios, the PAN coordinator (denoted by C) was positioned in a fixed location, in the center of the street about 70 cm above ground, as we can see in Fig.

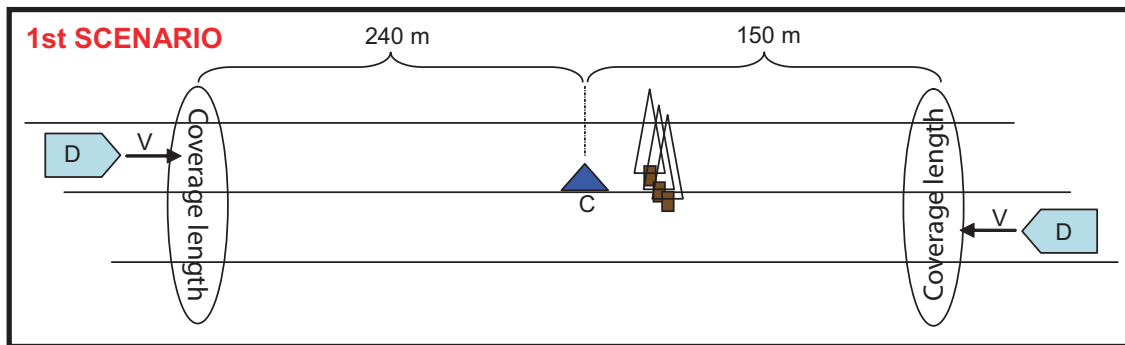


Figure 5.13: First test scenario

5.13. It's interesting to note that the group of trees decreases the signal intensity, making the coverage length different in the two opposite directions.

The transmission power has been changed during the tests from 0.4 to 3.6 dBm; the results do not point out a deep impact of the transmission power on the system performance. This is fair, because the receiver sensitivity is -92 dBm (see [82]), and a 3 dBm increase on the transmitted power little affects the device's received power.

The second tested scenario is characterized by two PAN coordinators separated by a distance of 150 m, denoted by C1 and C2 (see Fig. 5.14). The coordinators are independent: they autonomously start the initialization procedure, and scan the channels (see [82], choosing the one less interfered). The objective of this experiment was to test the capability of the mobile device D to properly associate and de-associate in a cellular scenario (in this test we have two coordinators, C1 and C2, and consequently two cells), and to correctly deliver the most data as possible to the coordinators. In particular, we examined how the Leaky Bucket procedure threshold affects both directly the association and de-association times and indirectly PER and throughput.

The third scenario could seem similar to the second, but it gives very different results. As in the previous case, two coordinators C1 and C2 are used, but the distance between them has been decreased to 50 m (as shown in Fig. 5.15), to enlarge the overlapping of the coverage areas related to the two coordinators. This enlargement, on one side increases the probability that D

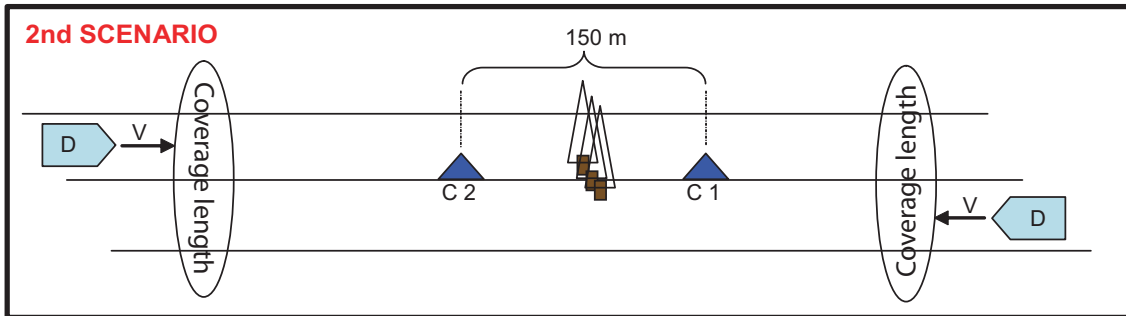


Figure 5.14: Second test scenario

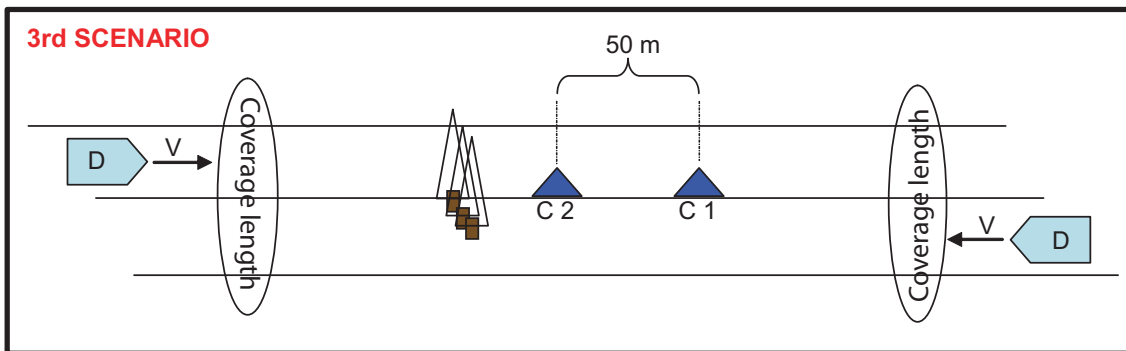


Figure 5.15: Third test scenario

can communicate with at least one coordinator when it is inside the overlapping zone, but on the other reduces the whole covered area. The main goal of this test was to measure the same quantities considered in the second scenario in order to compare the results, and determine the impact of the cells' overlapping on the performance of the system.

### 5.3.4 Final Test: Results

One of the main objectives of this second phase of tests was to verify the system behavior in a cellular scenario, and in particular to verify if the device is capable to de-associate from its coordinator in case of low quality of the received signal, and associate to the next coordinator that provide it a sufficient signal strength. The obtained results show that the device correctly executes the association and de-association procedures, successfully delivering its data to the

coordinators.

To evaluate the time taken by the device to change its PAN coordinator, we refer to the second and third scenario described above. We are going to examine the time for the device de-association from the first coordinator, and that for the association to the second coordinator. Through the experiments we obtained a good confirmation of the de-association times expected according to the implemented Leaky Bucket algorithm, as we can observe in Fig. 5.16. The Leaky Bucket is based on the counting of lost packets; with threshold equal to four, after five consecutive lost packets the device execute the de-association procedure; this implies that, if the device sends one packet every 0.5 seconds, the times obtained with the tests are exactly that expected. The values in Fig. 5.16 are averaged on the quantities obtained in both scenario 2 and 3, because the distance between the coordinators does not affect the de-association time.

Denoting by re-association time the time spent by the device to associate to another PAN

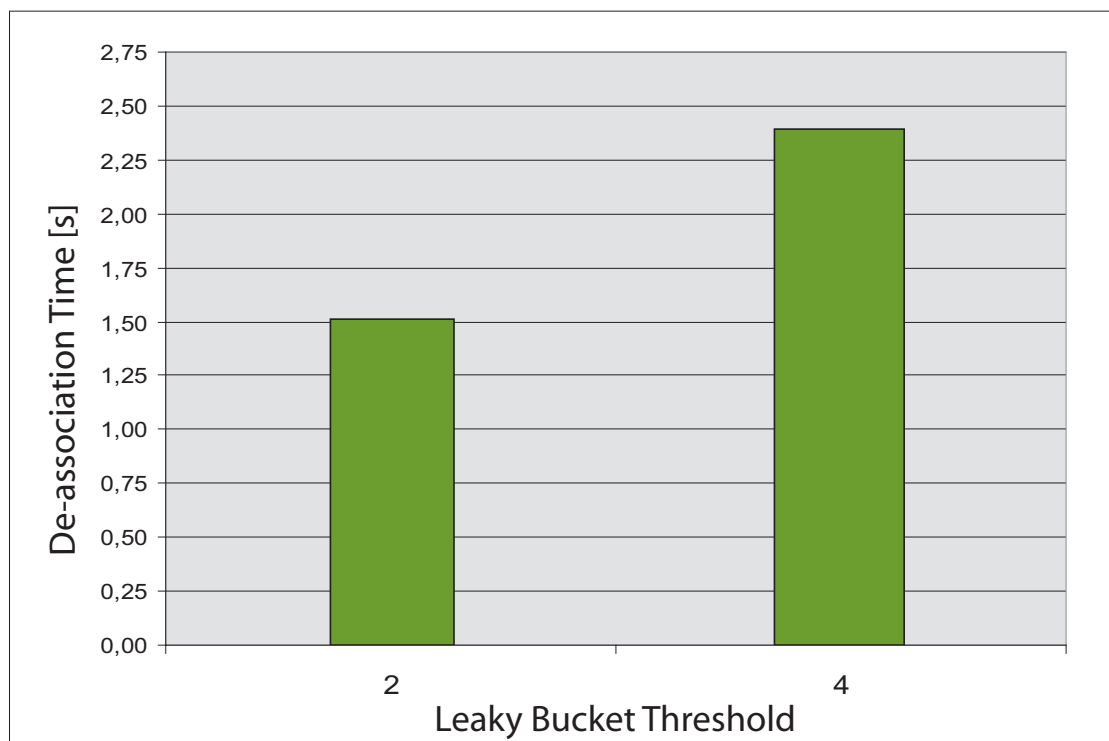


Figure 5.16: De-association time for different Leaky Bucket thresholds

coordinator after a de-association, Fig. 5.17 shows the re-association times related to the scenarios 2 and 3. The information on the two scenarios have been shown separated, to compare the two results.

If we denote by  $S_{LB}$  the value of the threshold of the Leaky Bucket algorithm, starting from the second scenario we can observe in Fig. 5.17 that for  $S_{LB} = 4$  the re-association time is lower than in the case  $S_{LB} = 2$ . This is due to the fact that with  $S_{LB} = 4$ , the device's de-association time is larger, therefore, when it tries to re-associate, it will be probably closer to the second coordinator than in the case  $S_{LB} = 2$ , and consequently it will experiment an high quality of the channel and connect quickly to the coordinator. This does not happens in the third scenario, where the coordinators are very close, so that, if  $S_{LB} = 4$ , when D is de-associated from the first coordinator probably it is to far from the second coordinator too, and the re-association fails. The same observation can be drawn if we compare the re-association

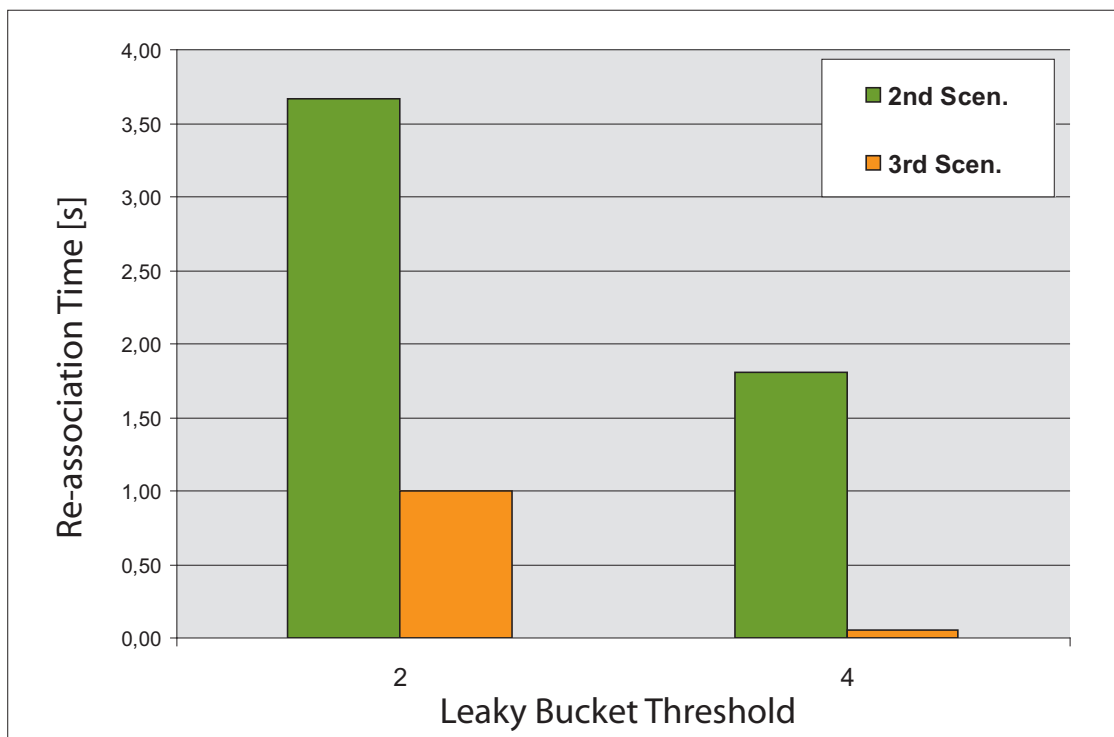


Figure 5.17: Re-association time for different Leaky Bucket thresholds

times in the two scenarios,  $S_{LB}$  being equal. Analyzing Fig. 5.17, we can then conclude that  $S_{LB}$  strongly impacts on the system performance, but does not exist an optimum value for that threshold;  $S_{LB}$  needs to be chosen in accordance with the cellular planning.

Concerning the data throughput and the PER, the results have been kept separated for both different scenarios and different  $S_{LB}$ . Moreover, the performance related to the two coordinators have been kept separated. In Fig. 5.18 it's possible to observe that the throughput related to the first coordinator (where we mean by first alternately C1 or C2 depending on the vehicle direction) does not change significantly, and it is similar to that in the case of one coordinator; this is obvious because the presence of a second coordinator, independent by the first and working on a different channel, does not generate interference. However, we can notice that in the  $S_{LB} = 4$  case, the throughput is slightly lower than in the  $S_{LB} = 2$  case, in particular in scenario 2; this is due to the fact that increasing  $S_{LB}$ , the time during which D remains connected to the

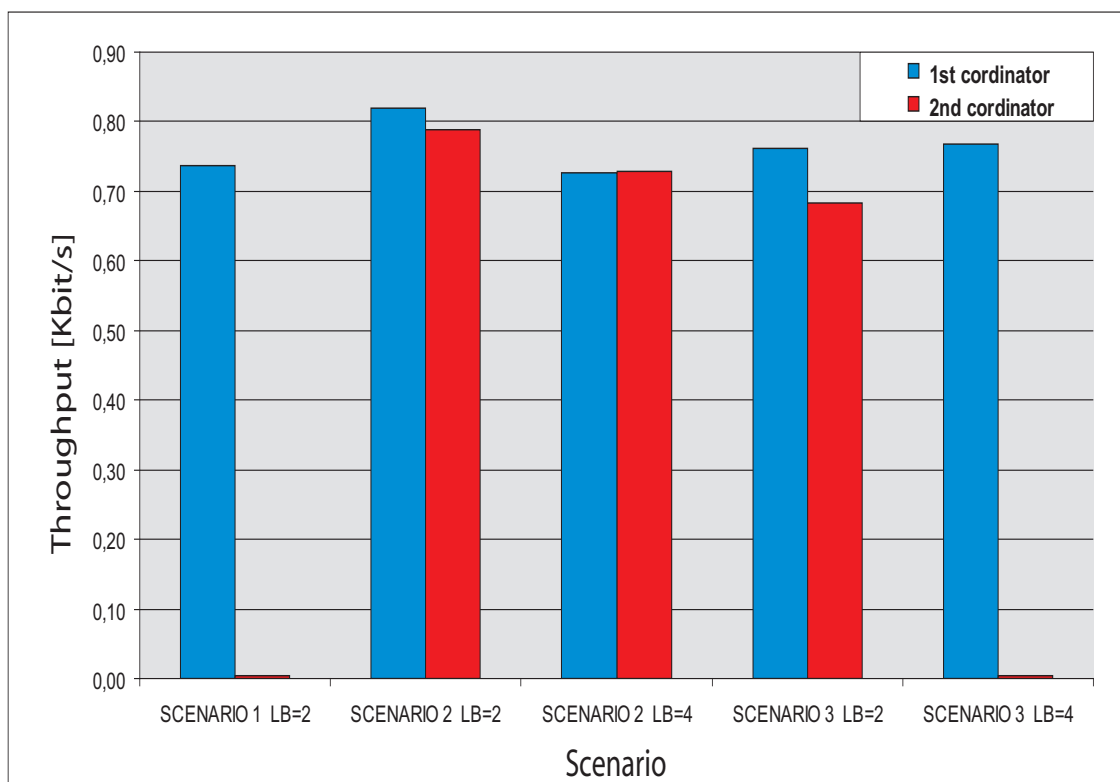


Figure 5.18: Throughput for different scenarios and Leaky Bucket thresholds

first coordinator increases, the number of corrected delivered packet being equal, therefore the throughput decreases. The figure shows also that the performance related to the second PAN coordinator vary for different  $S_{LB}$ ; as a matter of fact, in the second scenario the throughput for  $S_{LB} = 2$  is larger than in the case  $S_{LB} = 4$ . This suggests us that when the link quality decreases, the faster D de-associate from the first coordinator, the better are the performance; this behavior is confirmed if we observe the third scenario case, where the distance between the coordinators is minor.

Finally, Fig. 5.19 shows the system PER. As expected, the Figure substantially confirms the conclusions drawn from the throughput graph; as a matter of fact, the two quantities are strictly related, and the Figures carry the same results in a different way.

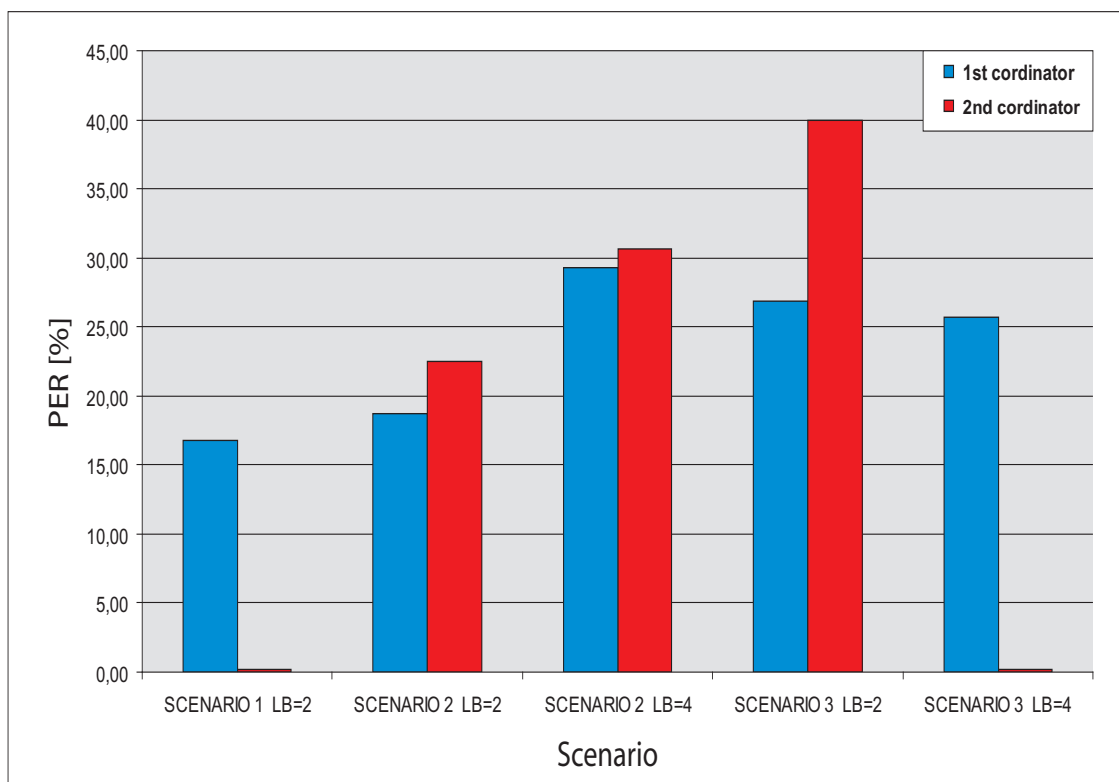


Figure 5.19: PER for different scenarios and Leaky Bucket thresholds

# Chapter 6

## Conclusions

In this thesis some issues concerning connectivity models in fourth generation wireless network have been proposed and analyzed, in particular by focusing on the performance evaluation of these systems.

To this aim, in Chapter 2 a statistical model to evaluate the distribution of the received power in wireless and sensor networks has been proposed. The model, which extends the result of [23], can be used to evaluate the useful and the interference power in a scenario of infinite area where all the terminals can communicate with each other using the same radio resource. The analysis, which allows the investigation of propagation environments characterized by distance-dependent loss and log-normally distributed shadowing, has been verified through simulation results which confirm the validity of the model.

Aiming to extend the previous consideration to the interesting finite area case, in Chapter 3 the contribution of interference provided by nodes located on regions of limited area has been studied. The propagation environment we have considered is characterized by a distance-

dependent deterministic path-loss and a superimposed log-normal shadowing. We have tried to overcome some limitations of existing interference models and proposed an analytical framework for the evaluation of any statistical moment of the interference provided by a Poisson field of nodes located on a given area. The main contributions of this Chapter have been:

- the derivation of an exact expression for the distribution of the channel gain for nodes located on an arbitrary finite area;
- an expression for the derivation of any moment of the amount of interference received by a given terminal;
- closed form approximate expressions for the moments of the interference in some reference scenarios.

The methodology presented can be used to provide a fast and accurate evaluation of the statistical distribution of the interference in many situations of interest.

In Chapter 4, the achievable rate of a wireless sensor network where the supervisor, which collects information from uniformly distributed sensors, is equipped with multiple antennas, has been investigated. Owing to the randomness of the node location and of the propagation environment, characterized by a distance-dependent loss, shadowing and Rayleigh fading, the number of sensors able to communicate with the supervisor is a random variable and the system can be considered as an equivalent MIMO with a random number of transmit antennas which provide different values of power on the receiving antennas. In this Chapter, we have derived an expression for the achievable rate and evaluated its average over the possible values of the signal-to-noise ratios on the receiving antennas and node positions.

Finally, Chapter 5 deals with the performance of next generation systems, but analyze the issue from the experimental point of view. A TCS (Tracking and Communication System) system based on a self-configuring wireless network consisting on IEEE802.15.4 nodes (equipped with positioning devices) in mobility conditions, has been designed, developed and tested, and its performance (that is, Throughput and Packet Error Rate) have been verified. The nodes carry out successful procedures of association, deassociation and data exchange, and experimental

tests and measurement shows that the system perform well even in a cellular scenario.



# Appendix A

## Discussion on the p.d.f. of the distance between a pair of communicating nodes

Among the contributions on wireless ad hoc and sensor networks appeared in the open literature in the past few years, the paper of Orriss and Barton [23] was important as it represented one of the first attempts to study the connectivity properties of networks composed of randomly located nodes in a propagation environment characterized by a distance dependent loss and log-normal shadowing. The following results were obtained in [23] for an infinite 2-dimensional area:

- a) the probability density function (p.d.f.) of the distance between a pair of *audible* nodes (a node is audible by others if the power loss does not exceed a given threshold);
- b) the probability distribution of the number of audible nodes with respect to a node taken as a reference. This distribution was proven to be Poisson and its mean was evaluated;
- c) the distribution for the number of audible nodes within a finite area of the plane. This distribution is still Poisson and its mean was evaluated.

Results a) and b) were also extended to the case where the path loss changes at a specified distance from the transmitting node.

In this appendix, we comment on the results obtained in [23]; more specifically, we prove that the p.d.f. expression for a) is wrong and derive a correct one, which is valid for an infinite  $d$ -dimensional area. The validity of the other results of [23] is also discussed.

## A.1 Review of eq. (7) of [23]

The scenario considered in [23] is characterized by an infinite 2-dimensional area where the nodes are distributed according to a Poisson point process (PPP) with density  $\rho$ . Let us consider a node  $N_1$  which attempts to communicate with another one (say,  $N_0$ ) located in the origin of a reference coordinate system. The channel model is affected by distance-dependent exponential path loss component and log-normal shadowing. Nodes  $N_1$  and  $N_0$  are  $l_1$ -audible if the path loss in decibels  $\hat{L}$  does not exceed a given threshold  $l_1$ , that is

$$\hat{L} = \hat{k} + k_\beta \ln D + \hat{S} \leq l_1, \quad (\text{A.1})$$

where, as in the previous chapters,  $\hat{k}$  and  $k_\beta$  are propagation constants,  $\hat{S}$  is the shadowing term, which is assumed to be a Normal random variable with zero mean and variance  $\sigma_S^2$ , and  $D$  represents the distance between the nodes. Let us also denote by  $\mathcal{C}$  the event of  $l_1$ -audibility between  $N_1$  and  $N_0$ . The steps followed in [23] to obtain  $f_{D|\mathcal{C}}(x|\mathcal{C})$ <sup>1</sup> can be summarized as follows:

- i): evaluation of the conditional density of  $D$  given  $\hat{S} = s$  (see [23, eq. (6)]);
- ii): evaluation of the joint pdf of  $D$  and  $\hat{S}$  (conditioned on the event  $\mathcal{C}$ );
- iii): evaluation of the pdf of  $D$  (conditioned on the event  $\mathcal{C}$ ), by integrating out  $\hat{S}$  from the joint p.d.f. of  $D$  and  $\hat{S}$  (see [23, eq. (7)]).

---

<sup>1</sup>Here  $f_D(x)$  and  $f_{\hat{S}}(s)$  denote the p.d.f. of the distance between two arbitrary nodes (regardless of the audibility) and the p.d.f. of the corresponding shadowing sample. The p.d.f of the distance between two  $l_1$ -audible nodes and the corresponding distribution of  $\hat{S}$  are here denoted as  $f_{D|\mathcal{C}}(x|\mathcal{C})$  and  $f_{\hat{S}|\mathcal{C}}(s|\mathcal{C})$ .

Let us consider step ii), which requires the evaluation of

$$f_{D,\hat{S}|\mathcal{C}}(x, s|\mathcal{C}) = f_{D|\hat{S},\mathcal{C}}(x|s, \mathcal{C})f_{\hat{S}|\mathcal{C}}(s|\mathcal{C}). \quad (\text{A.2})$$

To evaluate (A.2), the distribution of  $\hat{S}|\mathcal{C}$  is assumed in [23] to be normally distributed with zero mean and variance  $\sigma_S^2$ . This would be true in the absence of any condition on the audibility, but this assumption is wrong under condition  $\mathcal{C}$ . To prove this, we show that the mean value of  $\hat{S}|\mathcal{C}$  is nonzero. This can be checked by observing that in the presence of the events  $\mathcal{C}$  and  $\mathcal{D} = \{\text{the distance } D \text{ is equal to } x\}$ , the distribution of  $\hat{S}$  conditioned on  $\mathcal{C}$  and  $\mathcal{D}$  becomes

$$f_{\hat{S}|\mathcal{C},\mathcal{D}}(s|\mathcal{C}, \mathcal{D}) = \frac{K e^{-\frac{s^2}{2\sigma_S^2}}}{\sqrt{2\pi}\sigma_S} u(l_1 - \hat{k} - k_\beta \ln x - s), \quad (\text{A.3})$$

where  $K$  is a normalizing constant and  $u(z)$  is the unitary step function

$$u(z) \triangleq \begin{cases} 1 & \text{if } z \geq 0 \\ 0 & \text{if } z < 0 \end{cases}. \quad (\text{A.4})$$

Starting from (A.3), the p.d.f. of  $\hat{S}|\mathcal{C}$  can be calculated as

$$\begin{aligned} f_{\hat{S}|\mathcal{C}}(s|\mathcal{C}) &= \int_0^{+\infty} f_{\hat{S}|\mathcal{C},\mathcal{D}}(s|\mathcal{C}, \mathcal{D}) f_{D|\mathcal{C}}(x|\mathcal{C}) dx \\ &= \frac{K e^{-\frac{s^2}{2\sigma_S^2}}}{\sqrt{2\pi}\sigma_S} \int_0^{e^{\frac{l_1 - \hat{k} - s}{k_\beta}}} f_{D|\mathcal{C}}(x|\mathcal{C}) dx \\ &= \frac{K e^{-\frac{s^2}{2\sigma_S^2}}}{\sqrt{2\pi}\sigma_S} h(s), \end{aligned} \quad (\text{A.5})$$

where  $h(s) \triangleq \int_0^{e^{\frac{l_1 - \hat{k} - s}{k_\beta}}} f_{D|\mathcal{C}}(x|\mathcal{C}) dx > 0$  with limits  $h(-\infty) = 1$  and  $h(+\infty) = 0$ . The expectation of  $\hat{S}|\mathcal{C}$  becomes

$$\begin{aligned} \mathbb{E}\{\hat{S}|\mathcal{C}\} &= \frac{K}{\sqrt{2\pi}\sigma_S} \int_{-\infty}^{+\infty} s e^{-\frac{s^2}{2\sigma_S^2}} h(s) ds \\ &= -\frac{K\sigma_S}{\sqrt{2\pi}k_\beta} \int_{-\infty}^{+\infty} e^{-\frac{s^2}{2\sigma_S^2}} e^{\frac{l_1 - \hat{k} - s}{k_\beta}} h\left(e^{\frac{l_1 - \hat{k} - s}{k_\beta}}\right) ds. \end{aligned} \quad (\text{A.6})$$

Since the three integrands functions in (A.6) are positive, the integral is positive and therefore  $\mathbb{E}\{\hat{S}|\mathcal{C}\}$  is nonzero.

## A.2 Distribution of the distance between audible nodes and discussion on the validity of the other results of [23]

### A.2.1 Evaluation of $f_{D|\mathcal{C}}(\cdot)$

Since the evaluation of  $f_{\hat{s}|\mathcal{C}}(s|\mathcal{C})$  in (A.2) is not straightforward, the right expression for  $f_{D|\mathcal{C}}(x|\mathcal{C})$  and its generalization to an infinite  $m$ -dimensional area can be obtained using the following alternative approach.

We assume that nodes are spatially distributed in a  $(m - 1)$ -dimensional sphere of radius  $D_s$  and denote by  $\mathbf{y} = (y_1, \dots, y_x)$  the position of  $N_1$  with respect to  $N_0$  (whose position is assumed to be in the origin of the reference coordinate system). The distance between the two nodes is denoted by  $D = \|\mathbf{y}\|$ .<sup>2</sup>

Let us consider  $D = x$  (event  $\mathcal{D}$ ). The probability that inequality (A.1) is verified is given by

$$\text{Prob} \left\{ \hat{L} \leq l_1 | \mathcal{D} \right\} = \text{Prob} \{ \mathcal{C} | \mathcal{D} \} \triangleq C(x) = \frac{1}{2} \text{erfc} \left( \frac{\hat{k} + k_\beta \ln x - l_1}{\sqrt{2}\sigma_s} \right), \quad (\text{A.7})$$

where  $\text{erfc}(\cdot)$  denotes the complementary error function.

Starting from (A.7) and by means of the Bayes theorem, we can derive the probability distribution of the distances (conditioned on the event  $\mathcal{C}$ ) as

$$\begin{aligned} f_{D|\mathcal{C}}(x|\mathcal{C}) &= \frac{\text{Prob} \{ \mathcal{C} | \mathcal{D} \} f_D(x)}{\text{Prob} \{ \mathcal{C} \}} \\ &= \frac{C(x) f_D(x)}{\int_0^{D_s} \text{Prob} \{ \mathcal{C} | \mathcal{D} \} f_D(x) dx} \\ &= \frac{C(x) f_D(x)}{\int_0^{D_s} C(x) f_D(x) dx}. \end{aligned} \quad (\text{A.8})$$

It can be easily shown that  $f_D(x)$  has the expression

$$f_D(x) = \frac{m}{D_s^m} x^{m-1}, \quad 0 \leq x \leq D_s. \quad (\text{A.9})$$

Hence, by substituting (A.9) into (A.8) and letting  $D_s \rightarrow \infty$ , we obtain

$$f_{D|\mathcal{C}}(x|\mathcal{C}) = \frac{C(x)x^{m-1}}{\int_0^\infty C(x)x^{m-1}dx} = C(x)x^{m-1} e^{-\frac{m}{k_\beta}(l_1 - \hat{k})} e^{-\frac{\sigma_s^2 m^2}{2k_\beta^2}}. \quad (\text{A.10})$$

<sup>2</sup> $\|\mathbf{y}\|$  indicates the euclidean norm of the vector  $\mathbf{y}$ .

In the one-dimensional case, the previous result was also derived in [84, eq. 10].

In the 2-dimensional case, equation (A.10) becomes

$$f_{D|\mathcal{C}}(x|\mathcal{C}) = x e^{-\frac{2}{k_\beta}(l_1 - \hat{k} - \sigma_S^2/k_\beta)} \operatorname{erfc}\left(\frac{\hat{k} - l_1 + k_\beta \ln x}{\sqrt{2}\sigma_S}\right). \quad (\text{A.11})$$

An equivalent expression was also obtained in [85, eq. (20)]. Note that [23, eq. (7)] is very similar to the previous expression, it differs from (A.11) only for the presence of an additional coefficient  $\sqrt{2}\sigma_S/k_\beta$  in the argument of the erfc function<sup>3</sup>.

The comparison between (A.11) and [23, eq. (7)] is shown in Fig.A.1 for different values of  $\sigma_S$ .

### A.2.2 Discussion on the other results of [23]

Now, let us discuss the validity of the other results of [23]. We focus, in particular, on results b) and c) since their proofs required the knowledge of  $f_{D|\mathcal{C}}(d|\mathcal{C})$  (see for instance [23, eq. (8)]). Although the formula for the p.d.f. of  $f_{D|\mathcal{C}}(d|\mathcal{C})$  was wrong, these results are still correct. This can be proved by observing that the Poisson nature of the distribution of the number of audible nodes is a consequence of the Marking Theorem [86], valid under conditions which are more general than (A.1). The extension of result b) in the presence of arbitrary channel randomness was also given in [25] and [87]. The latter works showed that the number of audible nodes is Poisson whatever channel model is considered. Result c) can be seen as a special case of the Marking Theorem too.

---

<sup>3</sup>The function  $\Phi(\tilde{x})$  used in [23, eq. (7)] can be easily written as  $\frac{1}{2}\operatorname{erfc}\left(-\frac{\tilde{x}}{\sqrt{2}}\right)$ .

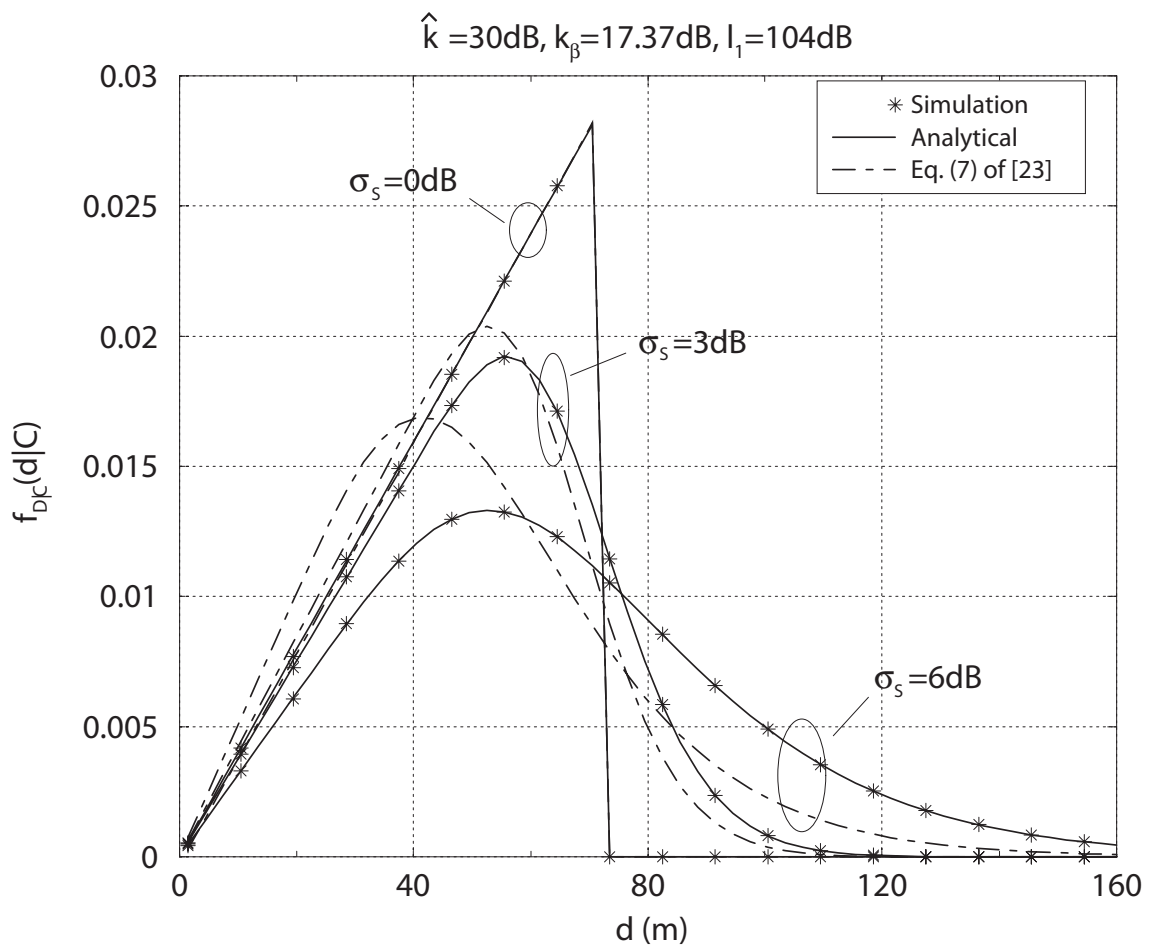


Figure A.1: The p.d.f. of distance between two audible nodes.

# Bibliography

- [1] J. G. Markoulidakis, G. L. Lyberopoulos, D. F. Tsirkas, E. D. Sykas, “ Mobility modeling in third-generation mobile telecommunications systems,” *Personal Communications, IEEE [see also IEEE Wireless Communications]*, pp. 41-56, Vol. 4, Aug. 1997.
- [2] A. Samukic, “ UMTS universal mobile telecommunications system: development of standards for the third generation,” *IEEE Transactions on Vehicular Technology* , pp. 1099 - 1104, Vol. 47, Nov. 1998.
- [3] A. G. Valko, A. Racz, G. Fodor, “ Voice QoS in third-generation mobile systems,” *IEEE Journal on Selected Areas in Communications* , pp. 109 - 123, Vol. 17, Jan. 1999.
- [4] F. Houeto, S. Pierre, R. Beaubrun, Y. Lemieux, “ Reliability and cost evaluation of third-generation wireless access network topologies: a case study,” *IEEE Transactions on Reliability* , pp. 229 - 239, Vol. 51, June 2002.
- [5] S. Dixit, G. Yile, Z. Antoniou, “ Resource management and quality of service in third generation wireless networks,” *IEEE Communications Magazine* , pp. 125 - 133, Vol. 39, Feb 2001.
- [6] K. R. Santhi, V. K. Srivastava, G. SenthilKumaran, A. Butare, “ Goals of true broadband’s wireless next wave (4G-5G),” *In Proc. of IEEE VTC 2003-Fall* , pp. 2317 - 2321, Vol. 4, Oct. 2003.
- [7] M. Munoz, C. G. Rubio, “ A new model for service and application convergence in B3G/4G networks,” *IEEE Wireless Communications*, pp. 6 - 12, Vol. 11, Oct. 2004.
- [8] Jun-Zhao Sun, J. Sauvola, D. Howie, “ Features in future: 4G visions from a technical perspective,” *In Proc. of IEEE GLOBECOM '01*, pp. 3533 - 3537, Vol. 6, Nov. 2001.
- [9] S. Frattasi, H. Fathi, F. H. P. Fitzek, R. Prasad, M. D. Katz, “ Defining 4G technology from the users perspective,” *IEEE Network*, pp. 35 - 41, Vol. 20, Jan.-Feb. 2006.
- [10] R. Agrawal, A. Bedekar, “ Network Architectures for 4G: Cost Considerations [Wireless Broadband Access],” *IEEE Communication Magazine*, pp. 76 - 81, Vol. 45, Dec. 2007.
- [11] M. Frodigh, S. Parkvall, C. Roobol, P. Johansson, P Larsson, “ Future-generation wireless networks,” *IEEE Personal Communications*, pp. 10 - 17, Vol. 8, Oct. 2001.

- [12] L. Benyuan, D. Towsley, "A study of the coverage of large-scale sensor networks," *IEEE International Conference on Mobile Ad-hoc and Sensor Systems, 2004*, pp. 475 - 483, Oct. 2004.
- [13] Dali Wei; H. A. Chan, "Clustering Ad Hoc Networks: Schemes and Classifications," *3rd Annual IEEE Communications Society on Sensor and Ad Hoc Communications and Networks, 2006*, pp. 920 - 926, Vol. 3, Sept. 2006.
- [14] S. Zhao, I. Seskar, D. Raychaudhuri, "Performance and scalability of self-organizing hierarchical ad hoc wireless networks," *In Proc. of IEEE Wireless Communications and Networking Conference, 2004*, pp. 132 - 137, Vol. 1, March 2004.
- [15] M. Tubaishat, S. Madria, "Sensor networks: an overview," *IEEE Potentials*, vol. 22, n. 2, April/May 2003.
- [16] H. Durrant-Whyte, "Data fusion in sensor networks," *Fourth International Symposium on Information Processing in Sensor Networks*, pp. 2 - 6, April 2005.
- [17] Tim Tau Hsieh, "Using sensor networks for highway and traffic applications," *IEEE Potentials*, pp. 13 - 16, Vol. 23, Apr-May 2004.
- [18] Z. Cheng, M. Perillo, W. B. Heinzelman, "General Network Lifetime and Cost Models for Evaluating Sensor Network Deployment Strategies," *IEEE Transactions on Mobile Computing*, pp. 484 - 497, Vol. 7, April 2008.
- [19] V. Mhatre, C. Rosenberg, "Homogeneous vs heterogeneous clustered sensor networks: a comparative study," *IEEE International Conference on Communications*, pp. 3646 - 3651, Vol. 6, June 2004.
- [20] J. Burdin, J. Duniak, "Enhancing the performance of wireless sensor networks with MIMO communications," *IEEE Military Communications Conference*, pp. 2321 - 2326, Vol. 4, Oct. 2005.
- [21] M. Haenggi, "Link modeling with joint fading and distance uncertainty," *4th Int. Symp. on Modeling and Optimiz. in Mob. Ad Hoc and Wireless Networks*, pp. 1-6, 3-6 Apr. 2006.
- [22] T.K. Philips, S.S. Panwar, A.N. Tantawi, "Connectivity properties of a packet radio network model," *IEEE Trans. on Inf. Theory*, vol. 35, n. 9, pp. 1044-1047, Sep. 1989.
- [23] J. Orriss, S.K. Barton, "Probability distributions for the number of radio transceivers which can communicate with one another," *IEEE Trans. on Communications*, vol. 51, n. 4, Apr. 2003.
- [24] C. Betstetter, C. Hartmann, "Connectivity of wireless multihop networks in a shadow fading environment," *Proc. of ACM MSWIM*, San Diego, CA, Sept 2003.

- [25] D. Miorandi, E. Altman, "Coverage and connectivity of ad hoc networks presence of channel randomness," in *Proc. of IEEE INFOCOM, 24th Annual Joint Conference*, vol. 1, pp. 491 - 502, 13-17 March 2005.
- [26] Y.-C. Cheng, T.G. Robertazzi, T.G., "Critical connectivity phenomena in multihop radio models," *IEEE Trans. on Communications*, Vol. 37, n. 7, pp. 770-777, July 1989.
- [27] J. Proakis, *Digital communications*, Fourth edition, Mc-Graw Hill.
- [28] G. L. Stuber, *Principles of Mobile Communication*, Kluwer Boston, Inc., 1996.
- [29] S. W. Wang, S.S. Rappaport, "Signal-to-interference calculations for corner-excited cellular communications systems," *IEEE Trans. on Communications*, vol. 39, n. 12, pp. 1886-1896, Dec. 1991.
- [30] Y. D. Yao, A.U.H. Sheikh, "Investigations into cochannel interference in microcellular mobile radio systems," *IEEE Trans. on Vehicular Technology*, vol. 41, n. 2, pp. 114-123, May 1992.
- [31] C. De Morais Cordeiro, D.P. Agrawal, D.H. Sadok, "Interference modeling and performance of Bluetooth MAC protocol," *IEEE Trans. on Wireless Communications*, vol. 2, n. 6, pp. 1240-1246, Nov. 2003.
- [32] D. Stoyan, W. S. Kendall, J. Mecke, *Stochastic geometry and its applications*, Sec. Ed., J. Wiley & Sons, 1995.
- [33] L. Kleinrock, J. Silvester, "Spatial reuse in multihop packet radio networks," *IEEE Proceedings*, vol. 75, n. 1, pp. 156-167, Jan. 1987.
- [34] P. Gupta, P. R. Kumar, "Critical power for asymptotic connectivity," *Proc. of IEEE Conference on Decision and Control*, vol. 1, pp. 1106-1110, Dec 1998.
- [35] P. Gupta, P. R. Kumar, "The capacity of wireless networks," *IEEE Trans. on Inf. Theory*, vol. 46, pp. 388-404, Mar 2000.
- [36] P. Santi, D. M. Blough, "The critical transmission range for connectivity in sparse wireless ad hoc networks," *IEEE Trans. on Mob. Comp.*, vol. 2, pp. 25-39, Mar 2003.
- [37] O. Dousse, F. Baccelli, P. Thiran, "Impact of interferences on connectivity in ad hoc networks," *IEEE Trans. on Networking*, vol. 13, n. 2, pp. 425-436, Apr 2005.
- [38] L. Booth, J. Bruck, M. Cook, M. Franceschetti, "Ad hoc wireless networks with noisy links," *Proc. of IEEE ISIT*, vol. 2, pp. 386-386, July 2003.
- [39] J. Orriss, A.R. Phillips, S.K. Barton, "A statistical model for the spatial distribution of mobiles and base stations," in *Proc. of IEEE Vehicular Technology Conference (VTC 1999 - Fall)*, Vol. 1, pp. 127-130, 19-22 Sept. 1999.

- [40] M. Haenggi, "Analysis and design of diversity schemes for ad hoc wireless networks," *IEEE Jour. on Sel. Areas in Comm.*, vol. 23, pp. 19-27, Jan 2005.
- [41] H. A. David, H. N. Nagaraja, *Ordered statistics*, Third edition, Wiley and Sons, 2003.
- [42] H. Bolcskei, R. U. Nabar, O. Oyman, A. J. Paulraj, "Capacity scaling laws in MIMO relay networks," *IEEE Transactions on Wireless Communications*, Vol.5, n.6, pp. 1433 - 1444, June 2006.
- [43] A. Papoulis, *Random variables and stochastic processes*, 2nd ed. New York: McGraw-Hill, pp. 104 and 148, 1984.
- [44] I. S. Gradshteyn and I. M. Ryzhik, *Tables of integrals, series, and products*.
- [45] S. D. Muruganathan, D. C. F. Ma, R.I. Bhasin, A. Fapojuwo, "A centralized energy-efficient routing protocol for wireless sensor networks," *IEEE Communications Magazine*, vol. 43, n. 3, pp. 8-13, March 2005.
- [46] J. H. Kotecha, V. Ramachandran, A.M. Sayeed, "Distributed multitarget classification in wireless sensor networks," *IEEE Selected Areas in Communications*, vol. 23, n. 4, pp. 703-713, April 2005.
- [47] R. Verdone, "An energy-efficient decentralised communication protocol for a network of uniformly distributed sensors polled by a wireless transceiver," in *Proc. of IEEE Intern. Conf. on Communications (ICC 2004)*, vol. 6, pp. 3491-3498, 20-24 June 2004.
- [48] M. Dohler, A. Gkelias, H. Aghvami, "Resource allocation for FDMA-based regenerative multihop links," *IEEE Transactions on Wireless Comm.*, vol. 3, n. 6, pp. 1989 - 1993, Nov. 2004.
- [49] E. S. Sousa, J. A. Silvester, "Optimum transmission ranges in a direct-sequence spread-spectrum multihop packet radio network," *IEEE Journal on Selected Areas in Communications*, Vol 8, Issue 5, pp. 762 - 771, June 1990.
- [50] E. Sousa, "Performance of a spread spectrum packet radio network link in a Poisson field of interferers," *IEEE Trans. on Inf. Theory*, vol. 38, n. 6, pp. 1743-1754, 1992.
- [51] J. Ilow, D. Hatzinakos, A. Venetsanopoulos, "Analytic alpha-stable noise modeling in a Poisson field of interferers or scatterers," *IEEE Trans. Signal Processing*, vol. 46, pp. 1601-1611, June 1998.
- [52] X. Yang, A. Petropulu, "Co-channel interference modelling and analysis in a Poisson field of interferers in wireless communications," *IEEE Trans. on Signal Processing*, vol. 51, n. 1, pp. 64-76, Jan. 2003.
- [53] P.C. Pinto, P.C., M.Z. Win, "Communication in a Poisson field of interferers," in *Proc. of 40th Annual Conference on Information Sciences and Systems (CISS 2006)*, pp. 432 - 437, 22-24 March 2006.

- [54] P.C. Pinto, P.C., M.Z. Win, "Communication in a Poisson field of interferers," *submitted to IEEE Transactions on Wireless Communications (2006)*.
- [55] W. Feller, *An introduction to probability theory and its applications*, vol. II, Wiley, 1966.
- [56] A. Conti, D. Dardari, G. Pasolini, O. Andrisano, "Bluetooth and IEEE 802.11b coexistence: analytical performance evaluation in fading channels,," *IEEE Jour. on Selected Areas in Communications*, vol. 21, n. 2, pp. 259-269, Feb. 2003.
- [57] R.P. Stanley, *Enumerative combinatorics, Volume 2*, Cambridge Studies in Advanced Mathematics 62, Cambridge University Press, Cambridge, 1999.
- [58] J. A. Shohat, J. D. Tamarkin, *The problem of moments*, Mathematical Surveys, vol. 1., American Mathematical Society, New York, 1943.
- [59] M. Chiani, D. Dardari, and M. K. Simon, "New exponential bounds and approximations for the computation of error probability in fading channels," *IEEE Trans. on Wireless Comm.*, vol. 2, n. 4, pp. 840-845, July 2003.
- [60] J. H. Winters, "On the capacity of radio communication systems with diversity in Rayleigh fading environment," *IEEE Journal in Select. Areas Commun.*, vol. SAC-5, pp. 871-878, June 1987.
- [61] J.H. Winters, J. Salz, R.D. Gitlin, "The impact of antenna diversity on the capacity of wireless communication systems," *IEEE Trans. on Communications*, vol. 42, n. 2/3/4, pp. 1740-1751, Feb/Mar/Apr. 1994.
- [62] A. Jovicic, P. Viswanath, S.R. Kulkarni, "Upper bounds to transport capacity of wireless networks," *IEEE Transactions Information Theory*, vol. 50, n .11, pp. 2555-2565, Nov.2004.
- [63] O. Leveque, I.E. Telatar, "Information-theoretic upper bounds on the capacity of large extended ad hoc wireless networks," *IEEE Transactions on Information Theory*, vol. 51, n. 3, pp. 858-865, March 2005.
- [64] M. Dohler, A. Gkelias, H. Aghvami , "A Resource Allocation Strategy for Distributed MIMO Multi-Hop Communication Systems," *IEEE Comm. Letters*, vol. 8, n. 2, pp. 99-101, Feb. 2004.
- [65] M. Dohler, A. Gkelias, A.H. Aghvami, "Capacity of distributed PHY-layer sensor networks," *IEEE Trans. on Vehicular Technology*, vol. 55, n. 2, pp. 622-639, March 2006.
- [66] O. Dousse, F. Baccelli, P. Thiran, "Impact of interferences on connectivity in ad hoc networks," *IEEE/ACM Trans. on Networking*, vol. 13, n. 2, pp. 425-436, April 2005.
- [67] J. Orriss, A.R. Phillips, S.K. Barton, "A statistical model for the spatial distribution of mobiles and base stations," in *Proc. of IEEE Vehicular Technology Conference (VTC 1999 - Fall)*, Vol. 1, pp. 127-130, 19-22 Sept. 1999.

- [68] V. P. Mhatre, C. Rosenberg, D. Kofman, R. Mazumdar, N. Shroff, "A minimum cost heterogeneous sensor network with a lifetime constraint," *IEEE Trans. on Mobile Computing*, Volume 4, Issue 1, Page(s):4 - 15, Jan-Feb 2005.
- [69] P. J. Wan, C. W. Yi "Coverage by randomly deployed wireless sensor networks," *IEEE Trans. on Information Theory*, Volume 52, Issue 6, Page(s):2658 - 2669, June 2006.
- [70] J. F. Chamberland, V. V. Veeravalli, "The impact of fading on decentralized detection in power constrained wireless sensor networks," in *Proc. of IEEE Int. Conf. on Acoustics, Speech, and Signal Processing (ICASSP '04)*, vol. 3, pp. 837-40, May 2004.
- [71] R. Niu, B. Chen, P. K. Varshney, "Fusion of decisions transmitted over Rayleigh fading channels in wireless sensor networks," *IEEE Trans. on Signal Processing*, [see also *IEEE Trans. on Acoustics, Speech, and Signal Processing*,] vol. 54, pp. 1018 - 1027, March 2006.
- [72] E. Telatar, "Capacity of multi-antenna Gaussian channels," *Europ. Trans. on Telecomm.*, vol. 10, pp. 585-595, Nov. Dec. 1999.
- [73] A. T. James, "Distributions of matrix variates and latent roots derived from normal samples," *Ann. Math. Statist.*, vol. 35, pp. 475-501, 1964.
- [74] R. J. Muirhead, *Aspects of multivariate statistical theory*, John Wiley & sons, 1982.
- [75] M. Chiani, M. Z. Win, A. Zanella, "On the capacity of spatially correlated MIMO Rayleigh fading channels," *IEEE Trans. on Inf. Theory*, vol. 49, n. 10, pp. 2363-2371, Oct. 2003.
- [76] A. Zanella, M. Chiani, M.Z. Win, "On the marginal distribution of the eigenvalues of Wishart matrices," Technical Report IEIIT-BO-07-06, Dec. 2006.
- [77] M. S. Aloini, A. Goldsmith, "Capacity of Rayleigh fading channels under different adaptive transmission and diversity techniques," *IEEE Trans. on Veh. Technology*, vol. 48, pp. 1165-1181, July 1999.
- [78] P. Smith, S. Roy, M. Shafi, "Capacity of MIMO systems with semi-correlated flat fading," *IEEE Trans. on Inf. Theory*, vol. 49, n. 10, pp. 2781-2788, Oct. 2003.
- [79] J. O. Berger, V. de Oliviera, and B. Sanso, "Objective bayesian analysis of spatially correlated data," *J. Amer. Statistical Assoc.*, vol. 96, no. 456, pp. 1361-1374, 2001.
- [80] M.C. Vuran, I.F. Akyildiz, "Spatial correlation-based collaborative medium access control in wireless sensor networks," *IEEE/ACM Transactions on Networking*, vol. 14, n. 2, pp. 316-329, April 2006.

- 
- [81] M. Chiani, Moe Z. Win, H. Shin, "A general result on hypergeometric functions of matrix arguments and application to wireless MIMO communication," in *Proc. International Conference on Next-Generation Wireless Systems (ICNEWS'06)*, Dhaka, Bangladesh, pp. 196-200, Jan. 2006.
- [82] IEEE, "IEEE 802.15.4: Wireless Medium Access Control (MAC) and Physical Layer (PHY) Specifications for Low-Rate Wireless Personal Area Networks (LR-WPANs)", 2006.
- [83] ZigBee Alliance, "ZigBee Specification", December 2006.
- [84] D. Dardari, "On the connected nodes position distribution in ad hoc wireless networks with statistical channel models", in *Proc. of IEEE International Conference on Communications (ICC)*, pp. 4741-4745, June 2007.
- [85] S. Mukherjee, D. Avidor, K. Hartman, "Connectivity, power, and energy in a multihop cellular - packet system," *IEEE Trans. on Veh. Technology*, vol. 56, n. 2, pp. 818-836, March 2007.
- [86] J.F.C. Kingman, *Poisson processes*, Oxford Univ. Press, 1993.
- [87] R. Verdone, D. Dardari, G. Mazzini, A. Conti, *Wireless sensor and actuator networks: technologies, analysis and design*, Elsevier, January 2008.



